論文 / 著書情報
Article / Book Information

題目(和文)	
Title(English)	Dissolution kinetics of elemental mercury and biosorption kinetics of dissolved inorganic mercury in freshwaters
著者(和文)	RosamondR.M.S Tshumah-Mutingwende
Author(English)	T.M Rosa
出典(和文)	学位:博士(工学), 学位授与機関:東京工業大学, 報告番号:甲第11499号, 授与年月日:2020年3月26日, 学位の種別:課程博士, 審査員:高橋 史武,日野出 洋文,中﨑 清彦,江頭 竜一,時松 宏治
Citation(English)	Degree:Doctor (Engineering), Conferring organization: Tokyo Institute of Technology, Report number:甲第11499号, Conferred date:2020/3/26, Degree Type:Course doctor, Examiner:,,,,
学位種別(和文)	博士論文
Type(English)	Doctoral Thesis

Dissolution kinetics of elemental mercury and biosorption kinetics of dissolved inorganic mercury in freshwaters

A thesis submitted to the School of Environment and Society, Tokyo Institute of Technology; in fulfilment of the requirements for the degree of

Doctor of Engineering

by Rosamond R.M.S. Tshumah-Mutingwende

Supervisor: Ass. Prof. Fumitake Takahashi

Dedication

...to my loving husband and son

Abstract

Artisanal and small-scale gold mining (ASGM) is undeniable a lucrative source of income to impoverished communities of developing countries such as Brazil, Colombia, Tanzania and Zimbabwe. However, owing to the unregulated use of elemental mercury (Hg^0) and the lack of reputable mine waste disposal facilities, its negative effects on the environment and human health tend to tarnish its economic benefits. Hg^0-rich amalgamation and or cyanide-processed amalgamation tailings are often discharged into nearby freshwaters. Here; Hg^0 droplets undergo several biogeochemical transformations whose end product is methylmercury (MeHg), a potent neurotoxin and teratogen. MeHg readily bioaccumulates and biomagnifies within the different trophic levels of the aquatic food chain, thus, exposing humans to Hg via MeHg-contaminated fish consumption. In order to estimate such dietary mercury (Hg) exposures using Hg environmental fate and transport mass balance models; knowledge of the Hg^0 dissolution rate coefficient is required yet it is limited in literature. Therefore, it was investigated in this study.

Dissolution tests in a 'dark chamber' revealed that an increase in medium pH resulted in a decrease in the dissolution rate, whereas, a large Hg^0 droplet specific surface area (SSA) and high Reynolds number (Re) resulted in a faster dissolution. A multivariate first order dissolution model of the form: $\hat{k} = -7.9 \times 10^{-5}[pH] + 7.0 \times 10^{-4}\,[\log Re] + 0.12[SSA] - 2.5 \times 10^{-3}$ was proposed (adjusted R^2 = 0.99). The Breusch-Pagan and White heteroscedasticity tests revealed that the model residuals are homoscedastic (p-value = 0.05) at the 5% significance level. Parameter sensitivity analysis suggests that slow Hg^0 dissolution in aquatic systems might mask emerging environmental risk of Hg. Even after Hg^0 use in ASGM is banned, Hg^0 dissolution and following contamination will continue for about 40 years or longer owing to previously discharged Hg^0 droplets. In the presence of Suwannee River fulvic acid (SRFA) (2 mg-C L^{-1}) it was observed that acidic pH enhances the dissolution of Hg^0 in humic substances'-rich freshwaters. However, the concentration of Hg-SRFA soluble organic complexes (Hg_{OC}) increased with increase in pH. The total dissolved Hg (Hg_T) concentration, dissolution rate coefficient and the Hg_{OC} concentration were proportional to the SRFA concentration (0 -30 mg-C L^{-1}). Ionic strength (0 – 3.0 mM KCl) did not result in any significant increase in the Hg^0 dissolution rate coefficient, Hg_T and Hg_{OC} concentrations. A multivariate first-order dissolution model of the form: $\hat{k} = 1.4 \times 10^{-3} - 1.1 \times 10^{-4}[pH] + 3.5 \times 10^{-5}[SRFA]$ was proposed (Adjusted R^2: 0.99). The p-values of 0.53

and 0.57 for the Breusch-Pagan and White heteroscedasticity test models respectively; revealed that the residuals are homoscedastic at the 5% significance level. Though Hg^0 dissolution is rapid in the presence of humic substances (it is expected to continue for at least 31 years); more Hg will be released into the water column, hence, there is need to pay close attention to Hg environmental risk.

Owing to the limited potable water sources in the vicinity of ASGM activities coupled with the high capital and operational costs of conventional water treatment technologies such as ion exchange and membrane processes; ASGMs and communities downstream of the mining activities in developing countries are often left with no option but to use the Hg contaminated river/stream water for domestic purposes. Thus, the potential use of an abundant living green freshwater algae, *Cladophora* sp., as an Hg biosorbent for Hg-contaminated freshwaters was assessed at different experimental conditions. A rapid uptake of Hg by *Cladophora* sp. was displayed. More than 99% of Hg in solution was removed within the first 5 min of contact and equilibrium was attained after 10 min of contact. A high adsorption capacity of 800 mg kg^{-1} was attained at pH 3 and at the optimum initial Hg concentration of 1.0 mg L^{-1}. Competitive adsorption studies showed that the selectivity of cations by *Cladophora* sp. was in the following order: Hg^{2+} >Fe^{2+}>Cu^{2+}> Zn^{2+} > Co^{2+}.The experimental results best fitted the pseudo-second order kinetic model and the Langmuir equilibrium isotherm model. The rapid uptake of Hg and the high extraction efficiency displayed will result in huge cost savings during industrial and domestic applications and further treatment of the water for Hg removal is not required.

For environmental remediation purposes, Hg release into the water column once Hg^0-rich amalgamation tailings are discharged into freshwaters was simulated based on the sensitivity analysis of the dissolution tests results. Based on the optimum conditions of Hg^{2+} adsorption by Cladophora sp. algae, a 1000 L batch reactor was designed and the mass of algae required at different Hg^{2+} initial concentrations in order to achieve the World Health Organization (WHO) Hg in drinking water threshold of 0.006 mg-Hg L^{-1} was determined. It was observed that, the mass of algae required depended on the concentration of Hg^{2+} available in solution and it increased with increase in concentration.

Acknowledgements

Special thanks to my supervisor Prof. F. Takahashi for granting me the opportunity to be under his great mentorship. He was also able to secure and avail financial support for my studies, without which it would be impossible to pursue them. Many thanks to my co-supervisor Prof. K. Tokimatsu for his comments and contributions towards this research work during our regular lab seminars. I would like to thank our lab Secretaries Ms. Ohno and Ms. Takahashi (retired) for all their assistance during the course of my studies.

Many thanks goes to Prof. Tomohiro Hayashi for allowing me to use facilities in his laboratory and Ryongsok Chang for assisting me with the analysis.

I am indebted to Tokyo Institute of Technology community as a whole, for their love and support during the course of my studies. Many thanks to Tokyo Institute of Technology financial aid for Doctoral students for all the provisions they made available to me. With much appreciation, I would like to thank JASSO Honors Scholarship for their financial support during the final year of my studies. This study was financially supported by Environment research and technology development fund [grant number 3K143002 and 3-1701], Ministry of the Environment, Japan and I would like to thank them so much.

Last but not least, I would like to thank my husband and son, for their unwavering encouragement, patience, constructive criticism, prayers, love and support, without which I would have not made it this far. I would like to thank my in-laws and family, for their constant communication with great words of encouragement. I would like to appreciate my Pastors and fellow congregants at City Vision Glory Church, Yokohama, Japan, for their love and prayers. It all means a lot to me!

If I have seen further than others, it is by standing on the shoulders of giants. - Isaac Newton

Table of Contents

CHAPTER 5: SIMULATED MERCURY RELEASE AND BIOSORPTION REACTOR DESIGN

CHAPTER 6: CONCLUSIONS AND RECOMMENDATIONS

List of Figures

List of Tables

List of Abbreviations

ASGM: Artisanal and small-scale gold mining

ASGMs: Artisanal and small-scale gold miners

DOC: Dissolved organic carbon

FA: Fulvic acid

HA: Humic acid

HSs: Humic substances

SRFA: Suwannee river fulvic acid

List of publications

1. Rosamond Tshumah-Mutingwende, Fumitake Takahashi, Ewa M. Cukrowska, Julien Lusilao-Makiese (2018) Cladophora sp. biosorption of metal-contaminated water, Applied Environmental Research, Vol.40, No.2, 17-31. DOI:10.35762/AER.2018.40.2.2
2. Rosamond R.M.S Tshumah-Mutingwende, Fumitake Takahashi (2019) Physio-chemical effects of freshwaters on the dissolution of elemental mercury, Environmental Pollution, Vol.252, 627-636. DOI:10.1016/j.envpol.2019.05.130

Chapter One

Introduction

This is the introductory chapter and it gives a general overview of the scope of the project, an outline of the problem statement together with the motivation for the research. The general objective and the specific objectives which provide the roadmap for fulfilling the general objective together with the key questions are given.

1.0 General Overview

Artisanal and small-scale gold mining (ASGM) employing the elemental mercury (Hg^0) amalgamation technique contributes about 37% (Esdaile and Chalker, 2018) to the global anthropogenic mercury (Hg) emissions pool to the environment. This makes it the largest source of Hg emissions when compared to fossil fuel combustion, cement production and chlor-alkali industry amongst others (AMAP/UNEP, 2013). Developing countries such Colombia, China, Brazil, Tanzania and Zimbabwe have the highest mean Hg demand due to ASGM in their territories (Fig 1.1). Abject poverty, high unemployment rate, hyper-inflation and political instability are notably its main drivers (Lassen et al., 2016; PACT, 2015).

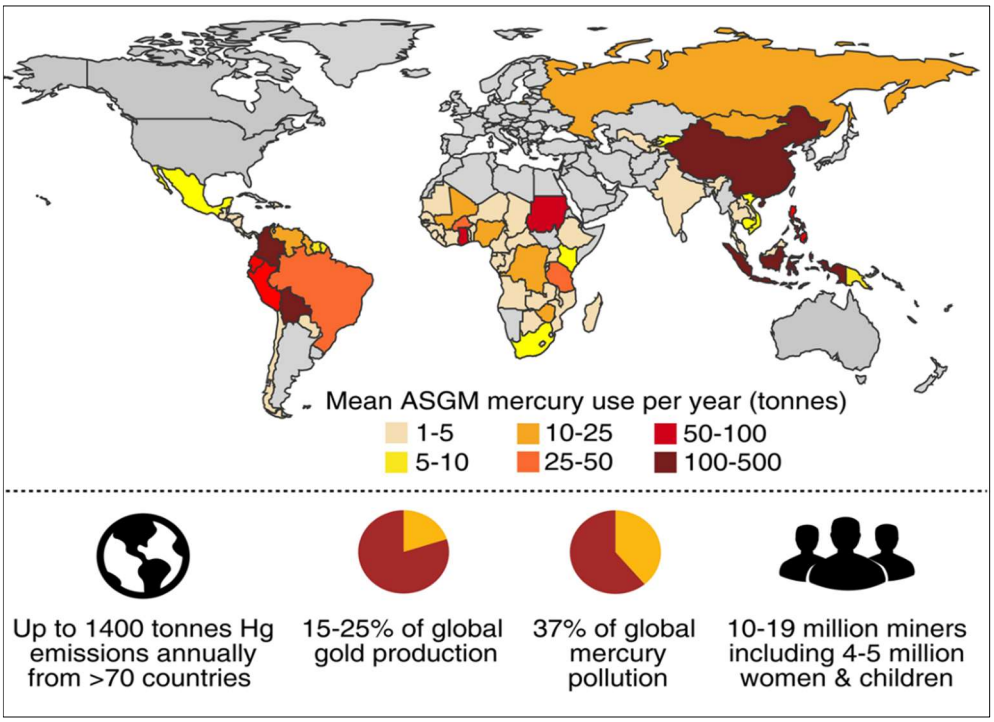

Fig. 1.1: Global Hg^0 use in ASGM

(Source: (Esdaile and Chalker, 2018))

Hg^0, a toxic and non-biodegradable heavy metal is preferably used in this rudimentary and unscrupulous practice due to its simplicity, as it does not require any sophisticated equipment in already poorly equipped field applications; accessibility and low cost (Telmer and Veiga, 2009). As a result, efforts to transition to non-Hg^0 gold mining technologies have failed to yield the desired results. Thus, the continuous use of Hg^0 by Artisanal and small-scale Gold Miners

(ASGMs) coupled with the lack of reputable mine waste disposal facilities has resulted in the pollution of nearby rivers and streams with Hg due to the discharge of Hg^0-rich amalgamation and or cyanide-processed amalgamation tailings (200-500 mg-Hg L^{-1}) (Chouinard and Veiga, 2008; Gunson et al., 2006; Veiga et al., 2014, 2006). Once in fresh waters, Hg^0 droplets tend to settle in bottom sediments and sediment/water interfaces which are usually poorly-lit to dark environments. Here, the gradual dissolution and oxidation of Hg^0 droplets takes place (Amyot et al., 2005). The end product of succeeding biogeochemical transformations is methylmercury (MeHg) (Morel et al., 1998), a potent neurotoxic (Salonen et al., 1995) and teratogenic (Sullivan and Krieger, 2001) organic compound. Owing to its lipophilic nature, MeHg readily bioaccumulates and biomagnifies within the different trophic levels of the aquatic food chain, thus, humans and wildlife are susceptible to Hg exposure as a result of MeHg-contaminated fish consumption (Fitzgerald and Clarkson, 1991) (Fig. 1.2).

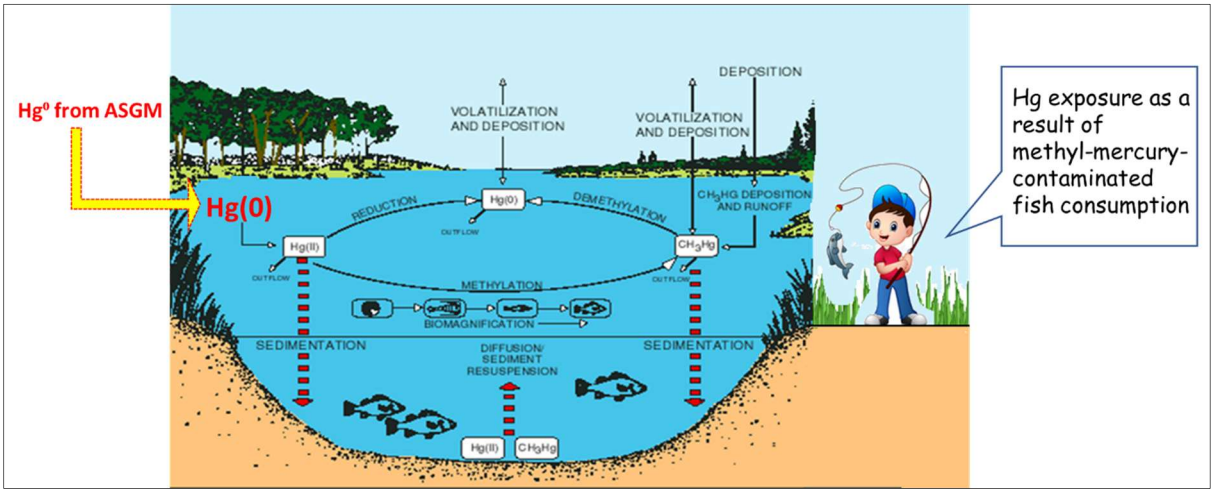

Fig. 1.2: Fate of Hg^0 in freshwaters

(Source: Adapted and modified from (U. S. Geological Survey, 1995))

High Hg concentrations, far exceeding the World Health Organization (WHO) safety limit of 0.5 µg g^{-1} on a fresh weight basis (World Health Organization, 1990) have been reported in fish tissues from rivers along ASGM activities. For example, fish consumed by ASGMs and the inhabitants of surrounding communities along the Muzvezve River, Zimbabwe and Tapajós River, Brazil; have total Hg concentrations as high as 2.61 µg g^{-1} (Billaud et al., 2004; Gunson et al., 2006) and 0.69 µg g^{-1} (Malm et al., 1995) respectively. At least 95% (Bloom, 1992) of the total Hg present

in fish tissue is MeHg. Such dietary Hg exposures are usually depicted by high MeHg concentrations in human hair samples. Typical symptoms of Hg intoxication include signs of a damaged central and peripheral nervous system such as ataxia, dysdiadochokinesia, pathological reflexes, coordination problems and concentration problems and in worst cases the Minamata disease (EPA, 2019; Gunson et al., 2006).

Owing to increased ASGM activities in the remote areas of developing nations, ASGMs and inhabitants of downstream non-mining communities are often left with no option but to use the Hg polluted water sources for domestic purposes including agriculture (Boese-O´Reilly et al., 2004; Esdaile and Chalker, 2018; World Health Organization (WHO), 2016). Most of these water sources have Hg concentrations far greater than the recommended WHO guideline value for inorganic mercury in drinking water of 6.0 μg-Hg L^{-1} (World Health Organization (WHO), 2005) or the maximum contaminant level limit (MCL) of 2.0 μg-Hg L^{-1} (WQA, 2019). For example, Ngwabalozi River, Zimbabwe, where Hg concentrations as high as 310 μg-Hg L^{-1} have been reported (Mudyazhezha and Kanhukamwe, 2014). Drinking such Hg-contaminated waters can cause kidney damage from short-term exposures at levels above the MCL. However, on a chronic basis, Hg has the potential to cause kidney damage from long-term exposure at levels above the MCL. High levels can damage the brain, kidneys, and developing fetus. Effects on brain functioning may result in irritability, shyness, tremors, changes in vision or hearing, and memory problems (WQA, 2019).

1.1 Problem Statement and Motivation

Cases of ASGM-related dietary Hg exposure have been reported in the Philippines (Drasch et al., 2001) Indonesia (Castilhos et al., 2006), Brazil (Gunson et al., 2006; Malm et al., 1995) and Zimbabwe (Billaud et al., 2004). However, these findings are based mainly on field investigations which are tedious, costly, time consuming and do not provide any time integrated Hg exposure measurements. Yet, Hg environmental fate and transport mass balance models can be successfully used to estimate Hg exposure to human bodies via MeHg-contaminated fish consumption (Takahashi, 2017). However, in freshwaters contaminated with Hg^0, its first-order dissolution rate coefficient must first be determined before incorporating consecutive biogeochemical transformation parameters in the model. But, unlike the solubility of Hg^0 in aquatic systems,

(Amyot et al., 2005; Canela and Jardim, 1997; Glew and Hames, 1971) there are several knowledge gaps on the Hg^0 first order dissolution rate coefficient. Based on laboratory investigations, it is estimated to be about 0.3 min^{-1} in air-equilibrated waters with a chloride concentration close to that of seawater (0.5 M) (Amyot et al., 2005). To the best of our knowledge, this is the only reported value in literature. The Hg^0 dissolution rate coefficient reported by Amyot and colleagues (Amyot et al., 2005) is inapplicable for freshwaters where the chloride concentration is in the range of 0 - 2.8 mM (0 - 100 mg L^{-1} (Goldman and Horne, 1983)), thus, it was investigated in this study under freshwater conditions. Furthermore, despite the abundance of humic substances (HSs) in freshwaters, their tendency to interact with Hg species influencing several aspects of the Hg biogeochemical cycle such as mobility, speciation, toxicity and solubility (Loux, 1998; Meech et al., 1998; Melamed et al., 2000, 1997; Ravichandran, 2004a; Ravichandran et al., 1998; Tromans et al., 1996; Waples et al., 2005); their effect on the Hg^0 first-order dissolution rate coefficient remains uncertain. As a result, it was also investigated. Also, owing to the limited potable water sources in the vicinity of ASGM activities coupled with the high capital and operational costs of passive and conventional water treatment technologies such as aerobic/ anaerobic wetlands and membrane technologies respectively (e.g. reverse osmosis) (Macingova et al., 2012; Skousen et al., 1990; Strydom and King, 2009; Udayabhanu and Prasad, 2010); ASGMs and surrounding communities are often left with no option but to utilize the Hg-contaminated river/stream water for domestic purposes. Therefore, the potential use of an abundant freshwater living green algae *Cladophora* sp. as a cheap alternative for the removal of Hg from contaminated freshwaters was assessed.

1.2 Research objectives

Chapter 2: To determine the Hg^0 reactive (oxidative) first-order dissolution rate coefficient in fresh waters and the factors influencing it.

Chapter 3: Investigate the effect of humic substances on the Hg^0 first-order dissolution rate coefficient in fresh waters and the factors influencing it.

Chapter 4 To assess the potential use of an abundant living green freshwater algae, *Cladophora* sp., as an Hg biosorbent for Hg-contaminated freshwaters.

Chapter 5 Simulate Hg release into the water column due to Hg^0 dissolution (based on Chapters 2&3) and then design a 1000 L batch reactor for the adsorption of the released Hg (based on Chapter 4).

1.3 Research questions

Chapter 2

1. Does Hg^0 dissolve under freshwater conditions?
2. What are the optimum Hg^0 dissolution conditions?

Chapter 3

1. Do humic substances have any significant effect on the Hg^0 dissolution rate coefficient?
2. What are the optimum dissolution conditions in the presence of humic substances?

Chapter 4

1. Can algae be used as a low cost biosorbent?
2. What are the optimum conditions for the uptake of mercury by algae?

Chapter 5

1. How much Hg is released into the water column due to Hg^0 dissolution?
2. What is the mass of algae required in a 1000 L batch reactor?

1.4 Chapter relation

The overall relationship between all the chapters of this study, summary of the research objectives and outcomes are summarized in Fig. 1.3.

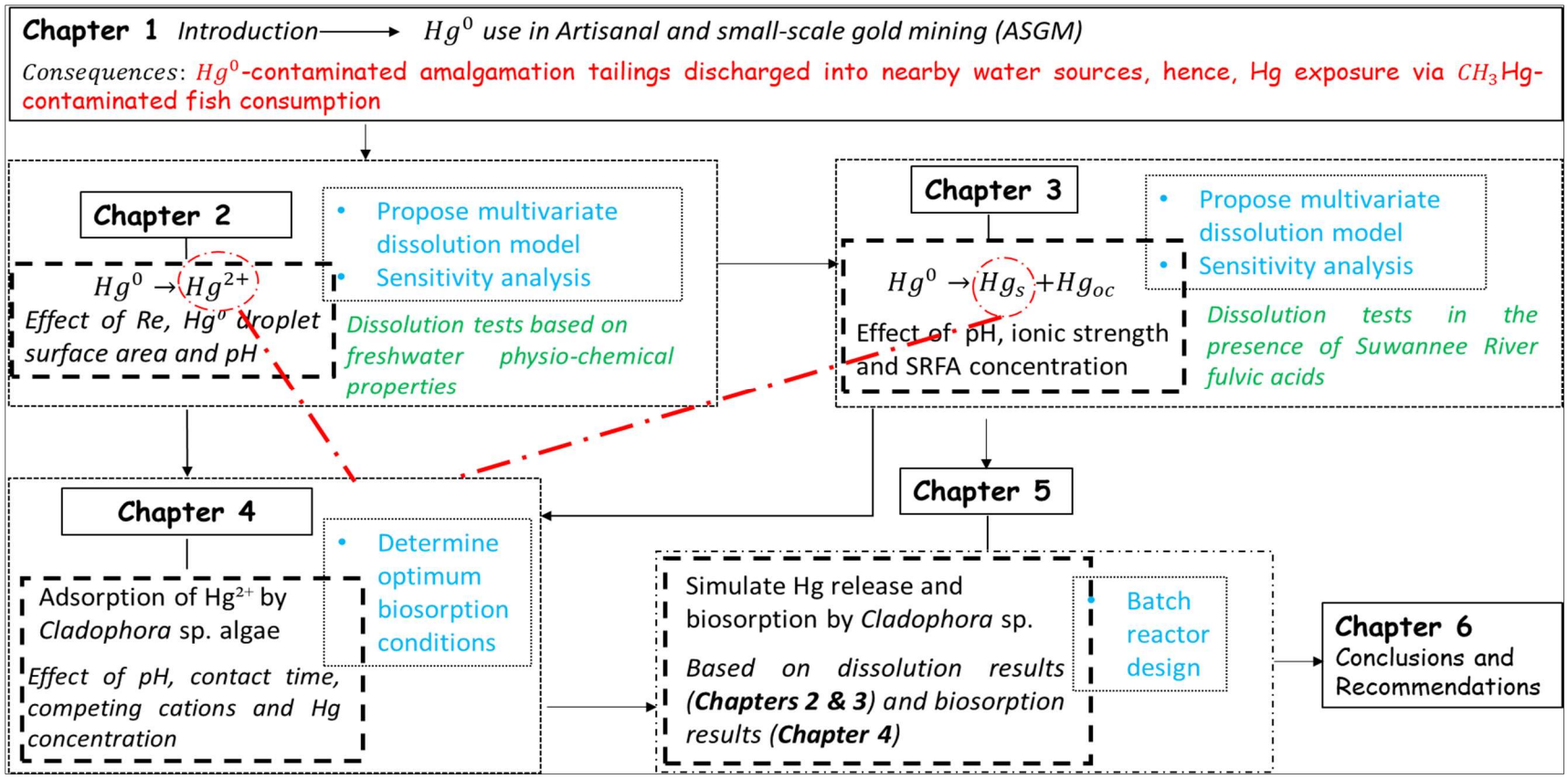

Fig. 1.3: Summary of Chapter relation

Chapter Two

Physio-chemical effects of freshwaters on the dissolution of elemental mercury

This chapter focuses on the physio-chemical effects of freshwaters such as pH, Reynolds number, Fe^{3+} concentration and Hg^0 droplet surface area on the oxidative-dissolution rate coefficient of elemental mercury in aquatic systems. The research and experimental approach used together with the kinetic study are elaborated. The key experimental findings are then simulated to develop a multivariate model for the Hg^0 first order dissolution model. Finally, a risk assessment on the impact of Hg^0 discharged into freshwaters by Artisanal and Small-scale Gold miners is conducted.

2.0 Introduction

Experimental investigations for Hg^0 dissolution in freshwaters is divided into two chapters. In this chapter, the physio-chemical effects of freshwaters such as pH, Re, Fe^{3+} concentration and Hg^0 droplet size were investigated. Based on the experimental results, a model for determining the Hg^0 first order reactive dissolution rate coefficient under different operational conditions will be proposed. Due to the aforementioned tendency of Hg^0 droplets to settle in bottom sediment and sediment/water interfaces, these investigations will be conducted under dark conditions. In **Chapter 3**, the effect of humic substances on the Hg^0 dissolution rate coefficient was investigated using commercially available Suwannee River fulvic acid (SRFA). The methodology and the experimental observations are detailed in the following sections.

2.1 Materials and methods

This section details the reagents used, methodology followed and machinery used for analysis.

2.1.1 Reagents

Reagents used in this study were of analytical grade, except for standards used for quantification purposes which were of high purity. All instrument standard solutions were prepared in 0.001% L-cysteine solution (Wako, Japan). Milli-Q water with an electrical resistivity of 18.2 MΩ cm (Millipore, USA) was used in reagent preparation.

2.2 Experimental setup

Dissolution tests were performed in 250 mL Erlenmeyer flasks in which 150 mL of Milli-Q water of desired pH was added. Hg^0 dissolution rate coefficient investigations were conducted at room temperature (23-25ºC). The entire reaction flask was wrapped in aluminium foil to avoid exposure to natural and/or laboratory light. After adding an appropriate Hg^0 droplet volume, the mouth of the vessel was first sealed with a parafilm followed by aluminium foil, thus the possibility of gaseous Hg escaping or reaching the reaction vessel is negligible. The aluminium-wrapped reaction flasks were then put in a cardboard box 'dark reaction chamber'. This was then placed on either a shaker (Riken, Japan) or magnetic stirrer (AS ONE Corporation, Japan) depending on the specific experiment (Fig. 2.1). All vessels used in this study were acid washed following a cleaning

protocol described by Monperrus and co-workers (Monperrus et al., 2005). Nitrile gloves were worn at all times during sample preparation and handling. All dissolution tests were performed in triplicates. The liquid Hg^0 used in this study was stored in tightly sealed dark glass containers away from any oxygen source, direct sunlight and heat in order to avoid its oxidation before the dissolution tests.

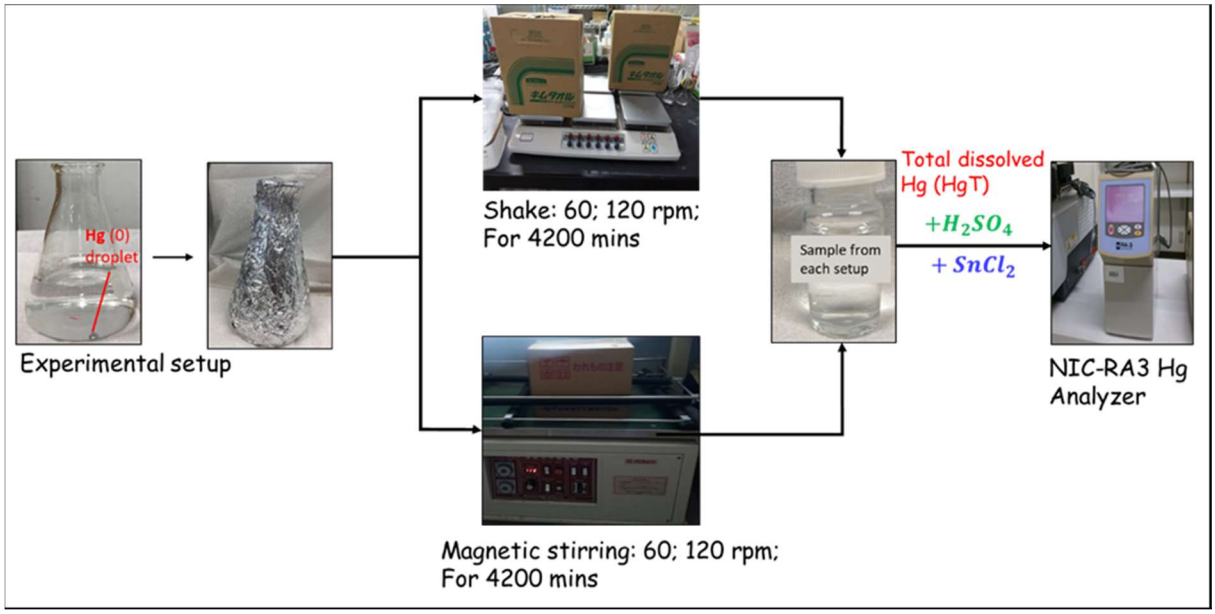

Fig. 2.1: Experimental procedure

2.2.1 Effect of pH

The effect of pH on the dissolution rate of Hg^0 was investigated at pH: 3.0, 6.5, 7.0, 8.0, and 10.0. The pH was adjusted by using either 0.1 M nitric acid (HNO_3) or 1.0 M sodium hydroxide (NaOH) solution. An initial Hg^0 droplet specific surface area of 0.0063 cm^2 cm^{-3} was used and the shaking rate was kept constant at 120 rpm. Since the optimum pH of freshwaters is in the range of 6.5 to 8.5 (Behar, 1996), pH 7.0 was chosen as the optimum pH and kept constant for all succeeding experiments in this study unless stated otherwise.

2.2.2 Effect of Hg^0 droplet surface area

Assuming the Hg^0 droplet is spherical in shape, the following surface areas: 0.19, 0.37, 0.55 and 0.94 cm^2 were obtained for the 0.01, 0.02, 0.04 and 0.09 mL droplet volumes respectively. This is

equivalent to a specific surface area of (0.0013, 0.0025, 0.0037 and 0.0063 $cm^2\ cm^{-3}$). The shaking rate was kept constant at 120 rpm.

2.2.3 Effect of Fe^{3+} concentration

The presence of Fe^{3+} in acidic mine waste waters is known to promote the dissolution of Hg from cinnabar (HgS) (Burkstaller et al., 1975). It is assumed that in such media, Fe^{3+} behaves as an oxidizing agent, thus facilitating the oxidative dissolution of Hg. Therefore, the oxidizing effect of Fe^{3+} on Hg^0 dissolution was investigated in this study.

A stock solution of 10 mg L^{-1} Fe^{3+} was prepared by weighing appropriate amounts of $Fe_2(SO_4)_3 \cdot nH_2O$. Suitable aliquots were taken from this standard for subsequent dilution to the desired concentration. The solutions were stored in a refrigerator at 4ºC prior to the relevant experiments. Hg^0 dissolution tests were investigated in 0, 0.5 and 1.0 mg L^{-1} Fe^{3+} solutions. A shaking rate of 120 rpm and Hg^0 droplet specific surface area of 0.0063 $cm^2\ cm^{-3}$ were used. In order to mimic acidic conditions of Acid Mine Drainage (AMD), tests were conducted at pH 3.0.

2.2.4 Effect of agitation type and rate

The effect of agitation type and rate on the dark dissolution rate coefficient of Hg^0 was investigated by shaking at 60 and 120 rpm and; magnetic stirring at 60 and 120 rpm. An Hg^0 droplet specific surface area of 0.0063 $cm^2\ cm^{-3}$ was used. The observed results were further elaborated based on the media Reynolds number (Re) which was computed using Eq. 3.1 (Büchs et al., 2000):

$$Re = \rho n d_i^2 / \eta \tag{2.1}$$

Where;

Re - is the Reynolds number (-)

ρ – is the reaction fluid density (kg m^{-3})

n – is the shaking or stirring frequency (min^{-1})

d_i – is the maximum inner diameter of reaction flask and stirrer diameter for shaking and magnetic stirring respectively (m)

η- is the dynamic viscosity of the reaction fluid (kg m^{-1} min^{-1})

2.3 Measurement of Total dissolved Hg (Hg_T)

For each investigation, the total dissolved Hg concentration (Hg_T) (referring to the sum of dissolved Hg^0 and Hg^{2+} was monitored over time from 0 to 4200 min. Any formed Hg_2^{2+} is assumed to rapidly disproportionate to Hg^0 and Hg^{2+} (Sanemasa, 1977). The Hg_T was determined using the Reducing Vaporization Mercury Analyser -RA3 (Nippon Instruments Corporation, Japan). Sulphuric acid (50%) and 10% tin (II) chloride were used as the carrier and reductant respectively.

2.4 Kinetic study

Based on Fick's first law of diffusion and assuming that the Hg^0 droplet surface area remains constant throughout all experiments, the Hg^0 first order reactive dissolution rate coefficient was determined using the Noyes-Whitney first order dissolution model (Eq. 2.2- 2.3) (Noyes and Whitney, 1897):

The Hg^0 first order dissolution rate coefficient was determined by fitting the Hg_T experimental data on the Noyes-Whitney first order dissolution model (Noyes and Whitney, 1897):

$$dC_t/dt = k_1(C_e - C_t) \qquad (2.2)$$

Integrating between the boundary t = 0 to t; C_t= 0 to C_t yields:

$$log(C_e - C_t) = log\, C_e - (k_1 t/2.303) \qquad (2.3)$$

The Hg^0 first order dissolution rate coefficient (k_1 [min^{-1}]) and the equilibrium Hg_T concentration (C_e [µg-Hg L^{-1}]) were determined from the intercept and gradient respectively

Where;

C_e – is the equilibrium or saturated total dissolved mercury concentration (µg-Hg L^{-1})

C_t - is the total dissolved mercury concentration at time t, (µg-Hg L^{-1})

k_1 - is the Hg^0 first order dissolution rate coefficient (min^{-1})

t- is the time (min)

2.5 Modelling and statistical analysis

Based on the experimental results, a multivariate Hg^0 first order dissolution model was proposed. The model coefficients were optimized and then assessed by the ANOVA statistical analysis at the 95% confidence interval. Also, the Breusch-Pagan and the White heteroscedasticity test methods were applied on the model residuals at the 5% significance level. Furthermore, the model was evaluated graphically by plotting the predicted against observed data and also quantitatively by determining the Modeling Efficiency (ME) and the Root Mean Square Error (RMSE) (Janssen and Heuberger, 1995).

2.6 Results and Discussions

This section reports and discusses the experimental observations which are then used to develop a multivariate Hg^0 first-order dissolution model.

2.6.1 Reducing Vaporization Mercury Analyser calibration

An excellent linearity was obtained with the Reducing Vaporization Mercury Analyzer for total mercury standards (Fig. 2.2). Calibration was performed using standards in the range of 1-30 µg Hg l^{-1}. A method limit of detection of 0.08 µg Hg L^{-1} (calculated as three times the standard deviation of blank samples).

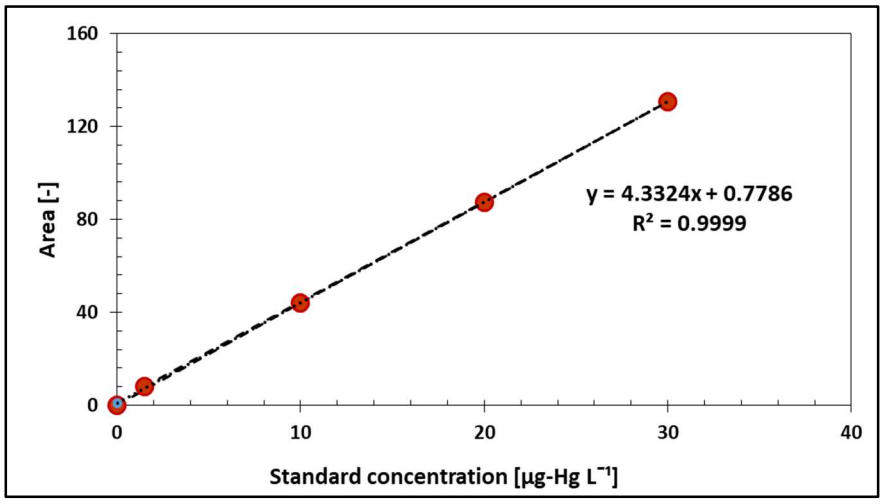

Fig. 2.2: Reducing Vaporization Mercury Analyser -RA3 calibration curve

2.6.2 Effect of pH

The dissolution of Hg^0 in low salinity waters is highly influenced by the media pH. The equilibrium Hg_T at pH 3.0 (734.2 µg-Hg L^{-1}) was six-fold more than that observed at pH 10.0 (124.6 µg-Hg L^{-1}). At optimum pH conditions for freshwaters (pH 6.5-8.0), the Hg_T ranged from 492.1 to 279.8 µg-Hg L^{-1} (Fig. 2.3 A). The observed solubility trend (increase in Hg_T with decrease in pH) was similar to that reported by Canela and co-worker (Canela and Jardim, 1997) However, owing to the difference in experimental conditions, the Hg_T results of this study were higher.

The observed Hg_T over the chosen pH range (pH 3.0 -10.0) were two orders of magnitude greater than the recommended World Health Organization (WHO) guideline value for inorganic mercury in drinking water of 6.0 µg L^{-1} (World Health Organization (WHO), 2005). This is a major threat to human health since some of the Hg-contaminated freshwaters located in the vicinity of ASGM activities are used for domestic purposes by both the ASGMs and downstream non-mining communities (Boese-O´Reilly et al., 2004; Esdaile and Chalker, 2018; Gafur et al., 2018; World Health Organization (WHO), 2016), for example, Bone River, Indonesia (Gafur et al., 2018) and Muzvezve River, Zimbabwe (Boese-O´Reilly et al., 2004). Also, the high concentration of dissolved Hg serves as a source of Hg available for the methylation process, thus, people depending on the polluted water body are also at risk of Hg exposure via MeHg-contaminated fish consumption.

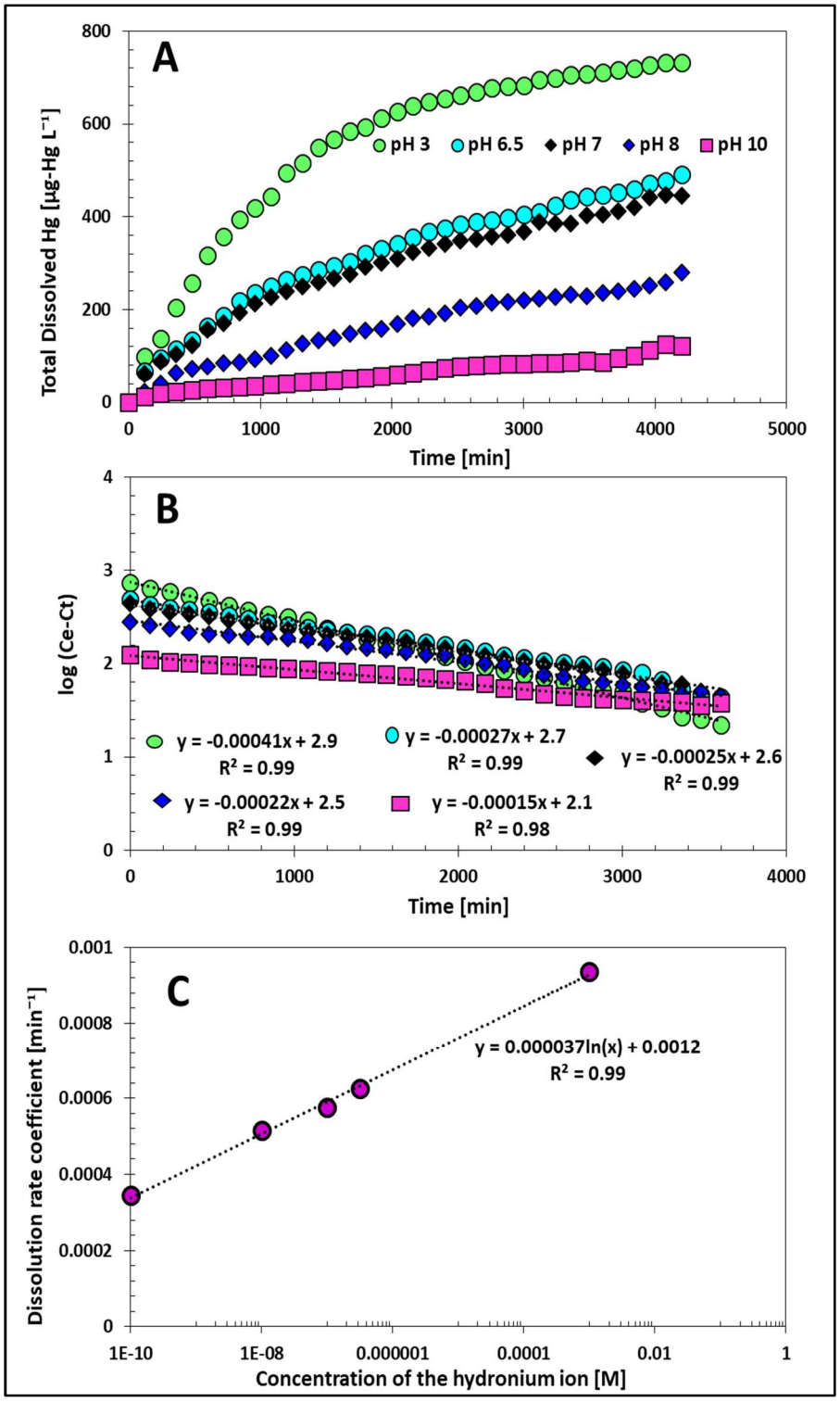

Fig. 2.3: (A) Effect of pH on the Hg_T concentration. (B) Noyes-Whitney first order dissolution model. (C) Effect of pH on the Hg^0 dissolution rate coefficient. (Shaking rate: 120 rpm; contact time: 4200 min; Hg^0 droplet surface area: 0.94 cm^2).

When the experimental data was fitted on the Noyes-Whitney first order dissolution model (Fig. 2.3B), good linearization (R^2: 0.98 – 1.0) was observed for all five scenarios. Also, the predicted equilibrium Hg_T (121.7 – 737.2 µg-Hg L^{-1}) was close to the experimental data (124.6 – 734.2 µg-Hg L^{-1}).

Generally, the dissolution of Hg^0 was slow throughout the chosen pH range (calculated as the hydronium ion concentration: $[H_3O^+]$ (M) = 10^{-pH}) (Fig. 2.3C). But, as expected, it was relatively faster at pH 3.0 (0.00094 min^{-1}) and decreased with increase in pH (0.00063-0.00034 min^{-1} for pH 6.5 - 10.0). The pH dependence of the Hg^0 dissolution rate coefficient can be attributed to the rapid oxidation of dissolved Hg^0 to Hg^{2+} under acidic conditions (pH 3.0). However, as the pH approaches slightly alkaline (pH 6.5) to alkaline levels (pH 7.0-10.0), oxidation of dissolved Hg^0 became less favorable, hence, the decrease in the dissolution rate coefficient as the pH increases.

2.6.3 Effect of Hg^0 droplet specific surface area

Owing to the uncontrolled and non-procedural nature of ASGM techniques all over the world, high uncertainties surround the quantities of Hg^0 used and lost into aquatic systems (Gunson et al., 2006; Lassen et al., 2016; Veiga et al., 2006; Veiga and Baker, 2004). Thus, it is important to investigate the effect of droplet size on the Hg^0 dissolution rate coefficient in freshwaters. The Hg_T increased with increase in Hg^0 droplet specific surface area (Fig. 2.4A). An increase in the droplet specific surface area from 0.0013 to 0.0063 cm^2 cm^{-3} resulted in two orders of magnitude increase in the equilibrium Hg_T. In the presence of the Hg^0 droplet with a specific surface area of 0.0013 cm^2 cm^{-3}, the Hg_T was below the method limit of detection of 0.08 µg-Hg L^{-1} for the majority of the experimental time. Thus, Hg_T of 1.1 and 447.9 µg-Hg L^{-1} were obtained in the presence of Hg^0 droplets with a specific surface area of 0.0013 cm^2 cm^{-3} and 0.0063 cm^2 cm^{-3} respectively.

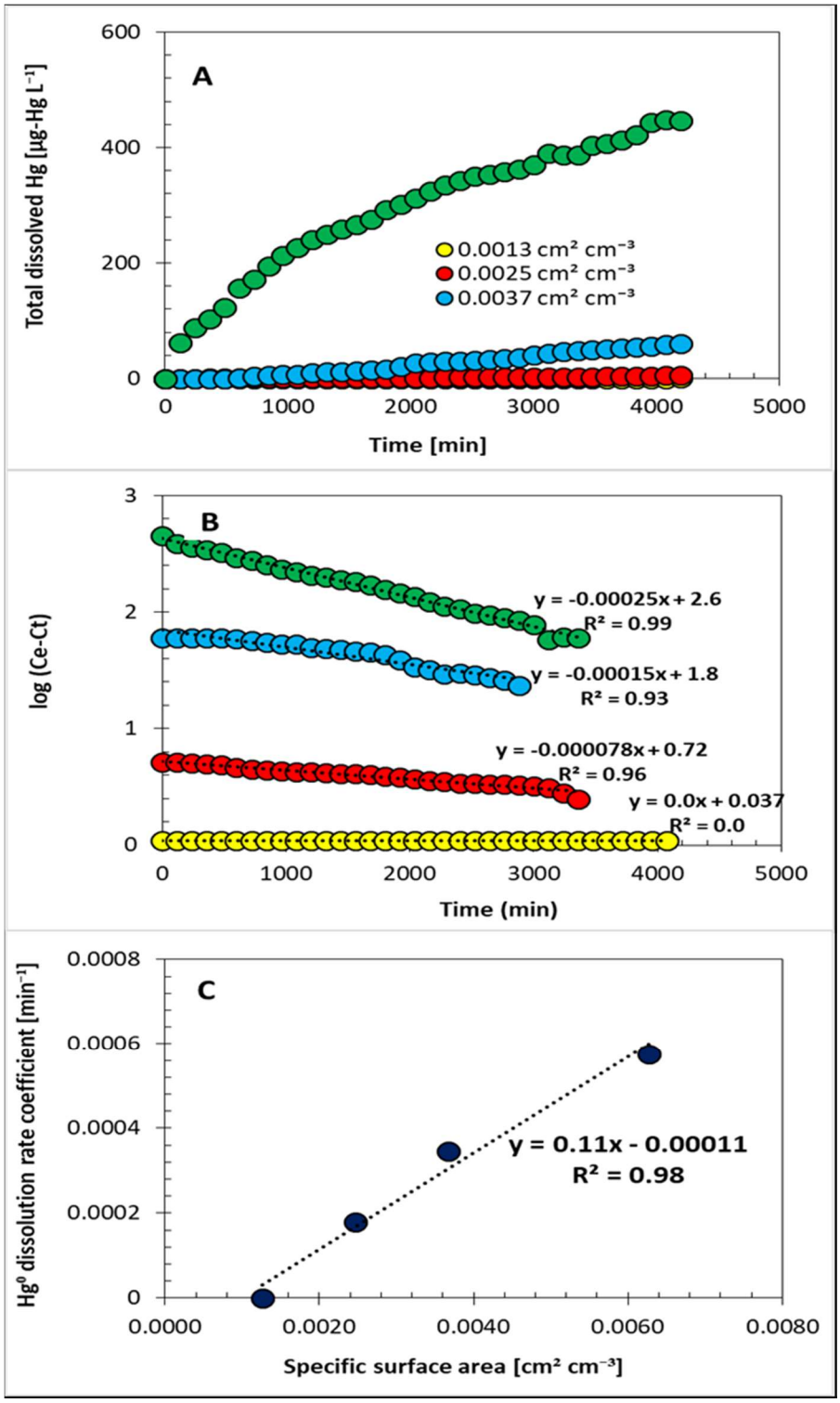

Fig. 2.4: (A) Effect of Hg droplet specific surface area on Hg_T concentration. (B) Noyes-Whitney first order dissolution model. (C) Effect of droplet specific surface area on the dissolution rate coefficient. (pH 7; shaking rate: 120 rpm; contact time: 4200 min).

When the experimental data was fitted on the Noyes-Whitney first order dissolution model (Fig. 2.4B), good linearization of experimental data was observed (R^2: 0.93 – 0.99) for the 0.37 to 0.94 cm^2 droplets (specific surface area: 0.0025 to 0.0063 cm^2 cm^{-3}). Since the Hg_T for the 0.0013 cm^2 cm^{-3} droplet was below the method limit of detection for most of the experiment, poor linearization of experimental data was observed ($R^2 = 0$). However, for the : 0.0025 to 0.0063 cm^2 cm^{-3} droplets, the predicted equilibrium Hg_T (5.3 – 398.1 µg-Hg L^{-1}) was close to the experimental data (5.2 – 447.9 µg-Hg L^{-1}).

An increase in the Hg^0 droplet specific surface area resulted in a rapid dissolution. When the droplet specific surface area was increased from 0.0025 to 0.0063 cm^2 cm^{-3}, the dissolution rate coefficient tripled (0.00018 to 0.00058 min^{-1}). This was expected since Hg^0 oxidation is faster in the presence of a larger droplet (Amyot et al., 2005). A linear relationship was observed between the dissolution rate coefficient and the droplet surface area (Fig. 2.4C).

2.6.4 Effect of Fe^{3+} concentration

The Hg_T increased with increase in Fe^{3+} concentration, however, insignificant (Fig. 2.5A). When the experimental data was fitted on the Noyes-Whitney first order dissolution model, a good correlation (R^2: 0.99 – 1.0) between experimental data was observed for all three Fe^{3+} concentrations investigated (Fig. 2.5B). Also, the model predicted equilibrium Hg_T (737.2 – 1382.3 µg-Hg L^{-1}) was close to the experimental data (734.2 µg-Hg L^{-1} – 1281.3 µg-Hg L^{-1}).
The Hg^0 dissolution rate coefficient increased from 0.00094 to 0.0013 min^{-1} upon addition of 1.0 mg-Fe^{3+} L^{-1} to the experimental solution (Fig. 2.5C). It was assumed that Fe^{3+} behaved as an oxidizing agent and facilitated the oxidative-dissolution of Hg^0.

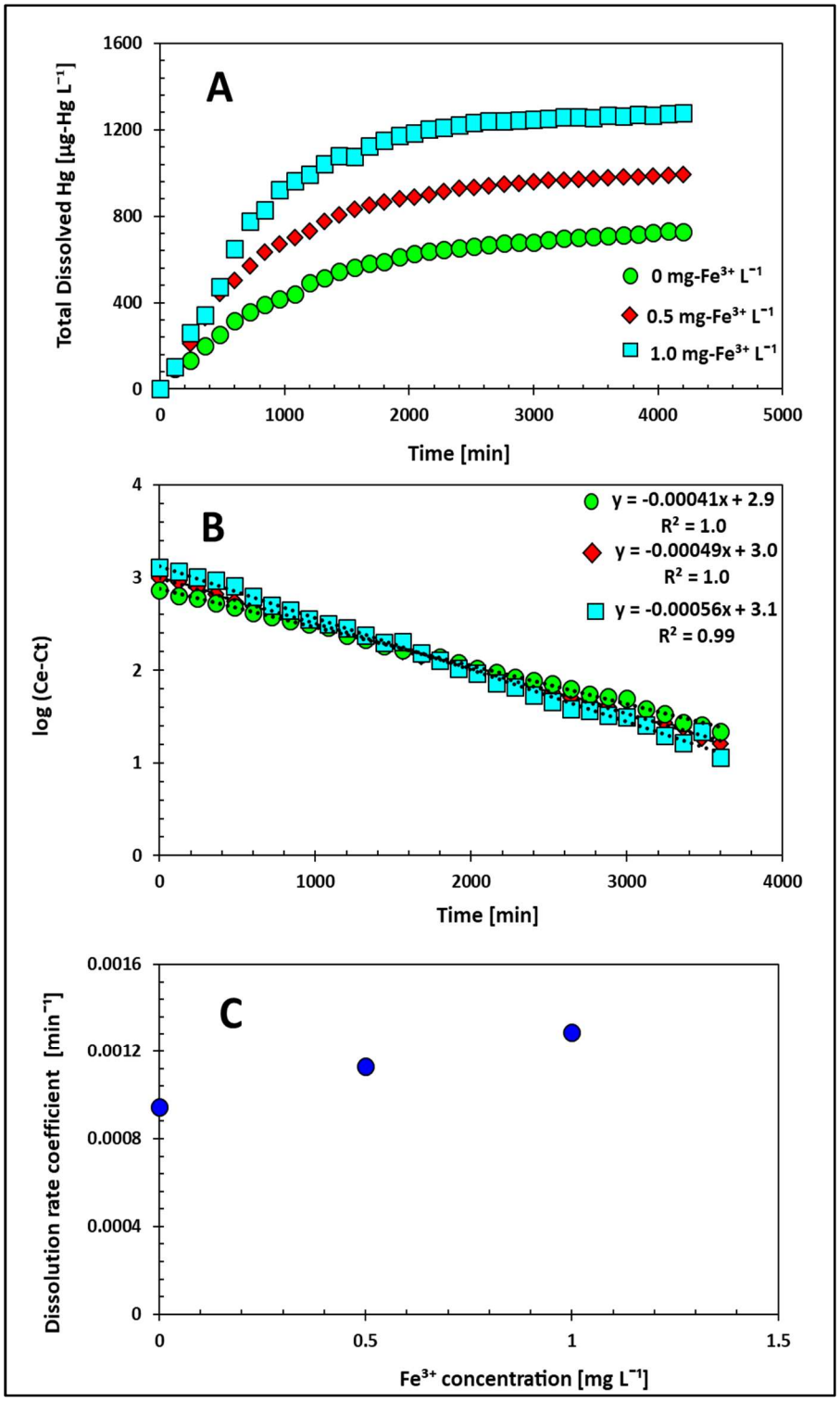

Fig. 2.5: (A) Effect of Fe^{3+} concentration on Hg_T concentration. (B) Noyes-Whitney first order dissolution model. (C) Effect of Fe^{3+} concentration on the Hg^0 dissolution rate coefficient. (pH 3; shaking rate: 120 rpm; contact time: 4200 min; Hg^0 droplet surface area: 0.94 cm^2).

2.6.5 Effect of agitation rate type and rate

As the frequency of shaking or magnetic stirring increased, the Hg_T increased (Fig. 2.6A). Good linearity (R^2: 0.76 – 0.99) was observed when the experimental data was fitted on the Noyes-Whitney dissolution model (Fig. 2.6 B). Also the predicted equilibrium Hg_T (2.5 – 398.1 µg-Hg L^{-1}) were close to the experimental data (2.3 – 447.9 µg-Hg L^{-1}).

The observed rate of dissolution of Hg^0 increased with increase in the agitation frequency (Fig. 2.6C). This is a result of convective mass transfer. The higher the agitation rate, the faster the solute molecules are removed from the Hg^0 droplet surface and the unsaturated solvent molecules are quickly introduced compared to shaking or magnetic stirring at a lower speed. Thus, as the agitation rate is increased, the thickness of the diffusion layer decreases, resulting in a faster mass transfer or dissolution of Hg^0 (Dutta, 2007; Jones et al., 1999). Furthermore, the dissolution rate coefficient of 0.00058 min^{-1} observed during shaking at 120 rpm was four times more than that observed during magnetic stirring (0.00014 min^{-1}) at the same frequency.

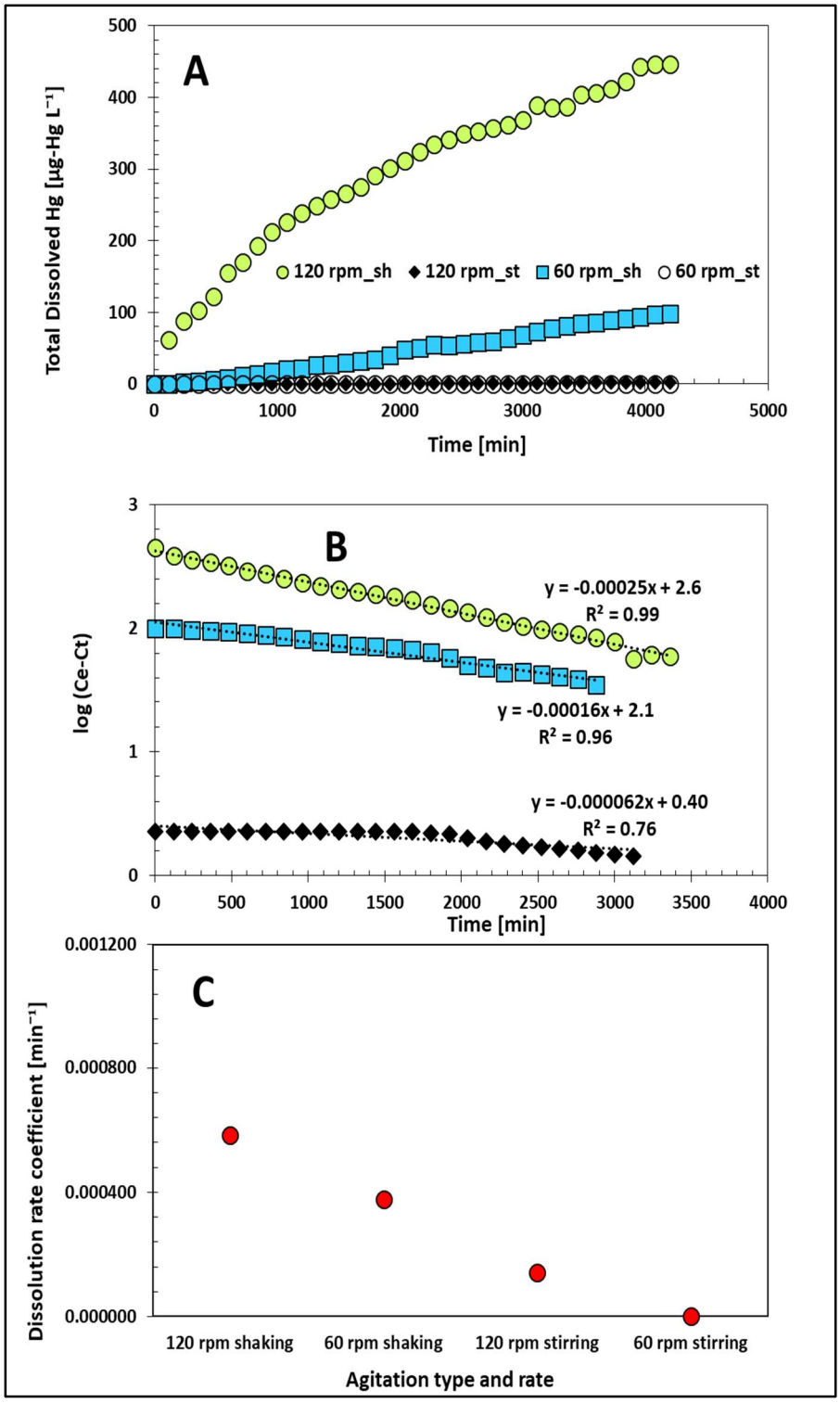

Fig. 2.6: (A) Effect of shaking and stirring on HgT concentration. (B) Noyes-Whitney first order dissolution model. (C) Effect of shaking and stirring on the Hg0 dissolution rate coefficient. (pH 7; contact time: 4200 min; Hg^0 droplet surface area: 0.94 cm2) †st -stirring and sh - shaking.

Based on the calculated Re for the two agitation scenarios (14382 and 3262 [-] for shaking and magnetic stirring respectively (Table 2.1)), the observed results can be attributed to the turbulent nature of the media during shaking which resulted in the disintegration of the Hg^0 droplet into smaller particles.

Table 2.1: Reynolds number at different agitation types and frequency

Agitation type and rate	Reynolds number
120 rpm shaking	14382
60 rpm shaking	7191
120 rpm stirring	3262
60 rpm stirring	1631

This resulted in an increase in the surface area available for contact between the water and Hg^0 molecules, hence, speeding up the dissolution of Hg^0. Thus, turbulent conditions result in faster Hg^0 dissolution compared to laminar flow (Fig. 2.7).

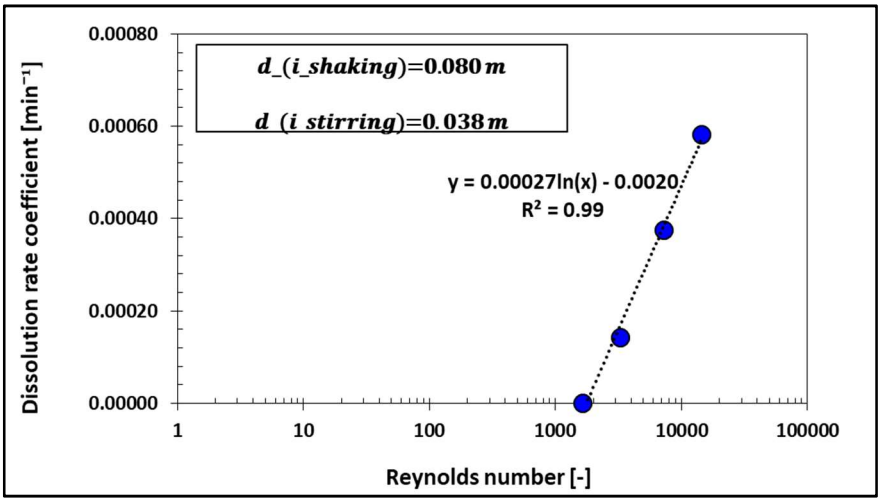

Fig. 2.7: Effect of Re on the Hg^0 dissolution rate coefficient.

Generally, the Hg^0 dissolution rate coefficients reported in this study were lower than that estimated by Amyot and colleagues (Amyot et al., 2005). This is mainly due to the high chlorides concentration they used in their study. Chlorides are known to accelerate the oxidation of Hg^0 in

aquatic systems (Amyot et al., 2005; Yamamoto, 1996). Consequently, Hg^0 dissolution is expected to be slow in freshwaters and rapid in high salinity waters.

2.7 Proposed Hg^0 first order dissolution rate coefficient model

From the experimental results, it was established that H_3O^+ concentration (Fig. 2.3C), Hg^0 droplet specific surface area (Fig. 2.4C) and Re (Fig. 2.7) have a significant effect on the Hg^0 oxidative first order dissolution rate coefficient. Thus, a multivariate model (Eq. 3.4) was proposed.

$$\hat{k} = \beta_o + \beta_1 \log[Re] + \beta_2 \log[H^+] + \beta_3[SSA] \quad (2.4)$$

Where;

$\hat{k}$ – is the predicted Hg^0 oxidative dissolution rate coefficient (min^{-1})

β_0 – is the intercept

$\beta_1, \beta_2 \; and \; \beta_3$ – are the model coefficients (-)

$[H_3O^+]$ – is the concentration of the hydronium ion (M)

Re – is the Reynolds number (-)

SSA – is the Hg^0 droplet specific surface area ($cm^2\ cm^{-3}$)

The following hypothesis were tested at the 5% significance level:

$$H_0: \beta_0, \beta_1, \beta_2, \beta_3 = 0 \quad (2.5)$$

$$H_1: \beta_0, \beta_1, \beta_2, \beta_3 \neq 0 \quad (2.6)$$

Where;

β_0 – is the intercept

$\beta_1, \beta_2 \; and \; \beta_3$ – are the model coefficients (-)

A good regression fit was obtained (Adjusted R^2 = 0.99). Also, the p-values of the model coefficients were less than 0.05 (Table 2.2), thus, the null hypothesis was rejected.

Table 2.2: ANOVA statistical analysis results

	df	*SS*	*MS*	*F*
Regression	3	1.7×10^{-6}	5.8×10^{-7}	496.8
Residual	17	1.9×10^{-8}	1.2×10^{-9}	
Total	20	1.7×10^{-6}		

	Coefficients	*Standard Error*	*t Stat*	*P-value*
Intercept	-2.5×10^{-3}	1.1×10^{-4}	-22.5	4.3×10^{-14}
log $[H_3O^+]$	7.9×10^{-5}	3.3×10^{-6}	24.1	1.4×10^{-14}
log Re	7.0×10^{-4}	2.5×10^{-5}	27.7	1.3×10^{-15}
SSA	0.12	4.5×10^{-3}	26.3	3.4×10^{-15}

The resulting Hg^0 first order oxidative dissolution model is given by Eq. 2.7:

$$\hat{k} = 7.9 \times 10^{-5}[\log H_3O^+] + 7.0 \times 10^{-4}\,[\log Re] + 0.12[SSA]\; - 2.5 \times 10^{-3} \qquad (2.7)$$

But;

$$pH = \; -\log[H_3O^+] \qquad (2.8)$$

Thus;

$$\hat{k} = -7.9 \times 10^{-5}[pH] + 7.0 \times 10^{-4}\,[\log Re] + 0.12[SSA]\; - 2.5 \times 10^{-3} \qquad (2.9)$$

2.7.1 Heteroscedasticity Test of error terms

From an eye observation of the plot of residuals (Fig. 2.8), the possibility of heteroscedasticity was suspected.

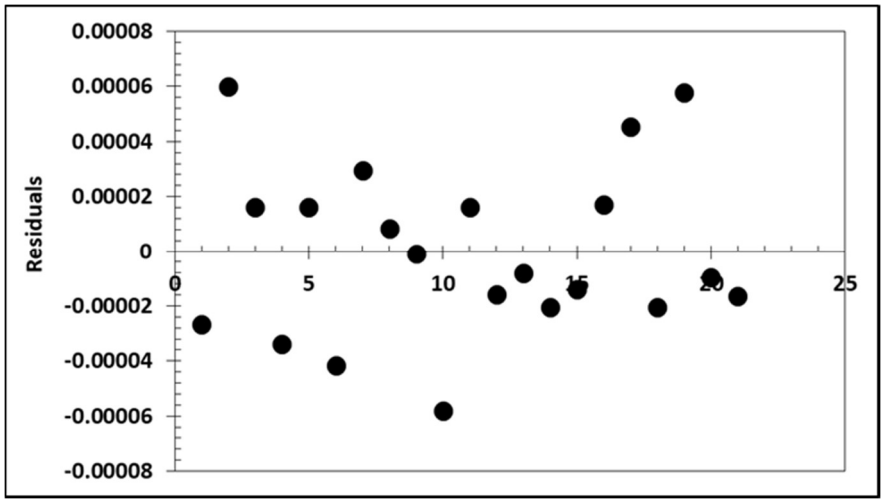

Fig. 2.8: Plot of the residuals.

Thus it was tested on the 5% significance level based on the following hypotheses:

$$H_0: the\ residuals\ are\ homoscedastic$$

$$H_1: the\ residuals\ are\ heteroscedastic$$

For both the Breusch-Pagan and White tests, the p-value is equal to 0.05, thus the null hypothesis cannot be rejected. Also, the observed LM is lower than the critical LM (χ^2), thus, the residuals are homoscedastic (Table 2.3).

Table 2.3: Heroscedasticity test results

Test method	**p-value**	**Degrees of freedom (df)**	**Observed LM**	**Critical LM (χ^2)**
Breusch-Pagan	0.05	3	4.4	7.8
White	0.05	8	14.6	15.5

2.7.2 Model evaluation

The predicted Hg^0 dissolution rate coefficients were very close to the experimental data (Fig. 2.8), as depicted by a high ME and coefficient of determination (R^2) of 0.99. In addition, the very low

RMSE (3.6×10^{-9}) signifies the closeness of the predicted data to the experimental data. Thus, the model is accurate and can be used for environmental purposes.

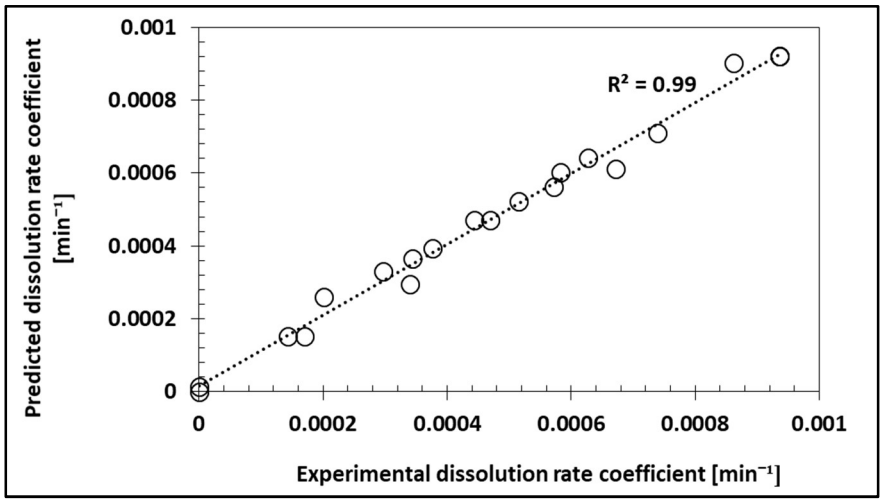

Fig.2.9: Comparison of observed and predicted data.

2.8 Parametric Sensitivity Analysis

Zimbabwe ranks amongst the top ten countries with the highest anthropogenic Hg emissions to the environment as a result of ASGM within its borders (Telmer and Veiga, 2009). The Hg^0 demand by each milling/amalgamation center is estimated to be about 2 kg-Hg^0 per week (Lassen et al., 2016). Since the whole ore amalgamation (WOA) technique on copper plates is mainly used by these ASGMs (Gunson et al., 2006), we assume that 70% (Chouinard and Veiga, 2008) of the Hg^0 used in the amalgamation process is lost into nearby creeks, rivers and streams via tailings. Thus, the model predicted oxidative dissolution rate coefficient of an Hg^0 droplet with a specific surface area of 0.0015 cm^2 cm^{-3} discharged in tailings into a nearby creek with a Re of 37453 [-] and pH 7.0 is 0.00033 min^{-1}. Considering that most ASGMs work between 5.9 and 8.6 h per day (average: 7.3 h per day) and a minority of them labor between 8.7 and 14.3 h per day (average: 11.5 h per day) (PACT, 2015) for 38.6 weeks per year (Persaud and Telmer, 2015); it will take between 39 and 62 years for such a droplet to dissolve when considering Hg^0 losses based on average minimum and maximum labor hours. Therefore, there is need to pay continuous attention to Hg environmental risk even after ASGM is banned.

Since this model was developed under ideal experimental conditions, it should be noted that in a natural freshwater system, several factors such as complexation with humic substances and entrapment in the sediments amongst others; are likely to affect the dissolution of Hg^0. Thus, the dissolution process can occur in a way not expected or rather predicted by the ideal experimental conditions.

The sensitivity of the Hg^0 dissolution rate coefficient model parameters to changes in operational conditions was tested using arbitrary values of pH, Re and Hg^0 droplet surface area. The pH and Re were varied from 3.0 to 8.5 [-] and 13 000 to 95 000 [-] respectively. An Hg^0 droplet specific surface area range of 0.00084 to 0.03 cm^2 cm^{-3} was used. The above-mentioned creek boundary conditions were used as the reference values (reference dissolution rate coefficient: 0.00033 min^{-1}). Simulation results revealed that this dissolution model is sensitive to changes in Hg^0 droplet surface area and the Re (Fig. 2.10).

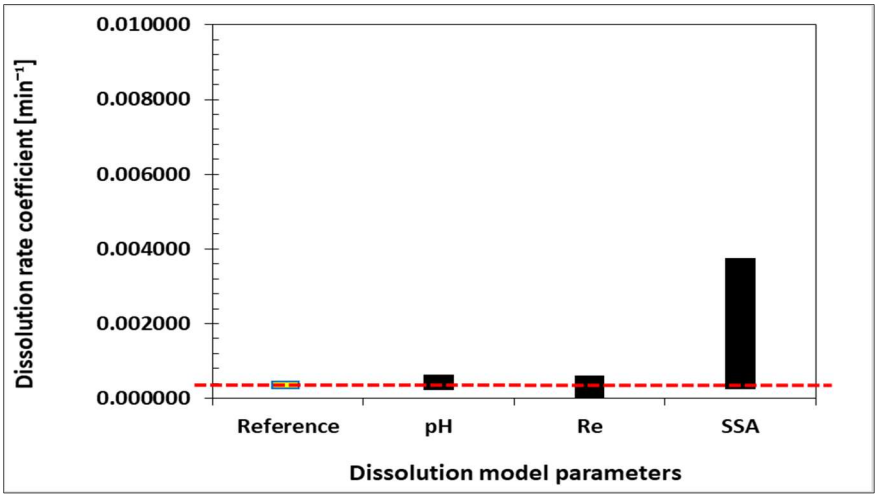

Fig.2.10: Sensitivity Analysis of Hg^0-dissolution model parameters

Fluctuations in the Hg^0 droplet specific surface area and Re resulted in one and two orders of magnitude range difference respectively; in the predicted dissolution rate coefficient. Changes in the media pH did not result in any order of magnitude range difference in the simulated dissolution rate coefficient (0.00021 – 0.00064 min^{-1}).

2.9 Conclusions

This study investigated the dissolution rate coefficient of Hg^0 in low salinity waters. The effect of Hg^0 droplet surface area, solution pH and Reynolds number was tested. Generally, the observed dissolution of Hg^0 was very slow. A relatively faster dissolution (0.00094 min^{-1}) occurred when a large Hg^0 droplet specific surface area (0.0063 cm^2 cm^{-3}) was placed in turbulent waters (Re = 14382) which were acidic (pH 3). However, despite the abundance of Fe^{3+} in most gold mine ores and acid mine drainage waters, its presence in the experimental solution did not result in any significant increase in the Hg^0 dissolution rate coefficient (0.00094 and 0.0013 min^{-1} for 0 and 1.0 mg-Fe^{3+} L^{-1} respectively). Based on these experimental results, a model for the oxidative dissolution of Hg^0 in freshwaters was proposed:

$$\hat{k} = -7.9 \times 10^{-5}[pH] + 7.0 \times 10^{-4}\,[\log Re] + 0.12[SSA]\ - 2.5 \times 10^{-3}$$

This model will serve as a simple but cost-effective tool for estimating the dissolution rate of Hg^0 in freshwaters. Due to the observed slow dissolution of Hg^0, we recommend that the Hg^0 dissolution rate coefficient be incorporated in model simulations for more accuracy and reliability. This is the only study that has proposed a model for the reactive dissolution of Hg^0 in freshwaters. The parametric sensitivity analysis revealed that the Hg^0 droplet surface area and Re have a significant impact on the simulated dissolution rate coefficient.

Owing to the abundance of humic substances in aquatic ecosystems, their strong interactions with Hg, and their ability to influence several aspects of its biogeochemical cycle such as solubility (Meech et al., 1998; Melamed et al., 2000; Ravichandran, 2004b; Tromans et al., 1996), further studies on their effect on the Hg^0 dissolution rate are currently underway.

Chapter Three

Effect of fulvic acid on the dissolution rate of elemental mercury in freshwaters

Based on the same concepts described in Chapter 2, the effect of humic substances on the Hg^0 dissolution rate coefficient was tested using commercially available Suwannee River fulvic acid (SRFA). The effects of pH, ionic strength and SRFA concentration were investigated under dark conditions. The dissolution tests results are given with an extensive discussion on their environmental implications.

3.0 Introduction

Based on the methodology described in **Chapter 2**, the effect of humic substances on the Hg^0 dissolution rate coefficient was investigated. Since dissolved fulvic acids (FA) are more abundant in the freshwater column than dissolved humic acid (Hessen and Tranvik, 1998; MacCarthy and Suffet, 1988; Tipping, 2002); the effect of humic substances Hg^0 dissolution rate coefficient was investigated using commercially available Suwannee River fulvic acid (SRFA). Owing to the sensitivity of the HSs' configuration to medium pH and ionic strength (De Haan et al., 1987; Ghosh and Schinitzer, 1979), the specific objectives are to investigate how variations in pH and ionic strength (chloride concentration) influence the Hg^0 dissolution rate coefficient. In addition, the solubility of Hg^0 is highly dependent on the concentration of organic acids in aquatic systems (Meech et al., 1998; Tromans et al., 1996), thus the influence of FA concentration on the dissolution rate coefficient was also tested. The methodology and the experimental observations are detailed in the following sections.

3.1 Methodology

This section details the reagents used, methodology followed and machinery used for analysis.

3.1.1 Reagent preparation

All reagents used in this study were of analytical grade except for the standards used for machine calibration which were of high purity. Reagents for instrument calibration were prepared as described by Tshumah-Mutingwende and colleague (Tshumah-Mutingwende and Takahashi, 2019). However, in this study, bromium chloride (BrCl) was used as an oxidizing agent. This was prepared in a fume hood using reagent grade potassium bromate ($KBrO_3$) (Sigma-Aldrich, Germany), 30% hydrochloric acid (HCl) (Wako, Japan) and potassium bromide (KBr) (Wako, Japan); following the methodology described by the United States Environmental Protection Agency (United States Environmental Protection Agency, 2002). It is recommended to wear the proper protective clothing including safety goggles and a face mask.

Suwannee River Fulvic Acid (SRFA) purchased from the International Humic Substance Society (IHSS) (Catalogue No. 3S101F) was used for the dissolution tests. Based on the SRFA carbon (C) content of 53.3% (w/w) (IHSS, 2018); stock solutions of 100 mg-C L^{-1} were prepared in Milli-Q

water (18.2 MΩ cm (Millipore, USA)) adjusted to the desired pH. The stock solutions were stored in 100 mL volumetric flasks which were wrapped with aluminium foil to prevent exposure to laboratory and or natural light. The flasks were then placed on a shaker (Riken, Japan) set at 120 rpm for at least 24 h after which they were stored at 4ºC prior to use. Serial dilution to the desired concentrations was achieved by using Milli-Q water adjusted to the desired pH.

3.1.2 Experimental procedure

The overall experimental setup described by Tshumah-Mutingwende and colleague (Tshumah-Mutingwende and Takahashi, 2019) was adopted except for the Hg species measurement techniques. Briefly, 150 mL of dissolved SRFA solution at the desired pH and concentration was poured into a 250 mL Erlenmeyer flask into which an Hg^0 droplet with a specific surface area of 0.0063 cm^2 cm^{-3} was placed. To avoid exposure to direct sunlight, the flask was wrapped with aluminium foil and put in a cardboard box 'dark chamber' prior to placing it on a shaker (Riken, Japan) set at 120 rpm (Fig. 3.1).

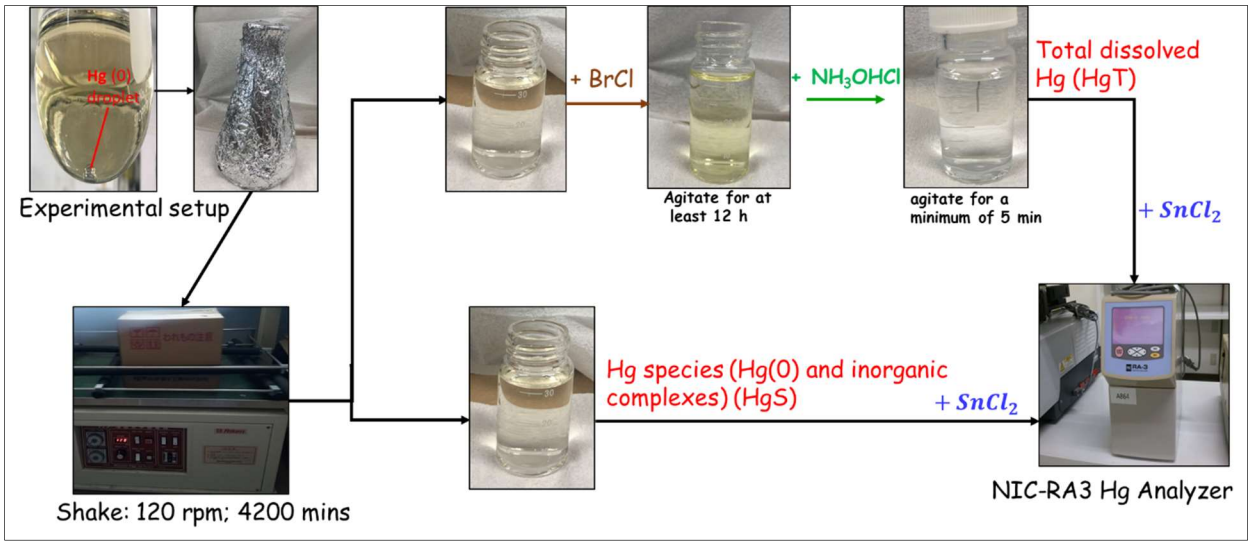

Fig. 3.1: Experimental procedure

Nitrile gloves were worn at all times during sample handling, preparation and analysis. All investigations were conducted in triplicates. Since the opening 'mouth' of the Erlenmeyer flask was first sealed with a parafilm followed by aluminium foil, the exit or entrance of gaseous mercury from / into the reaction vessel was assumed to be negligible. Proper precaution such as

storing Hg^0 in dark and tightly sealed containers away from any direct source of sunlight, heat and oxygen was taken in order to prevent its oxidation before the dissolution tests.

3.1.2.1 Effect of pH

The influence of pH on the Hg^0 dissolution rate and Hg-FA complex formation in FA-rich freshwaters was investigated at pH 3.0, 7.0, 8.0 and 10.0. The pH was adjusted using either 0.1 M nitric acid (HNO_3) or sodium hydroxide (NaOH) solution. The pH of most freshwaters is in the range of 6.5 to 8.5 (Behar, 1996); thus, pH 7.0 was chosen as the optimum pH and kept constant for all succeeding experiments. For all investigations, the solution pH was constantly checked and adjusted accordingly.

The average concentration of dissolved HSs in some of the clear surface waters of the United States of America (USA) is 2.2 mg-C L^{-1} (MacCarthy and Suffet, 1988). Since the ratio of FA: HA in natural waters is 9:1 (MacCarthy and Suffet, 1988); the dissolution tests for this and succeeding investigations were conducted at a FA concentration of 2.0 mg-C L^{-1} (typical FA concentration for freshwaters (Oriekhova and Stoll, 2016)); unless stated otherwise.

3.1.2.2 Effect of ionic strength

The average chloride concentration of freshwater rivers and streams is in the range of 0 - 2.8 mM (0 - 100 mg L^{-1} (Goldman and Horne, 1983)). Based on Lewis and Randall's definition of ionic strength (Lewis and Randall, 1921); this is equivalent to an ionic strength of 0 – 2.8 mM KCl. Therefore, the effect of ionic strength on the Hg^0 dissolution rate coefficient and Hg-FA complex formation was investigated at 0, 0.5, 1.5 and 3.0 mM KCl. Yamamoto observed that KCl accelerated the oxidation of Hg^0 to the same extent as NaCl (Yamamoto, 1996). Thus, since this study investigates the oxidative-dissolution of Hg^0 in freshwaters, the use of KCl has the same effect as NaCl. The FA concentration was kept constant at 2.0 mg-C L^{-1}. For comparison, dissolution tests in the absence of SRFA were conducted at the same ionic strength range (0 – 3.0 mM KCl). The solution pH and shaking rate were maintained at pH 7 and 120 rpm respectively.

3.1.2.3 Effect of FA concentration

Climate, changes in season, geographical location, size and productivity of the aquatic ecosystem, quantity and nature of pollutants discharged into an aquatic system are some of the principal factors influencing the concentration of dissolved HSs in that water body (Boggs et al., 1985; Thurman, 1985; Tipping, 2002). The concentration of dissolved organic carbon (DOC) (humic and non-humic compounds which can pass through a 0.45 μm filter (Pagano et al., 2014)) in the majority of the world's freshwater lakes, rivers and streams ranges from less than 0.5 to 100 mg-C L^{-1} with an average concentration of 5 mg-C L^{-1} (Thurman, 1985). Thus, assuming that on average; 65% (about 50% and 80 % of the total DOC in clear and colored surface waters respectively; accounts for dissolved HSs (MacCarthy and Suffet, 1988)) of the total DOC constitutes of HSs and 90% (MacCarthy and Suffet, 1988) of the dissolved HSs is FA; the effect of FA concentration on Hg^0 dissolution and Hg-FA complex formation was investigated for SRFA concentrations ranging from 0 to 30.0 mg-C L^{-1}.

3.1.3 Total dissolved Hg (Hg_T) and Hg-FA complex concentration (Hg_{OC}) determination

At pre-determined time intervals, two aliquots were collected from each experimental vessel and made up to 30 mL. This was stored in acid washed vials and one of the samples was oxidized using BrCl which also served as a preservative. About 150 μL of BrCl solution was added to the 30 mL sample (United States Environmental Protection Agency, 2002). The oxidized sample was agitated at 120 rpm for a minimum of 12 h. A permanent yellow colour was observed throughout the oxidation period. The excess BrCl solution was eliminated by adding 75 μL of 30% (w/v) ammonium hydroxyl chloride (NH_3OHCl) solution and agitating the samples for 5 min. Successful elimination of excess BrCl solution was indicated by the disappearance of the yellow colour (United States Environmental Protection Agency, 2002). The total dissolved Hg (Hg_T) and Hg-FA soluble organic complex concentration (Hg_{OC}) were determined using the methodology described by Melamed and colleagues (Melamed et al., 2000). That is, both the BrCl-oxidized and non-oxidized samples were reduced to volatile Hg^0 using 10% tin (II) chloride solution and analysed for Hg_T and concentration of Hg species (Hg_S) (Hg^0 and inorganic complexes) respectively; using the Reducing Vaporization Mercury Analyzer -RA3 (Nippon Instruments Corporation, Japan). Based on the mass balance theory, the Hg_{OC} concentration was determined as shown in Eq. (3.1):

$$Hg_{OC} = Hg_T - Hg_S \quad (3.1)$$

Where;

Hg_{OC} – is the soluble organic Hg-SRFA complex concentration [µg-Hg L^{-1}]

Hg_T – is the total dissolved Hg concentration [µg-Hg L^{-1}]

Hg_S – is the concentration of Hg species (Hg^0 and inorganic complexes) [µg-Hg L^{-1}]

3.1.4 Kinetic study

The Hg^0 first order dissolution rate coefficient was determined by fitting the Hg_T experimental data on the Noyes-Whitney first order dissolution model (Noyes and Whitney, 1897):

$$dC_t/dt = k_1(C_e - C_t) \quad (2.2)$$

Integrating between the boundary t = 0 to t; C_t= 0 to C_t yields:

$$log(C_e - C_t) = log\, C_e - (k_1 t/2.303) \quad (2.3)$$

The Hg^0 first order dissolution rate coefficient (k_1 [min^{-1}]) and the equilibrium Hg_T concentration (C_e [µg-Hg L^{-1}]) were determined from the intercept and gradient respectively

Where;

C_e – is the equilibrium or saturated total dissolved Hg concentration (µg-Hg L^{-1})

C_t - is the total dissolved mercury concentration at time t, (µg-Hg L^{-1})

k_1 - is the Hg^0 first order dissolution rate coefficient (min^{-1})

t- is the time (min)

3.2 Results and Discussions

This section reports and discusses the experimental observations which are then used to develop a multivariate Hg^0 first-order dissolution model.

3.2.1 Effect of pH

Compared Hg_T concentration results from our previous study (734.2 - 124.6 μg-Hg L^{-1}) for pH 3 to 10 (Tshumah-Mutingwende and Takahashi, 2019); the presence of SRFA in the experimental solutions enhanced the solubility of Hg^0 throughout the chosen pH spectrum (pH 3-10). An increase in pH from pH 3 to 10 resulted in a decrease in the Hg_T concentration from 1256.8 to 301.4 μg-Hg L^{-1} (Fig. 3.2A); thus, irrespective of the presence or absence of SRFA, acidic conditions favor the solubility of Hg^0.

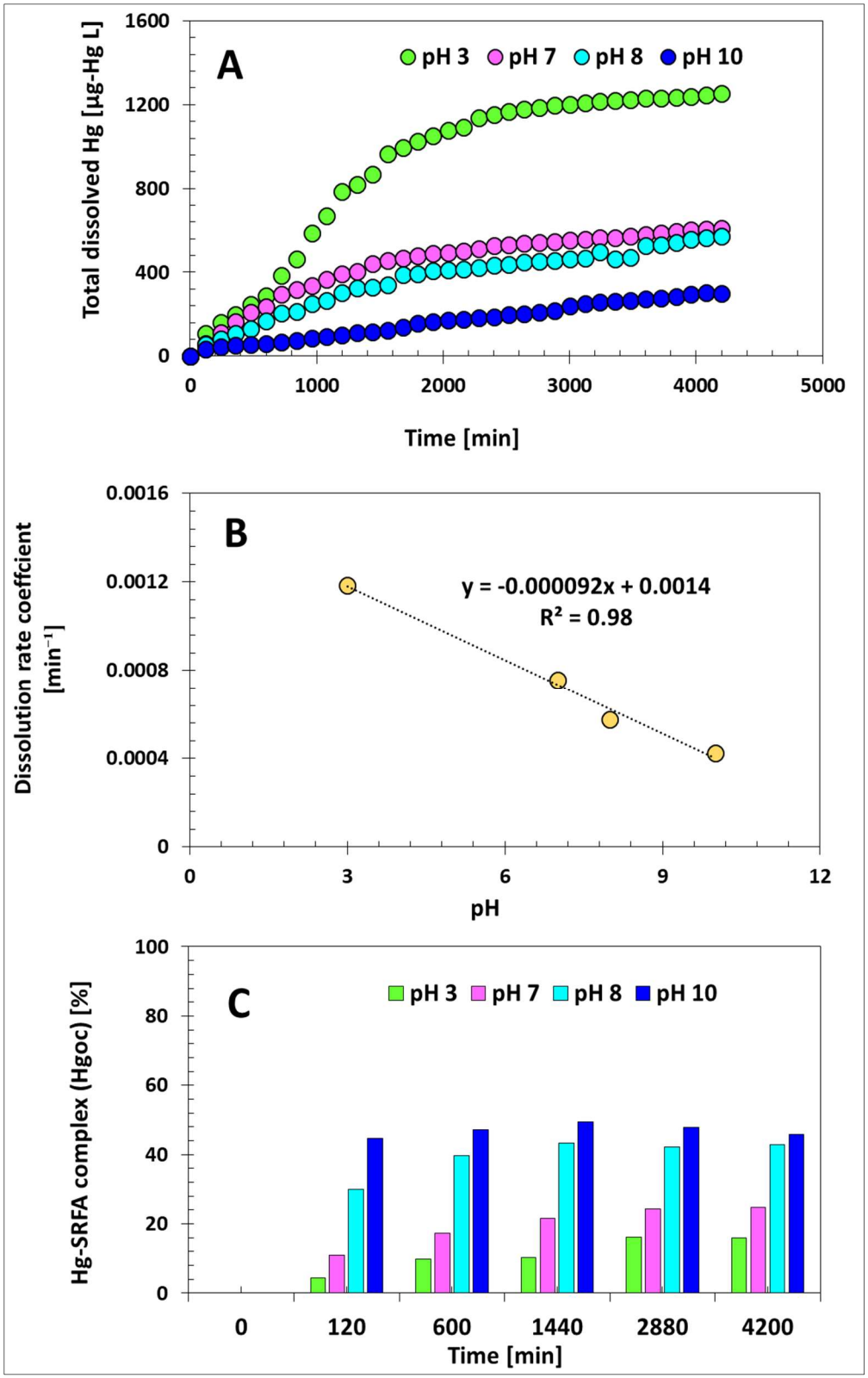

Fig. 3.2: (A) Effect of pH on the Hg_T concentration. (B) Effect of pH on the Hg^0 dissolution rate coefficient. (C) Effect of pH on Hg_{OC} concentration.

The observed trend of high Hg_T concentration in acidic compared to alkaline conditions was similar to that observed by Melamed and colleagues, however, they used humic acid in their Hg^0 solubility investigation (Melamed et al., 2000).

Good linearization (0.98-0.99) was obtained for all pH investigations when the experimental data was fitted on the Noyes-Whitney first order dissolution model (Fig. S3.2) (in Appendix A). Also, the model projected C_e (571.6 - 311.8 µg-Hg L^{-1}) was close to the experimental data (614.5 - 301.4 µg-Hg L^{-1}) for pH 7-10. However, at pH 3, the difference between the simulated C_e (1800.7 µg-Hg L^{-1}) and observed C_e (1256.8 µg-Hg L^{-1}) was significant. This can be due to the reduction of Hg^{2+} to volatile Hg^0 (under dark conditions, this is possible at high Hg_T concentrations and low pH (Chakraborty and Vudamala, 2015)) by electron-donating semi-quinone moieties present in SRFA (Alberts et al., 1974). Thus, the produced Hg^0 is likely to accumulate in the reaction vessel headspace before finally escaping during sample collection when the reaction vessel is opened. Therefore, it is expected that in low pH freshwaters such as Ngwabalozi River, Zimbabwe (pH: 3; Hg_T: 310 µg-Hg L^{-1}) (Mudyazhezha and Kanhukamwe, 2014), the interaction of HSs with Hg^0 will not only enhance its solubility but will also promote the evasion of $Hg^0_{(g)}$ into the atmosphere as a result of HSs-mediated Hg^{2+} reduction. Fig. 3.2 B illustrates the effect of pH on the Hg^0 dissolution rate coefficient. Acidic conditions (pH 3) resulted in a faster dissolution rate (0.0012 min^{-1}) compared to neutral and alkaline conditions; were the dissolution rate was in the range of 0.00076-0.00042 min^{-1} for pH 7-10. In the absence of SRFA, the Hg^0 dissolution rate coefficient was in the range of 0.00094 – 0.00034 min^{-1} for pH 3-10 (Tshumah-Mutingwende and Takahashi, 2019); thus the presence of SRFA resulted in a faster Hg^0 dissolution. A linear relationship was observed between increase in pH and the Hg^0 dissolution rate coefficient. The Hg_{OC} concentration gradually increased with increase in pH (Fig. 3.2 C). For example, after 120 min, 4.4% and 44.7% of the Hg_T present in solution is Hg_{OC} at pH 3 and 10 respectively. This can be attributed to the increase in negative charge of the HSs' surface under alkaline conditions. Thus, strong covalent bonds between Hg^{2+} and the oxygen atoms of the carboxylic and phenolic groups are formed. However, under acidic conditions, the Hg_{OC} concentration is lower due to the abundance of H^+ and Hg^{2+} ions, hence, competition for active sites between these two cations (Boggs et al., 1985; Kinniburgh et al., 1998; Klucakova et al., 2000; Melamed et al., 2000). In addition, since SRFA-mediated reduction of Hg^{2+} to Hg^0 is likely to occur in low pH waters, this will result in a reduced

concentration of Hg^{2+} available for complexing with SRFA, hence, the observed low Hg_{OC} concentration (Chakraborty and Vudamala, 2015).

Consequently, the low Hg_{OC} concentration in acidic waters results in a large pool of Hg^{2+} available for microbial methylation (Ravichandran, 2004a); whereas, the high concentration of Hg_{OC} in alkaline waters makes microbial methylation unfavorable due to decreased Hg^{2+} concentration. Thus, the MeHg concentration in fish tissue from low pH aquatic systems rich in dissolved HSs is likely to be higher compared to those fetched from high pH waters with almost the same concentrations of dissolved HSs (Kelly, 2003). Though microbial methylation of Hg_{OC} has not yet been fully understood, Hg_{OC} can be adsorbed on colloidal organic matter which serves as a substrate for methylating bacteria (Meech et al., 1998; Veiga and Baker, 2004). The observed constant to slight decrease in the Hg_{OC} concentration is most likely to be due to the exhaustion of active sites available on the SRFA molecule for complexation with Hg^{2+}. However, further investigations are necessary in order to elaborate on this finding.

3.2.2 Effect of ionic strength

When Hg^0 dissolution investigations were conducted in solutions with an ionic strength of 0 – 3.0 mM KCl in the absence of SRFA; no significant increase in the Hg_T concentration and Hg^0 first-order dissolution rate coefficient was observed. Amyot and colleagues (Amyot et al., 2005) observed a similar trend for Hg_T concentration when the dissolution tests were conducted under freshwater chloride concentrations. However, a comparison of the different ionic strength subsets showed that the Hg_T (447.9 – 474.7 µg-Hg L^{-1}) (Fig. 3.3 A) increased with increase in ionic strength from 0 – 3.0 mM KCl. Good regression coefficients (R^2: 0.98 – 0.99) (Fig. 3.3 B) were obtained when the experimental data from each subset was fitted on the Noyes-Whitney first order dissolution model. The simulated Ce (427.0 – 461.9 µg-Hg L^{-1}) were close to the experimental values (447.9 - 474.7 µg-Hg L^{-1}). Increasing the ionic strength also facilitated the rapid dissolution of Hg^0, thus, first-order dissolution rate coefficients of 0.00058 - 0.00065 min^{-1} where observed when the ionic strength was increased from 0 -3.0 mM KCl (Fig. 3.3 C). The observed high Hg_T and rapid Hg^0 dissolution as ionic strength increased can be attributed to the oxidizing ability of chlorides thus promoting Hg^0 dissolution (Amyot et al., 2005; Yamamoto, 1996).

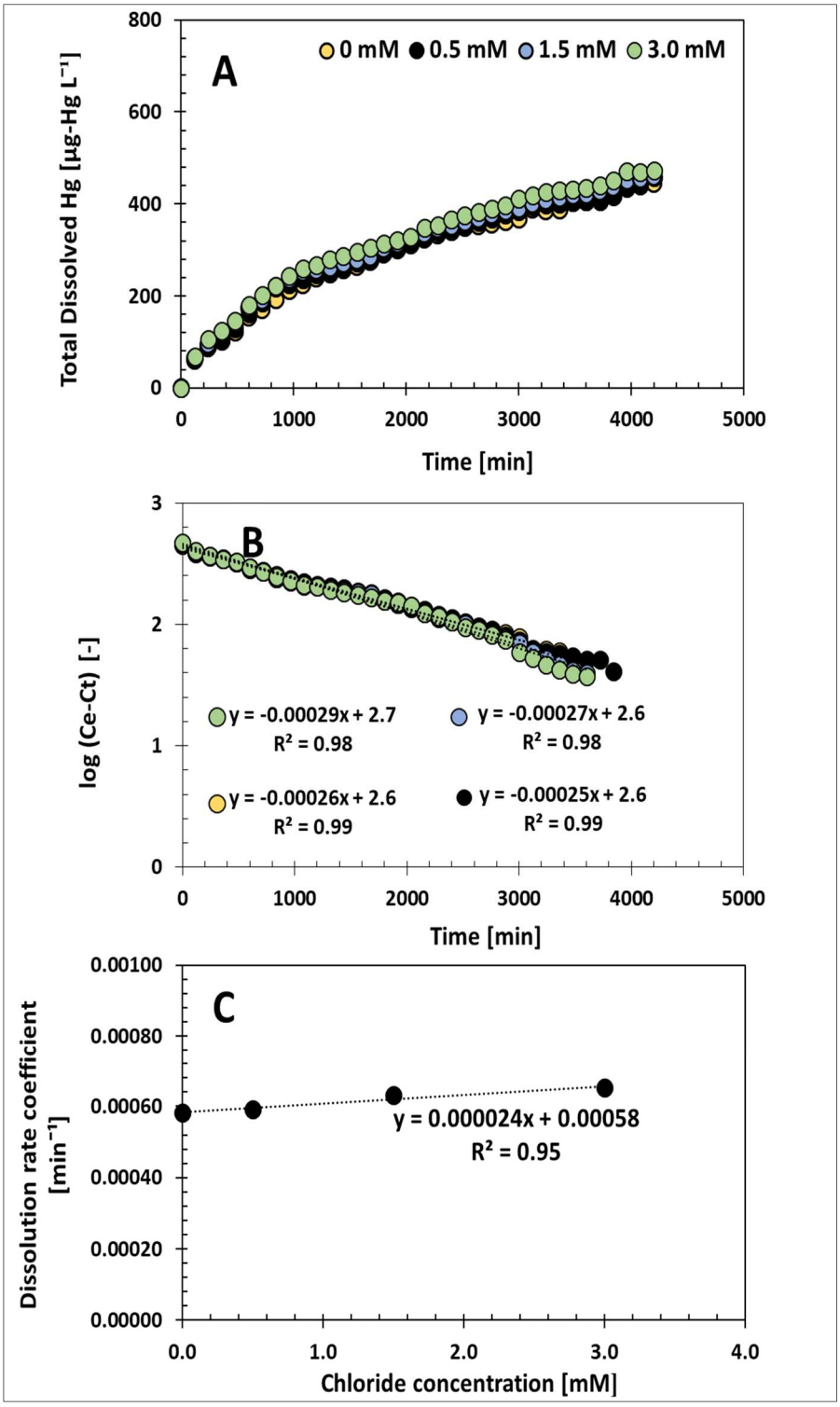

Fig. 3.3: (A) Effect of ionic strength on the Hg_T concentration. (B) Noyes-Whitney dissolution model. (C) Effect of ionic strength on the Hg^0 dissolution rate coefficient.

A comparison of the dissolution results of this study and those obtained by Amyot and colleagues (Amyot et al., 2005), reveal that Hg^0 dissolution is stimulated by Cl^- addition. This is a result of the accelerated oxidation of Hg^0 to Hg^{2+} due to a shift in equilibrium between Hg^0 and dissolved Hg^{2+} caused by the formation of a stable Cl^-—Hg^{2+} complex (Fig 3.4) at high Cl^- concentrations. As the concentration of Cl^- increases in the solution, Hg^{2+} forms $HgCl^+$, $HgCl_2$, $HgCl^{3-}$ and $HgCl_4^{2-}$ complexes. But, the Cl^- concentration of freshwaters (0 – 3.0 mM) is too low to form such stable Cl^-—Hg^{2+} complexes ($Hg(OH)_2$ or $HgCl_2$ molecules predominate in most fresh waters with a low Cl^- level); hence, there was no significant difference in the observed Hg^0 dissolution rate coefficients in the presence and absence of Cl^- (0 -3.0 mM KCl) (Fig. 3.3 C). The dissolved Hg^{2+} in freshwaters is likely to be reduced to Hg^0 and diffuse into the atmosphere (Yamamoto, 1996).

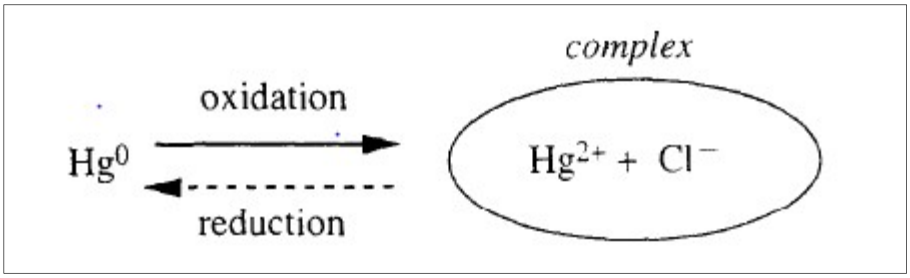

Fig. 3.4: A hypothetical scheme of Hg^0 oxidation in the presence of Cl^- in aqueous solution.
Source: (Yamamoto, 1996)

When the same experiment was repeated in 2 mg-C L^{-1} SRFA solution with a similar ionic strength (0 – 3.0 mM KCl) range, the Hg_T concentration decreased from 614.5 µg-Hg L^{-1} to 600.5 µg-Hg L^{-1} (Fig. 3.5 A).

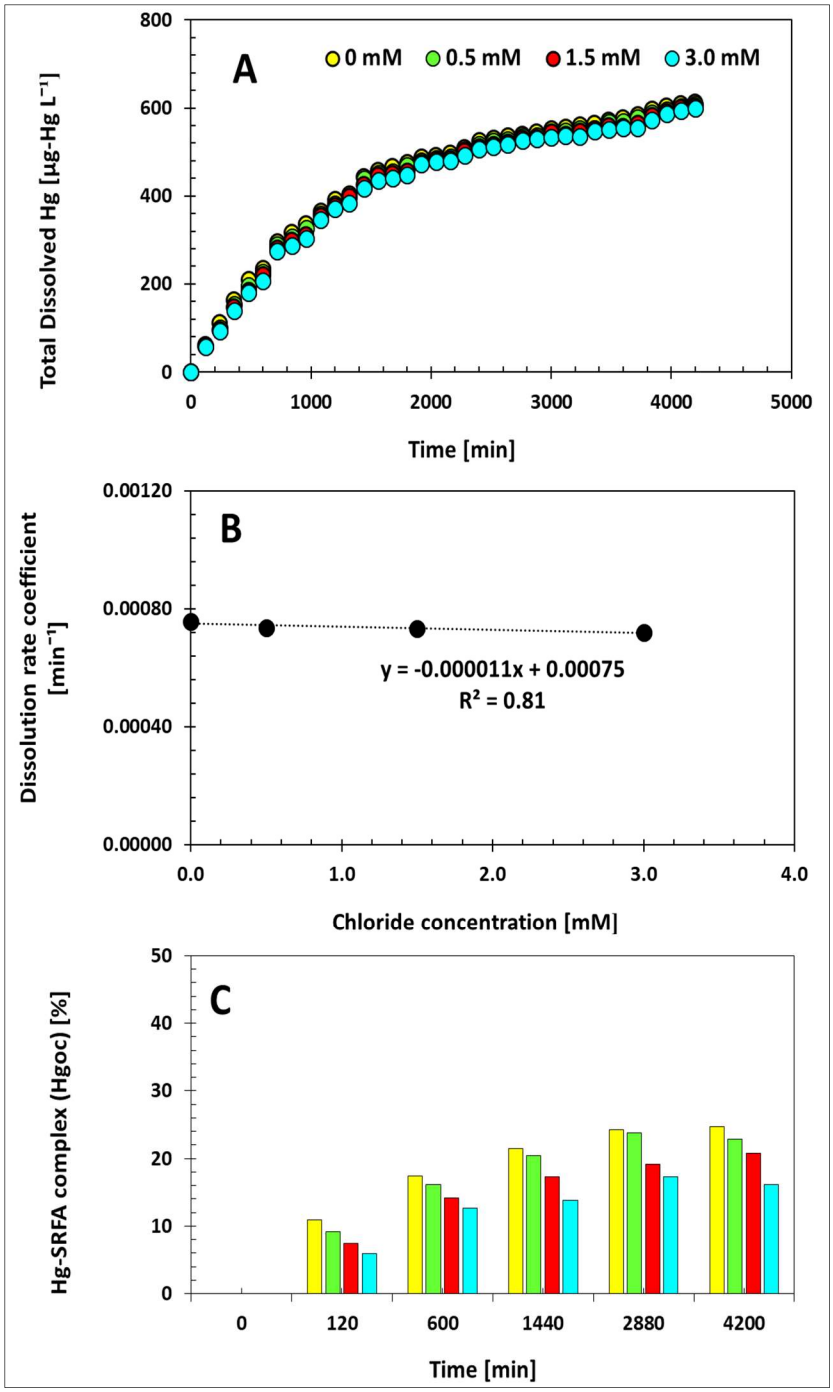

Fig. 3.5: (A) Effect of ionic strength on the Hg_T concentration. (B) Effect of ionic strength on the Hg^0 dissolution rate coefficient. (C) Effect of ionic strength on Hg_{OC} concentration.

Good linearity (R^2: 0.99) was obtained when the Hg_T concentration data was fitted on the Noyes-Whitney first-order dissolution model (Fig. S3.5) (in Appendix A). For each set, no significant difference between the model simulated C_e (571.6 – 564.9 µg-Hg L^{-1}) and the experimental value

(614.5 – 600.5 µg-Hg L^{-1}) was observed for the chosen ionic strength range. The Hg^0 first-order dissolution rate coefficient decreased with increase in ionic strength (Fig. 3.5 B). It varied from 0.00076 min^{-1} to 0.00072 min^{-1} when the ionic strength was increased from 0 – 3.0 mM KCl. A linear relationship was observed between increase in ionic strength and the Hg^0 dissolution rate coefficient. An increase in ionic strength resulted in a decrease in the Hg_{OC} concentration. A maximum of 24.7% and 17.3% of the total Hg species in solution were in the form of Hg_{OC} at 0 and 3.0 mM KCl concentrations respectively (Fig. 3.5 C). This can be attributed to several factors such as: (i) change in configuration of the SRFA molecules with increase in ionic strength. That is, as ionic strength increases, the SRFA molecules are likely to exist as tight, globular-shaped spherical colloids with most of the active sites hidden within the sphere and unavailable for cations in solution; whereas, at low ionic strength, they are likely to be flexible, linear and loose with most of the active sites exposed and accessible for complexation with cations (Akkanen, 2002; Stevenson and Cole, 1999); (ii) decreased stability of the Hg-SRFA complex as a result of increased competition for active sites between the Hg^{2+} and K^+ cations (Boggs et al., 1985; Stevenson and Cole, 1999); (iii) the possible interaction and complexation of Hg^{2+} with Cl^- will diminish the concentration of Hg^{2+} available for the formation of Hg_{OC} and (iv) decreased solubility of SRFA as the ionic strength increases (Pagano et al., 2014) can have a negative impact on the ability of SRFA to complex with Hg^{2+} in solution.

3.2.3 Effect of SRFA concentration

The observed Hg_T concentration was directly proportional to the SRFA concentration. An increase in SRFA concentration from 2 mg-C L^{-1} (Hg_T: 614.5 µg-Hg L^{-1}) to 30 mg-C L^{-1} (Hg_T: 3625.1 µg-Hg L^{-1}) resulted in almost a six-fold increase in the Hg_T concentration (Fig. 3.6 A).

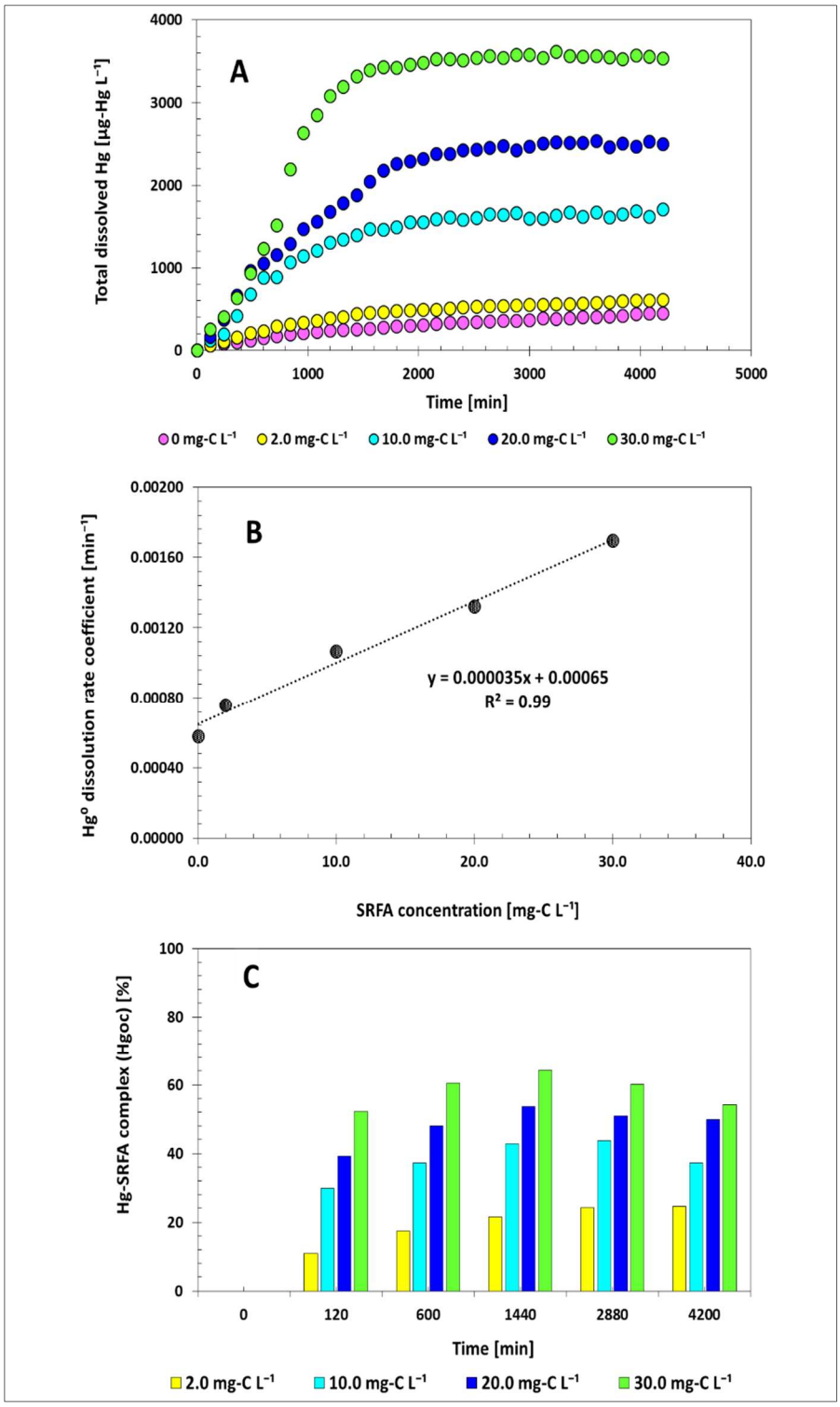

Fig. 3.6: (A) Effect of SRFA concentration on the Hg_T concentration (B) Effect of SRFA concentration on the Hg^0 dissolution rate coefficient. (C) Effect of SRFA concentration on Hg_{OC} concentration.

Good linearity (R^2: 0.95-0.99) was obtained when the Hg_T concentration data was fitted on the Noyes-Whitney first order dissolution model (Fig. S3.6) (in Appendix A). In addition, the model predicted C_e of 571.6 - 4673.8 µg-Hg L^{-1} was close to the experimental data 628.5 – 3625.1 µg-Hg L^{-1} for the chosen SRFA concentration range. Furthermore, increasing the SRFA concentration resulted in a faster dissolution. Thus, the Hg^0 dissolution rate coefficient increased from 0.00058 to 0.0017 min^{-1} when the SRFA concentration was increased from 0 to 30 mg-C L^{-1} (Fig. 3.6 B). A linear relationship was observed between increase in SRFA concentration and the Hg^0 dissolution rate coefficient. The availability of binding sites for complexation is proportional to the concentration of humic substances in solution (Schnitzer and Kerndorff, 1981). Thus, an increase in the SRFA concentration resulted in a high Hg_{OC} concentration due to the increase in the concentration of binding sites available for Hg-SRFA complex formation. A maximum of 67.2% of the total Hg species in solution was present as Hg_{OC} for a 30 mg-C L^{-1} solution compared to 24.7% for a 2 mg-C L^{-1} solution (Fig. 3.6 C). However, in aquatic ecosystems such as lakes, the increased Hg_{OC} concentration is a cause for concern since these soluble Hg complexes are highly mobile, and have the potential to be adsorbed on colloidal organic matter which serves as a substrate for methylating bacteria (Meech et al., 1998; Veiga and Baker, 2004). The constant and or gradual decrease in Hg_{OC} concentration can be due to the depletion of active sites available for Hg^{2+} and SRFA complexation.

3.3 Proposed Hg^0 dissolution rate coefficient model

Based on the dissolution tests findings (Fig. 3.2B, 3.4B, 3.5B and 3.6B), a multivariate Hg^0 dissolution model (Eq. (3.4)) was proposed:

$$\hat{k} = \beta_0 + \beta_1[pH] + \beta_2[Cl^-] + \beta_3[SRFA] \qquad (3.2)$$

Where;

$\hat{k}$ – is the predicted Hg^0 dissolution rate coefficient [min^{-1}]

β_0 – is the intercept [-]

$\beta_1, \beta_2 \; and \; \beta_3$ – are the model coefficients [-]

pH – solution pH [-]

Cl^- - ionic strength (expressed as concentration of KCl [mM]) [mM]

SRFA – Suwannee river fulvic acid concentration [mg-C L^{-1}]

The following hypothesis were tested at the 5% significance level:

$$H_0: \beta_0, \beta_1, \beta_2, \beta_3 = 0 \quad (3.3)$$

$$H_1: \beta_0, \beta_1, \beta_2, \beta_3 \neq 0 \quad (3.4)$$

Where;

β_0 – is the intercept

$\beta_1, \beta_2 \; and \; \beta_3$ – are the model coefficients (-)

The model coefficients were optimized using ANOVA statistical analysis on Microsoft Excel. The first optimization Table S2 (Appendix A) revealed that; at the 95% confidence level, $[Cl^-]$ is not significant since its p-value of 0.99 is far greater than 0.05. Hence, the regression was repeated without the $[Cl^-]$ data and the following multivariate model was obtained:

$$\hat{k} = 1.4 \times 10^{-3} - 1.1 \times 10^{-4}[pH] + 3.5 \times 10^{-5}[SRFA] \quad (3.5)$$

The model adjusted R^2 of 0.99 implies that the regression is a good fit. Also, as shown in Table 3.1, the p-values of the model coefficients were less than 0.05, thus, H_0 was rejected.

Table 3.1: ANOVA statistical analysis results

	df	*SS*	*MS*	*F*
Regression	2	1.34×10^{-6}	6.71×10^{-7}	238.69
Residual	5	1.40×10^{-8}	2.81×10^{-9}	
Total	7	1.36×10^{-6}		

	Coefficients	*Standard Error*	*t Stat*	*P-value*
Intercept	1.43×10^{-3}	7.67×10^{-5}	18.70	8.06×10^{-6}
pH [-]	-1.11×10^{-4}	1.04×10^{-5}	-10.72	1.22×10^{-4}
SRFA concentration [mg-C/L]	3.49×10^{-5}	1.83×10^{-6}	19.04	7.37×10^{-6}

The predicted Hg^0 dissolution rate coefficient was close to the experimental values (R^2: 0.99) (Fig. 3.7). Thus, for constant Hg^0 droplet surface area and Reynolds number, this model can be used to determine the Hg^0 dissolution rate coefficient in freshwaters rich in humic substances.

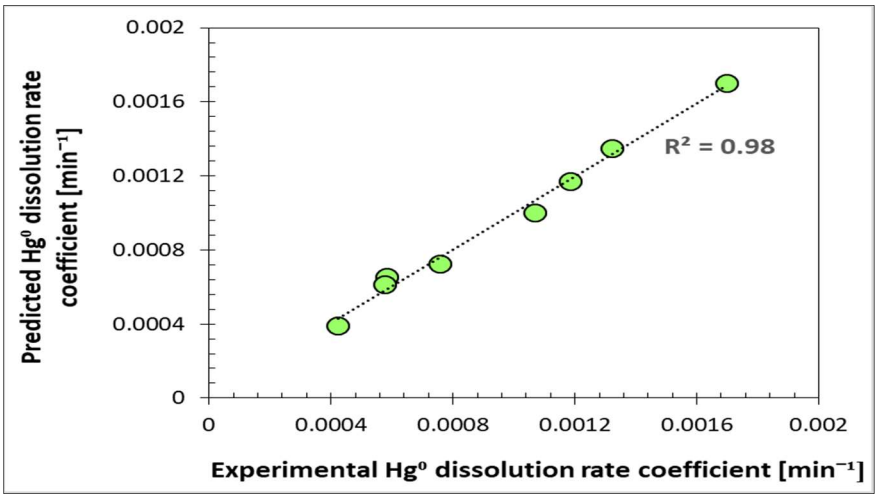

Fig.3.7: Comparison of observed and predicted data

3.4 Heteroscedasticity Test of error terms

From an eye observation of the plot of residuals (Fig. 3.8), the possibility of heteroscedasticity was suspected.

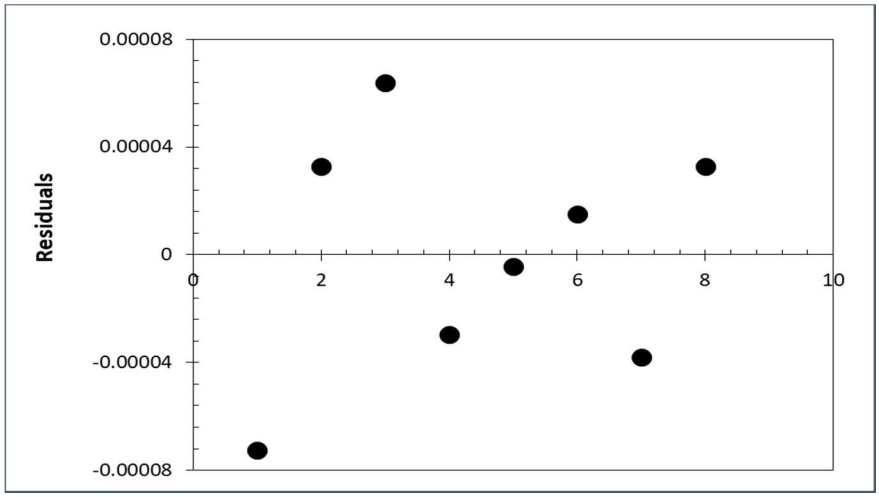

Fig. 3.8: Plot of the residuals

Thus it was tested on the 5% significance level based on the following hypotheses:

$$H_0: the\ residuals\ are\ homoscedastic$$

$$H_1: the\ residuals\ are\ heteroscedastic$$

For both the Breusch-Pagan and White heteroscedasticity test models, the computed p-values (0.53 and 0.57 for the Breusch-Pagan and White test respectively) are greater than the significance level ($\alpha = 0.05$) (Table 3.2), thus, the residuals are homoscedastic and the null hypothesis (H_0) cannot be rejected.

Table 3.2: Heteroscedasticity test results

Parameter	Breusch-Pagan test	White test
LM (Observed value)	1.3	3.9
LM (Critical value)	6.0	11.1
DF	2	5
p-value (Two-tailed)	0.53	0.57
alpha	0.05	0.05

3.5 Mercury pollution duration estimated by parametric sensitivity analysis

Compared to other developing countries in the sub-Saharan region, Zimbabwe's ASGM sector is said to be both significant and advanced. It encompasses informal artisanal miners, known as 'Makorokozas', to highly mechanized small-scale mining operations (Lassen et al., 2016). The Hg^0 demand by each milling/amalgamation center is estimated to be about 2 kg-Hg^0 per week (Lassen et al., 2016). Since the whole ore amalgamation (WOA) technique on copper plates is mainly used by these ASGMs (Gunson et al., 2006), we assume that 70% (Chouinard and Veiga, 2008) of the Hg^0 used in the amalgamation process is lost into nearby creeks, rivers and streams via tailings. Thus, the model predicted dissolution rate coefficient of an Hg^0 droplet with a specific surface area of 0.0015 cm^2 cm^{-3} discharged in tailings into a nearby creek rich in SRFA (2 mg-C L^{-1}) with a Re of 37453 [-] and pH 7.0 is 0.00042 min^{-1} (Calculated from the combined multivariate dissolution models of Chapter 2 (eq. 2.9) and 3 (eq. 3.7) (see Appendix A (eq. 5.6 and Table S1) and Chapter 5 for more details)) Considering that most ASGMs work between 5.9 and 8.6 h per day (average: 7.3 h per day) and a minority of them labor between 8.7 and 14.3 h per day (average: 11.5 h per day) (PACT, 2015) for 38.6 weeks per year (Persaud and Telmer, 2015); it will take between 30.9 and 48.1 years for such a droplet to dissolve when considering Hg^0 losses based on average minimum and maximum labor hours. Thus, though the dissolution time is shorter (compared to 39 - 62 years in the absence of SRFA (Chapter 2 results)) more Hg will be released into the water column owing to the humic substances' enhanced dissolution. Therefore, even after Hg^0 use in ASGM is replaced by non-Hg^0 methods such as using sodium borate 'borax box' (Appleton et al., 1999; Stoffersen et al., 2018) and or alternative Hg^0-rich tailings disposal facilities are put into place; there is need to pay continuous attention Hg environmental risk.

The sensitivity of the Hg^0 dissolution model in SRFA-rich waters was tested using arbitrary values of pH (3 - 8.5) and SRFA concentration (0 – 150 mg-C L^{-1}). The Hg^0 droplet surface area (0.94 cm^2) and Reynolds number (14382 [-]) were kept constant. The sensitivity of the model parameters was compared with the Hg^0 dissolution rate coefficient calculated using the following reference conditions: of pH: 7; SRFA concentration: 2 mg-C L^{-1}; Reynolds number: 14382 [-] and Hg^0 droplet specific surface area: 0.0063 cm^2 cm^{-3} (Hg^0 dissolution rate coefficient: 0.00070 min^{-1}). Model simulations revealed that the Hg^0 dissolution rate coefficient was highly sensitive to fluctuations in the SRFA concentration (Fig. 3.9). Changes in SRFA concentration (0.00063 – 0.0059 min^{-1}) and pH (0.00054 – 0.0011 min^{-1}) resulted in an order of magnitude range difference in the simulated Hg^0 dissolution rate coefficient.

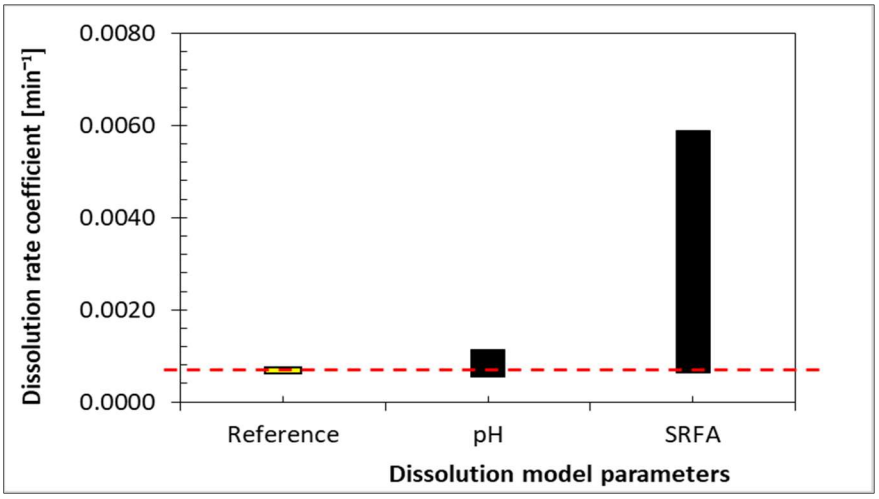

Fig.3.9: Sensitivity Analysis of Hg^0-dissolution model parameters

3.6. Conclusions

Owing to the abundance of humic substances in the freshwater column and their influence on the Hg biogeochemical cycle, this study investigated their effect on the Hg^0 first order dissolution rate coefficient by using commercially available Suwannee River fulvic acid (SRFA). The effects of SRFA solution pH, concentration and ionic strength on the dissolution rate coefficient of an Hg^0 droplet with a surface area of 0.94 cm^2 was investigated in a 'dark chamber'. Acidic pH, low salinity (ionic strength) and high SRFA concentration resulted in a rapid dissolution. The concentration of Hg-SRFA soluble organic complexes (Hg_{OC}) increased with increase in pH and SRFA concentration but decreased with increase in ionic strength. Under low pH conditions,

methylation is said to be rapid due to the increased uptake Hg^{2+} by methylating bacteria (Kelly, 2003), thus, the inhibited Hg_{OC} formation in acidic freshwaters results in a large pool of Hg^{2+} available for microbial methylation. Though microbial methylation of Hg_{OC} is not yet fully understood, the observed high Hg_{OC} concentration in alkaline pH and increased SRFA concentration; has the potential to be adsorbed on colloidal organic matter which serves as a substrate for methylating bacteria. Ionic strength in the range of freshwater chloride concentration (0 – 3.0 mM KCl) did not result in any significant increase in the total dissolved mercury concentration (Hg_T) and the Hg^0 dissolution rate coefficient in the absence of SRFA. Though insignificant, there was noticeable increase in the Hg_T and Hg^0 dissolution rate coefficient upon increasing the ionic strength. A multi-variate Hg^0 dissolution model of the form: $\hat{k} = 1.4 \times 10^{-3} - 1.1 \times 10^{-4}[pH] + 3.5 \times 10^{-5}[SRFA]$ was proposed. Based on this model, Hg^0 dissolution rate coefficient in freshwaters rich in humic substances can be estimated for a constant Hg^0 droplet specific surface area and Re. The parametric sensitivity analysis revealed that the model is sensitive to variations in the SRFA concentration and pH. In both cases; an order of magnitude range difference in the simulated Hg^0 dissolution rate coefficient was observed. Furthermore, even after Hg^0 use in ASGM is fully replaced by non-Hg^0 gold mining technologies such as the borax box, Hg^0 dissolution will continue for at least 31 years in already Hg^0-contaminated freshwaters. Thus, Hg environmental risk must always be considered and contaminated freshwaters monitored closely.

Chapter Four

Cladophora sp. biosorption of metal-contaminated water

This chapter focuses on the adsorption of mercury from contaminated waters using Cladophora sp., an abundant living green freshwater algae. The experimental design and methodology is elaborated. Results of the kinetic study, equilibrium models, and effect of the presence of other cations amongst others are given.

4.0 Introduction

Various physiochemical technologies such ion exchange, chemical precipitation, electrokinetics and membrane processing, have been widely used for the removal of heavy metal contaminants in waste waters (Skousen et al., 1990; Strydom and King, 2009; Udayabhanu and Prasad, 2010). However, these are often characterized by high capital and operational costs, incomplete removal of contaminants and secondary pollutants such as waste sludge rich in toxic and radioactive heavy metals – which is also difficult to dispose; hence, difficult to sustain in crumbling economies of developing nations. On the other hand, the removal of heavy metal contaminants by biosorption using natural biosorbents such as algae has proven to be an efficient, safe, and more economical method. The use of algae offers several advantages such as (1) diverse multifunctional groups on their surface, (2) relatively small and uniform distribution of binding sites on the surface, (3) requires minimal preparatory steps, (4) no and / or minimal use of chemicals, (5) naturally renewable, recyclable, and easily available all year round, and (6) high adsorption capacities (7) low operational costs. Thus, compared to physio-chemical techniques, the use algae as biosorbents is cost-effective (Bilal et al., 2018). Therefore, the potential use of an abundant freshwater living green algae *Cladophora* sp. as an Hg biosorbent was investigated in this chapter. The methodology and experimental observations are detailed in the following sections.

4.1 Materials and methods

This section details the reagents used, machinery and experimental methodology followed.

4.1.1 Reagents

Reagents used for the sorption studies were of analytical grade, except for standards used for quantification purposes which were high purity reagents (i.e. certified “heavy metals free”). All instrument standard solutions were prepared on the day of use. De-ionized water with an electrical resistivity of 18.2 MΩ cm (Millipore, USA) was used for reagent preparation.

4.1.2 Algae collection and storage

The filamentous green algae strain used in this research was collected from Alexander dam, in Springs, on the East Rand of Gauteng Province, South Africa (Fig. 2.1).

Fig. 4.1: Site map of Alexander dam in Springs, Gauteng. (The red oval shape shows the area where the algae samples were randomly picked)

Algae samples were handpicked from the dam. To minimise the risk of contamination, nitrile gloves were used during sample collection (Fig. 2.2) and in the removal of foreign material such as papers, grass and plant leaves which were attached to the algae. The dam water in which the algae were growing in was collected into polyethylene plastic containers in which the algae were placed. The containers were tightly sealed and placed in refrigerated bags for transportation to the laboratory were some of the algae were treated by washing thoroughly with tap water and rinsed with de-ionized water until all the foreign material was removed. The rigorous washing of the algae also enabled the removal of metals attached to the algae surface. The rest of the algae which was not to be immediately used were stored in the refrigerator at 4°C until use (Tshumah-Mutingwende, 2014). For all vessels used during sampling and batch reaction tests, a rigorous cleaning procedure as described by Monperrus and colleagues (Monperrus et al., 2005) was implemented.

Fig 4.2: Handpicking of algae from Alexander dam

4.1.3 Algae characterization

Identification of the freshwater algae was carried out under a light microscope (Olympus Instruments, Melville, NY, USA) equipped with a DMX 1200 digital camera at 200 X magnification (Nikon, Japan). The various functional groups present on the algae surface before batch adsorption tests were determined using Fourier Transform Infra-red (FTIR) analysis. FTIR spectra were measured directly from *Cladophora* sp. using a Tensor 27 (Bruker, Germany) device in the range of 4 000 to 400 cm^{-1}.

4.1.4 Algae culture

The algae samples were grown in an algae culture for 2-3 days and then acclimated in distilled water at room temperature and natural light for a day before use for experiments (Ji et al., 2012). The Acidic Bold-Basal Medium (ABM) algae culture was prepared as shown in Table 4.1 and 4.2 (Culture collection of alagae and protozoa (CCAP), 2013).

Table 4.1: Essential elements

Salt	Concentration (g L^{-1})
$NaNO_3$	25.0
$MgSO_4.7H_2O$	7.5
NaCl	2.5
$K_2HPO_4.3H_2O$	7.5
KH_2PO_4	17.5
$CaCl_2.2H_2O$	2.5

To 800 mL of distilled water, 250 mg of $(NH_4)_2SO_4$ were added as well as 10 mL of each of the essential elements in Table 4.1.

Table 4.2: Trace elements

Salt	Quantity (mg)
$FeCl_3.6H_2O$	97.0
$MnCl_2.4H_2O$	41.0
$ZnCl_2.6H_2O$	5.0
$CoCl_2.6H_2O$	2.0
$Na_2MoO_4.2H_2O$	4.0

To 1000 mL of deionised water, 0.75 g of Na_2-EDTA was added as well as the trace elements in the manner they appear in Table 4.2. To the 800 mL of deionized water in which 250 mg of $(NH_4)_2SO_4$ and 10 mL of each of the essential elements was added, 6.0 mL of each of the trace elements was also added. The resulting solution was made up to 1 L with deionised water and the pH was maintained at 6.5 since this was the pH of the dam water where the algae were collected. The solution was then autoclaved using a Precise Shaking Incubator WIS-30 (Daihan Scientific Co., Ltd, Korea) at 121ºC and 1000 Pa for 15 minutes so as to sterilise the culture media by inactivating microbial life such as bacteria (Barsanti and Gualtieri, 2006).

4.2 Batch adsorption tests

All batch experiments were conducted in triplicates and for each set a control which contained the metal contaminant but lacked algae were setup so as to determine if anything besides algae caused the observed effects. Stock solutions of 10 mg L^{-1} of Hg^{2+}, Co^{2+}, Cu^{2+}, Zn^{2+} and Fe^{2+} were prepared by weighing appropriate amounts of the following salts: $HgSO_4$, $Co(NO_3)_2{\cdot}6H_2O$, $Cu(NO_3)_2{\cdot}3H_2O$, $Zn(NO_3)_2{\cdot}6H_2O$ and $FeSO_4$. Appropriate aliquots were taken from these standards for subsequent dilution to the desired concentration level. To prevent precipitation of the metals, prepared solutions were acidified using 1% ultrapure HNO_3 (v/v) and stored in a refrigerator at 4^{o}C prior to the relevant experiments. Single component batch tests were performed in 250 mL conical flasks and a solution volume of 200 mL was used and competitive adsorption tests were performed in 500 mL Erlenmeyer flasks and a solution volume of 500 mL was used. At different equilibrium time intervals, 2 mL of the sample volume was withdrawn for analysis. This volume was such that the total volume drawn was less than 10% of the initial volume used so as to minimize the change in the ratio between the metal concentration and the sorbent mass (Nsimba, 2012). Of the 2 mL volume collected during the batch tests, 500 µL were used for analysis. This volume was placed in acid washed 15 ml centrifuge tubes and made up to 10 mL. The dilution factor was calculated and taken into account in determining the actual mercury concentration from the results obtained from the mercury analyzer. In the batch adsorption tests, the effects of pH, initial Hg concentration, contact time and the presence of competing cations were investigated.

4.2.1 Effect of initial concentration

The effect of initial Hg concentration was investigated by using a stock solution of 10 mg L^{-1} to make working solutions of 0.25, 0.50, 0.75, 0.85 and 1.0 mg Hg L^{-1}. An algae adsorbent mass of 2.0 ± 0.05 g was used and the agitation rate was fixed at 150 rpm. The effect of initial Hg concentration was studied at ambient temperature. The contact time was varied from 0-120 min.

4.2.2 Effect of pH

The effect of pH on the adsorption of Hg by *Cladophora* sp. algae was investigated at the optimum concentration (1.0 mg Hg L^{-1}) by adjusting the pH of the solution to pH 3.0, 6.5 and 8.5 by using either 0.1 M NaOH or HNO_3 at ambient temperature. An algae mass of 2.0 ± 0.05 g was used; the contact time was varied from 0-120 min at a fixed agitation rate of 150 rpm.

4.2.3 Effect of contact time

The effect of contact time on the adsorption of Hg by algae was investigated at the optimum pH (pH 3), optimum concentration (1.0 mg Hg L^{-1}) at ambient temperature. An algae mass of 2.0 ± 0.05 g was used at a constant agitation rate of 150 rpm. The contact time was varied from 0 to 120 min and the Hg concentration in solution as well as the Hg adsorbed by algae (i.e. bioavailable Hg) was determined at the end of each contact time. The obtained equilibrium capacities (q_e) were then plotted against the equilibrium time for kinetic modeling.

4.2.4 Effect of competing cations

Competitive adsorption tests were performed by using the same procedure as that for Hg adsorption on algae in a single component solution. The effect of Hg^{2+}, Fe^{2+}, Co^{2+}, Zn^{2+} and Cu^{2+} cations on the adsorption of Hg by algae in a multicomponent solution was investigated for an algae mass of 4.0 ± 0.05 g, cation concentration of 1.0 mg L^{-1}, optimum pH (pH 3) and ambient temperature. The agitation rate was maintained at 150 rpm whereas the contact time varied from 0 to 120 min.

4.3 Sample preparation

After batch adsorption tests, the experimental solution containing algae was filtered through a 0.45 µm filter paper (ACE, South Africa). The treated algae were then freeze dried in a Lyophilizer (Labconco, USA) at -40°C for 2 days. After drying, the samples were crushed into a fine powder using liquid nitrogen and stored in a cool dry place until further use.

4.4 Analytical method

A mass of 0.25 ± 0.005 g of homogenized dry algae samples were weighed using an analytical balance (Precisa 180A, Switzerland) and placed into acid washed digestion tubes (PTFE-TFM liners) into which 16 ml HNO_3 and 4 ml H_2O_2 were added before being placed into the Multiwave 300 microwave digester (Anton Paar, Switzerland). The digested samples were then transferred into 50 ml acid washed volumetric flasks and the volumes were completed with distilled water after which the samples were kept at 4°C until metal analysis. Total Hg in water and digested algae samples were determined using an automated Flow Injection-Cold Vapour Atomic Absorption Spectrometry system (FI-CVAAS) FIMS 400 (Perkin Elmer, USA) whereas the concentrations of

competing cations (Fe^{2+}, Co^{2+}, Cu^{2+}, and Zn^{2+}) were obtained by using an Inductively Coupled Plasma-Optical Emission Spectroscopy (ICP-OES) instrument (Spectro Genesis, Germany). All measurements were performed in triplicates and the mean value was reported. A certified reference material (BCR 482 Lichen) was also prepared in triplicate using the above mentioned digestion procedure and analysed to validate the used methodology (Tshumah-Mutingwende, 2014).

4.5 Data evaluation

4.5.1 Extraction efficiency

The extraction efficiency (r) of Hg by algae refers to the maximum amount of Hg ions removed from solution compared to the initial concentration of Hg ions. The mass balance equation used to calculate the extraction efficiency is shown below (Ji et al., 2012):

$$r = (C_0 - C_t/C_0) \times 100\% \qquad (4.1)$$

Where;

r - is the extraction efficiency (%)

C_0 - is the initial cation concentration (mg L^{-1})

C_t - is the equilibrium cation concentration (mg L^{-1})

4.5.2 Distribution coefficients

Metal analysis results for competitive adsorption obtained from the ICP-OES were used to calculate the distribution coefficients K_d $(L\,mol^{-1})$ of the different cations as shown in the following equation (U.S. Environmental Protection Agency (U.S. EPA), 1999):

$$K_d\ (L\,mol^{-1}) = (C_0 - C_t)V/C_tM \qquad (4.2)$$

Where;

V- is the volume of media (L)

C_0 - is the initial cation concentration (mg L^{-1})

C_t - is the equilibrium cation concentration (mg L^{-1})

M – is the mass of algae used (g)

4.5.3 Kinetic models

The computational procedures for the Pseudo 1st and 2nd kinetic models are detailed in this section.

4.5.3.1 Pseudo 1st order model

The pseudo 1st order model is given by (Lagergren., 1898):

$$log\ (q_e - q_t) = lo\ g\ q_e - (k_1/2.303)t \qquad (4.3)$$

A plot of $log\ (q_e - q_t)$ against time t, gives the values of q_e and k_1 on the intercept and slope of the plot respectively.

Where;

q_e - is the adsorption capacity at equilibrium (mg g^{-1})

q_t - is the adsorption capacity at time t (mg g^{-1})

k_1 - is the rate constant (min^{-1})

4.5.3.2 Pseudo 2nd order model

The pseudo second order model is given by (Ho and Mckay, 1999):

$$t/q_t = 1/k_2 q_e^2 + (1/q_e)t \qquad (4.4)$$

A plot of t/q_t against t gives a straight line and the values of q_e and k_2 are determined from the slope and intercept of the plot respectively.

Where;

q_e - is the adsorption capacity at equilibrium (mg g^{-1})

q_t - is the adsorption capacity at time t (mg g^{-1})

k_2 - is the rate constant (g mg^{-1} min^{-1})

4.5.4 Intra-particle diffusion model

The intra-particle diffusion model is given by (Weber and Morris, 1963):

$$q_t = K_{id} t^{0.5} \qquad (4.5)$$

Where;

q_t - is the adsorption capacity at time t (mg g^{-1})

K_{id} - is the rate constant for intra-particle diffusion ($mg\ g^{-1}\ min^{-0.5}$)

A plot of q_t against $t^{0.5}$ gives a straight line, which, if not passing through the origin indicates that pore diffusion is not the rate limiting step for the adsorption of Hg^{2+} on *Cladophora* sp. algae.

4.5.6 Equilibrium adsorption capacity

The equilibrium adsorption capacities (q_e) were determined using the following mass balance equation (Ji et al., 2012):

$$q_e = V(C_o - C_e)/m \qquad (4.6)$$

Where;

$q_e -$ is the amount of metal adsorbed per gram of adsorbent (algae) $(mg\ g^{-1})$

$V -$ is the volume of media (L)

$C_o -$ is the initial cation concentration in media $(mg\ L^{-1})$

$C_e -$ is the equilibrium cation concentration $(mg\ L^{-1})$

$m -$ is the mass of adsorbent (algae) used (g)

4.5.7 Equilibrium isotherm models

The experimental results for both the single and multi-component systems were fitted on equilibrium isotherm models and the methods are detailed in the following section.

4.5.7.1 Single component system

The experimental results for the single component adsorption tests were fitted on the Langmuir and Freundlich equilibrium isotherms and the methodology is detailed in the following sections.

4.5.7.1.1 Langmuir equilibrium isotherm model

The linearized form of the Langmuir equilibrium isotherm is given by (Langmuir, 1918):

$$q_e = (q_m b C_e)/(1 + bC_e) \qquad (4.7)$$

Where;

q_e - is the amount of metal adsorbed per gram of adsorbent (algae) $(mg\ g^{-1})$

q_m- is the amount of adsorption corresponding to complete monolayer coverage (i.e. maximum adsorption capacity) $(mg\ g^{-1})$

b - is the adsorption constant related to binding energy $(L\ mg^{-1})$

C_e- is the equilibrium cation concentration in media $(mg\ L^{-1})$

4.5.7.1.2 Freundlich equilibrium isotherm model

The linearized form of the Freundlich equation is given by (Freundlich, 1907):

$$In\ q_e = InK_f + 1/n\ In\ C_e \qquad (4.8)$$

A plot of $In\ q_e$ against $In\ C_e$ gives a straight line and the values K_f and n are determined from the intercept and slope of the graph respectively.

Where;

$q_e -$ is the amount of metal adsorbed per gram of adsorbent (algae) $(mg\ g^{-1})$

$C_e -$ is the equilibrium cation concentration in media $(mg\ L^{-1})$

K_f and n - are temperature dependent Freundlich constants related to adsorption capacity and intensity respectively. For favorable adsorption, the values of n must be between 0 and 1

4.5.7.2 Equilibrium adsorption isotherm for multi-component system

The methodology for computing the Extended Langmuir, Freundlich and Sips Equilibrium isotherm models is detailed in this section.

4.5.7.2.1 Extended Langmuir Equilibrium Isotherm model

The extended Langmuir equilibrium isotherm model for adsorption in a multicomponent system is given by (Hajahmadi et al., 2015):

$$q_{ei} = q_m b C_e \Big/ 1 + \sum_{i=1}^{n} b_i C_{ei} \qquad (4.9)$$

Where;

q_{ei} – is the amount of metal adsorbed per gram of adsorbent (algae) ($mg\ g^{-1}$)

q_m – is the amount of adsorption corresponding to complete monolayer coverage (i.e. maximum adsorption capacity) ($mg\ g^{-1}$)

b - is the adsorption constant related to binding energy ($L\ mg^{-1}$)

C_{ei} – is the equilibrium concentration of the cations in media ($mg\ L^{-1}$)

4.5.7.2.2 Extended Freundlich Equilibrium Isotherm model

The extended Freundlich equilibrium isotherm model for adsorption in a multicomponent system is given by (Hajahmadi et al., 2015):

$$q_{ei} = k_{fi} \sum_{i=1}^{n} C_{ei}^{1/ni} \qquad (4.10)$$

Where;

q_{ei} – is the amount of metal adsorbed per gram of adsorbent (algae) ($mg\ g^{-1}$)

C_{ei} – is the equilibrium concentration of cation in media ($mg\ L^{-1}$)

k_{fi} - is a temperature dependent Freundlich constants related to adsorption capacity $mg\ g^{-1}$ ($mg\ L^{-1})^n$

n_i - is a temperature dependent Freundlich constants known as the adsorbent intensity

4.5.7.2.3 Sips Equilibrium isotherm model

The Sips equilibrium isotherm model for adsorption in a multicomponent system is given by (Hajahmadi et al., 2015):

$$q_{ei} = K_s C_e^{\gamma} \Big/ 1 + \sum_{i=1}^{n} a_{si} C_{ei}^{\gamma i} \qquad (4.11)$$

Where;

$q_{ei} -$ is the amount of metal adsorbed per gram of adsorbent (algae) $(mg\ g^{-1})$

K_s - is the Sips isotherm constant (L g^{-1})

a_{si} –is the Sips isotherm constant $(L\ mg^{-1})$

$\gamma -$ is the Sips isotherm constants $[-]$

$C_{ei} -$ is the equilibrium concentration for the cation in media $(mg\ L^{-1})$

4.8 Results and discussion

The results for the experimental investigations and kinetic and equilibrium model optimization are given in this section.

4.8.1 Method validation

An excellent linearity was obtained with the FIMS instrument for total mercury standards (Fig. 4.3). Calibration was performed using standards in the range of 1-10 µg Hg L^{-1}. A method limit of detection of 0.009 µg Hg L^{-1} was obtained which makes the method suitable for ultra-trace analysis of mercury.

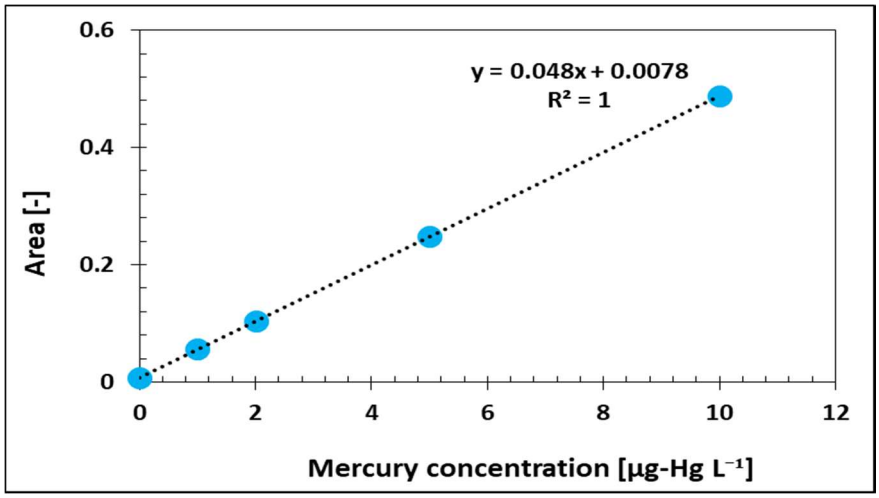

Fig.4.3: Calibration curve for the FIMS

The CRM BCR 482 of lichens was analyzed as described in **section 4.4 (Analytical method)** and the results shown in Tables 4.3 and 4.4 were obtained with the developed analytical methods. More than 99% of mercury recovery was obtained with the FIMS. This confirms that no considerable mercury loss or contamination occurred during samples preparation and subsequent analysis. The obtained results also demonstrated the excellent repeatability and reproducibility of the methodology with RSD always below 5%. Overall, the analysis of CRMs has shown that the optimized analytical method can be successfully used for the precise and accurate detection of mercury in plant materials.

Table 4.3: Hg concentration in CRM BCR 482 lichen

Sample ID	Hg ± SD (µg kg^{-1})	Mean ± SD(µg kg^{-1})	RSD (%)	Certified (µg kg^{-1})	% Recovery
CRM 1	456 ± 0.04				
CRM 2	502 ± 0.67	476 ± 23	4.8	480 ± 20	99
CRM 3	471 ± 0.02				

Table 4.4: Selected metals concentrations in CRM BCR 482 lichen

CRM BCR482	Cd (mg kg^{-1})	Cu (mg kg^{-1})	Zn (mg kg^{-1})
Mean (n = 3)	0.66 ± 0.13	6.90 ± 0.31	91.5 ± 1.0
Certified Values	0.56 ± 0.02	7.03 ± 0.19	100.6 ± 2.2
% Recovery	95	98	91

ICP-OES results of the same CRM generally exhibited the same trend since, with the exception of aluminum, all the analyzed metals also showed a recovery beyond 90%.

4.8.2 Algae structure

Observations made on algae under a light microscope (Fig. 4.4) showed that the algae collected from Alexander dam was filamentous, with cells joined from end to end. Though this alga was not branched like the common *Cladophora* species (e.g. *Cladophora glomerata*), its hair-like nature and rough texture fitted well the description of *Cladophora* sp. In addition, the order of *Cladophora* sp., *Cladophorales*, stipulates that it is filamentous, with cells joined end to end in definite series, with or without branching of multinucleate cells (Johnson et al., 1996).

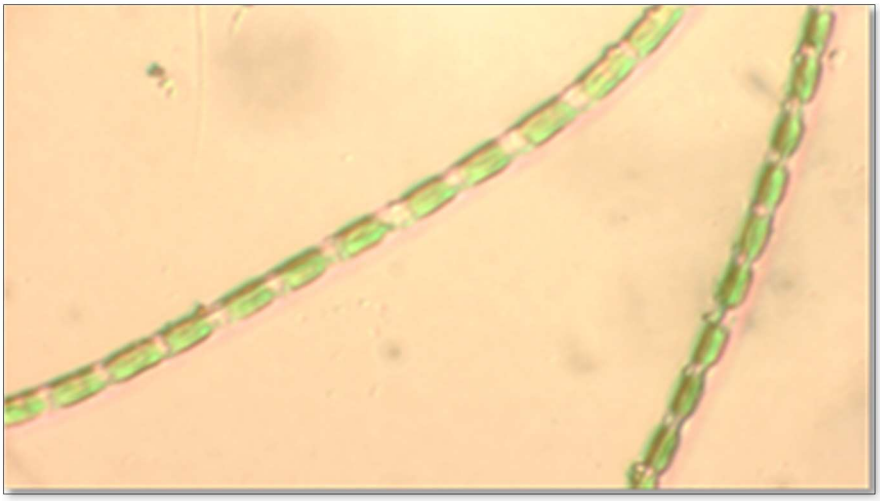

Fig. 4.4: Algae structure

4.8.3 Algae functional groups

From the FTIR spectrum of *Cladophora* sp. the functional groups present in algae were O-H (alcohol) observed at 3300-3600 cm^{-1}, N-H (amine) observed at 3200-3500 cm^{-1} and ν(C=O) observed at 1780-1680 cm^{-1} for carboxylic acids (Fig. 4.5). For algae species, this band is shifted to lower frequencies at 1700-1600 cm^{-1} (Deng et al., 2007). It has been reported that the majority of the algae functional groups responsible for metal sorption such as the carboxyl are acidic and are available at low pH (Mehta and Gaur, 2005). Also, at high pH values, the surface charge of algae is negative due to the presence of the hydroxyl (-OH) functional group thus facilitating metal adsorption due to attraction between the negative algae surface charge and the positively charged metal cation. Therefore, with reference to the FTIR results obtained, most of the metal adsorption is expected to occur at acidic and alkaline conditions.

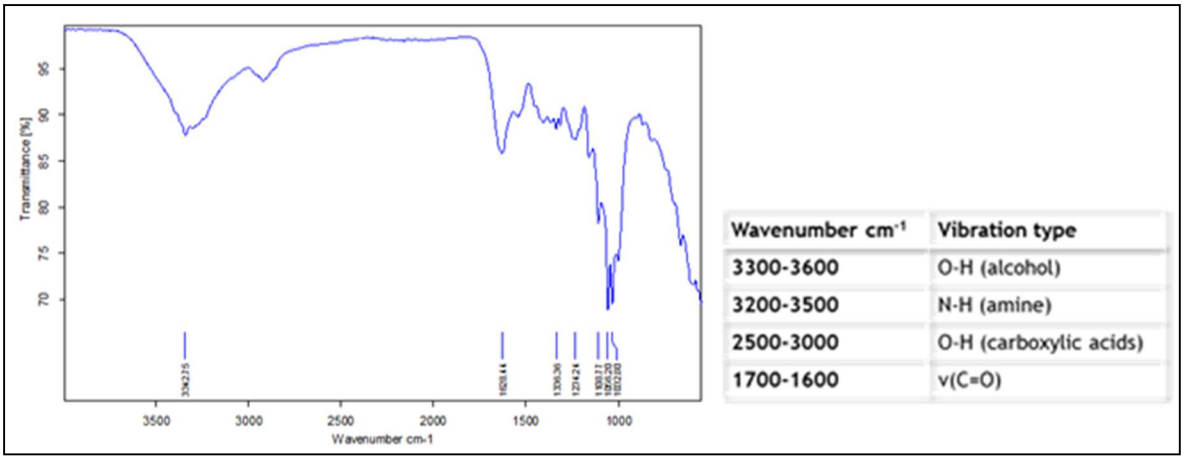

Wavenumber cm^{-1}	Vibration type
3300-3600	O-H (alcohol)
3200-3500	N-H (amine)
2500-3000	O-H (carboxylic acids)
1700-1600	v(C=O)

Fig.4.5: FTIR spectrum of *Cladophora* sp.

4.8.4 Effect of pH

pH plays a major role on the adsorption of heavy metals by algae as it influences the solution chemistry of the metals, the activity of functional groups (carboxylate, phosphate, thiol and amino groups) on the cell wall as well as the competition of cations for the binding sites (Pansamrit, K. Ruangsomboon, 2010; Rezaee and Ramavandi, 2006). Maximum Hg^{2+} adsorption (adsorption capacity of 805 mg kg^{-1}) was observed at pH 3 (Fig. 4.6), which is also algae point of zero charge (Yalcin et al., 2008). Due to the high adsorption capacity observed, it was concluded that under the given experimental conditions, the surface charge of alga at the point of zero charge developed

as negative, thus more binding sites such as the carboxyl functional group, which are acidic, were available for mercury adsorption (Hg^{2+}). Though low pH values have been reported to result in a decrease in metal sorption due to the increased concentration of the hydrogen ions (H^{+}) which are preferentially adsorbed onto the alga surface compared to cations (Mehta and Gaur, 2005); the results obtained were in agreement with the findings of Le Faucheur and colleagues (Faucheur et al., 2011) who concluded that Hg^{2+} uptake by algae seems to be stimulated by proton addition after investigating the influence of pH on Hg^{2+} uptake by a green, unicellular alga, *Chlamydomonas reinhardtii*. Therefore, pH 3 was chosen as the optimum pH.

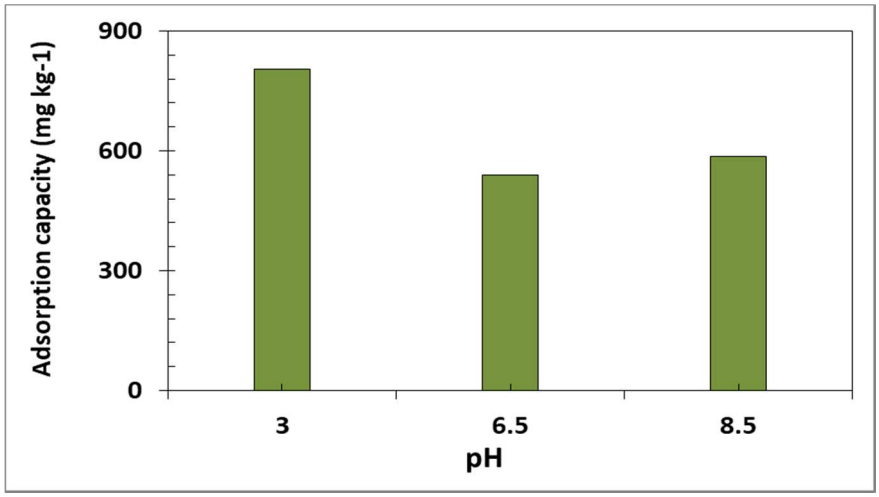

Fig. 4.6: Effect of pH on the adsorption of mercury on *Cladophora* sp. algae

4.8.5 Effect of initial Hg concentration

As the concentration of Hg^{2+} ions increased so was the amount of Hg^{2+}ions adsorbed. This can be attributed to the increasing concentration of Hg^{2+} ions in solution that competed for a finite number of binding sites on the algae surface. A maximum adsorption capacity of 805 mg kg^{-1} was attained at an initial concentration of 1.0 mg L^{-1} and optimum pH 3 (Fig. 4.7).

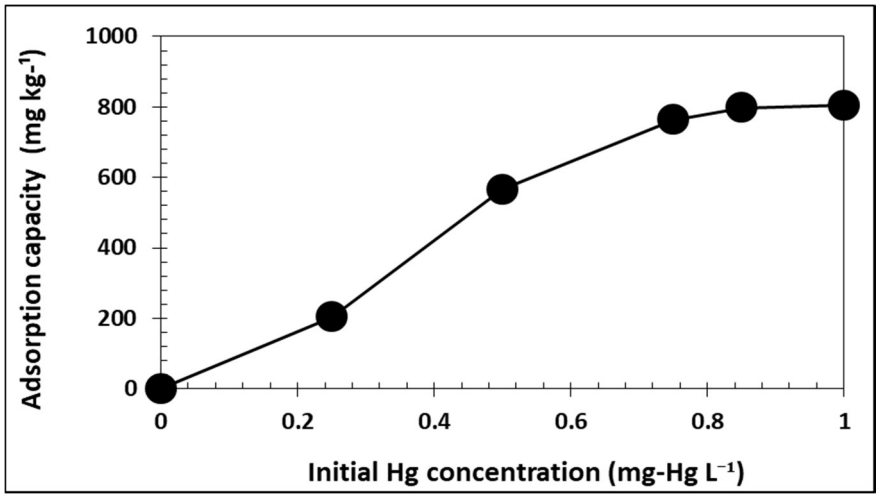

Fig. 4.7: Effect of initial Hg concentration on the adsorption of mercury on *Cladophora* sp. algae

4.8.6 Effect of contact time

The effect of contact time on the adsorption of Hg^{2+} by *Cladophora* sp. was investigated at the optimum pH (pH 3) and optimum concentration of 1.0 mg L^{-1}. The concentration of Hg in solution rapidly decreased within the first 5 min, attaining more than 99% Hg removal and equilibrium was attained after 10 min which was chosen as the optimum contact time (Fig. 4.8). Mechanism of heavy metal uptake consists of passive and active uptake (Mehta and Gaur, 2005; Satyanarayana et al., 2012). The biosorption mechanisms are further classified according to its dependence on cell metabolism and to the location within the cell and the metal removed, although most of them are not yet fully understood (Veglio and Beolchini, 1997). The rapid uptake of Hg by algae is of great importance in environmental applications and the observed short retention times will result in huge operation cost savings.

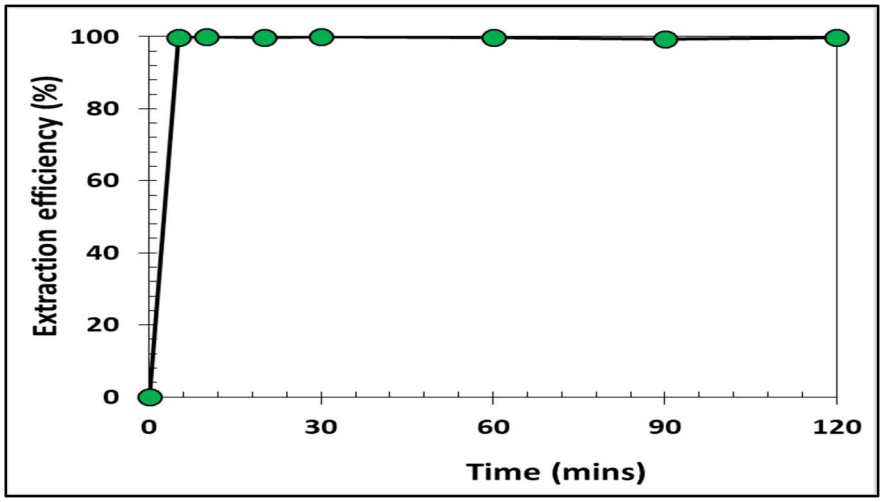

Fig.4.8: Effect of contact time on the adsorption of mercury on *Cladophora* sp. algae

4.8.7 Effect of competing metal cations

The removal efficiency of Hg^{2+} decreased from greater than 99% in a single component system to 67.2% in a multi component system (Fig. 4.9). However, this extraction efficiency is still high compared to the results obtained by other scholars, for example, Plaza and colleagues (Plaza et al., 2011) studied the biosorption of Hg in the presence of Zn, Cd and Ni using a brown algae biomass and observed a significant decrease of Hg uptake by more than 50%. Therefore, *Cladophora* sp. can be still used as a biosorbent material in environmental applications. The selectivity of cations by *Cladophora* sp. was in the following order: Hg^{2+} >Fe^{2+}>Cu^{2+}> Zn^{2+} > Co^{2+}. The difference in sorption affinities may be attributed to differences in electronegativity of the atoms which also follows the same order. Therefore, the greater the electronegativity or ionic radii the higher the sorption affinity, explaining the high extraction efficiency of Hg^{2+} obtained in the presence of competing cations (Al-rub and Ashour, 2006; Andrade and Nobrega, 2005; Mohamed and Anita, 1998). The observed trend for Hg^{2+} adsorption is most likely to be a result of adsorption and desorption occurring simultaneously. However, further work must be carried out in order to validate this assumption.

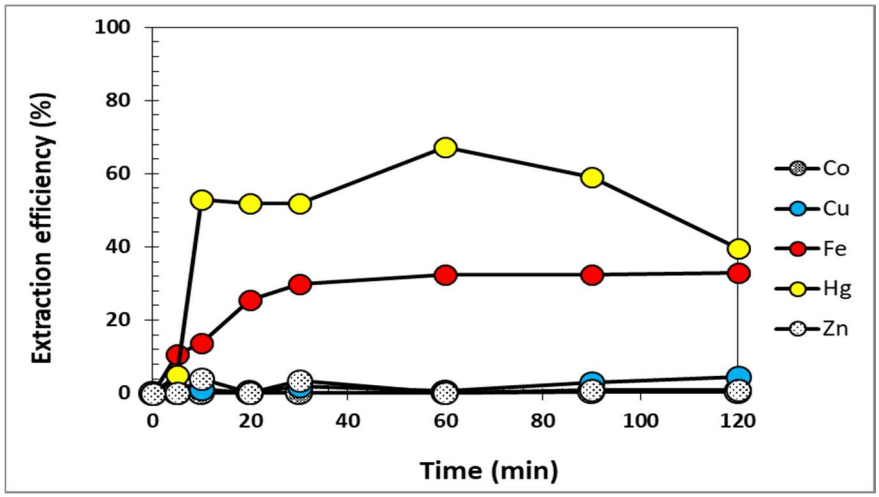

Fig.4.9: Effect of competing cations on the adsorption of mercury on *Cladophora* sp. algae

The extraction efficiency of Hg^{2+} by *Cladophora* sp. was compared with that of other adsorbents reported in literature at different conditions (Table 4.5). High extraction efficiencies in the range of 97-99% were observed when living green algae was used as Hg^{2+} biosorbent (Henriques et al., 2015; Shanab et al., 2012). These reported results were close to the results obtained in this study. However, unlike our study; longer retention times of 30 min (Shanab et al., 2012) and 96 h (Henriques et al., 2015) were reported at pHs 7 and 7.9 respectively. Though in their studies the influence of variations in pH was not investigated (Henriques et al., 2015; Shanab et al., 2012); as explained in Section 4.8.4; it can be assumed that the observed slow biosorption at pH 7 and 7.9 is a result of a positive algae surface charge at high pH, thus repulsion of Hg^{2+} ions (Yalcin et al., 2008); and also Hg toxicity to the algae cells at high concentrations (10 mg-Hg L^{-1}), thus, inhibiting its biosorption (Shanab et al., 2012).

Table 4.5: Comparison of Hg^{2+} extraction efficiencies for different adsorbents

Adsorbent	Hg^{2+} extraction efficiency (%)	Conditions	Ref.
Cladophora sp. algae (*living green algae)*	**>99**	**pH: 3** **room temperature** **Initial Hg^{2+} concentration: 1.0 mg L^{-1}** **Equilibrium contact time: 10 min**	**This study**
Pseudochlorococcum typicum *(living green algae)*	97	pH: 7 Temperature: 25˚C Initial Hg^{2+} concentration: 10 mg L^{-1} Equilibrium contact time: 30 min	(Shanab et al., 2012)
Ulva lactuca (*living green algae*)	99	pH: 7.9 Temperature: - Initial Hg^{2+} concentration: < 1.0 μg L^{-1} Equilibrium contact time: 96 h	(Henriques et al., 2015)
Cladophora fracta algae *(dried green algae biomass*)	98	pH: 5 Temperature: 18˚C Initial Hg^{2+} concentration: 1.0 mg L^{-1} Equilibrium contact time: -	(Ji et al., 2012)
Filamentous algae Spirogyra species (*dried green algae biomass*)	90	pH: 4 Temperature: 25˚C Initial Hg^{2+} concentration: 1.0 mg L^{-1} Equilibrium contact time: 30 min	(Rezaee and Ramavandi, 2006)
Activated carbon from carbonized eucalyptus wood	>90	pH: 3 Temperature: 25˚C Initial Hg^{2+} concentration: 40 mg L^{-1} Equilibrium contact time: -	(Silva et al., 2010)

Table 4.5: Comparison of Hg^{2+} extraction efficiencies for different adsorbents (*continued*.)

Adsorbent	Hg^{2+} extraction efficiency (%)	Conditions	Ref.
Rice Husk Ash	98	pH: 6 Temperature: 25˚C Initial Hg^{2+} concentration: 100 mg L^{-1} Equilibrium contact time: 3 h	(Tiwari et al., 1995)
2-mercaptobenzimidazole loaded natural clay	>99	pH: 4-8 Temperature: 30˚C Initial Hg^{2+} concentration: 50.0 mg L^{-1} Equilibrium contact time: 8 h	(Manohar et al., 2002)
Sargassum Glaucescens biomass	94.5	pH: 5 Room temperature Initial Hg^{2+} concentration: 0.2 mg L^{-1} Equilibrium contact time: 90 min	(Esmaeili et al., 2015)

For dried algae adsorbents, high extraction efficiencies in the range of 90-98% were reported at low pH (pH: 4-5) (Esmaeili et al., 2015; Ji et al., 2012; Rezaee and Ramavandi, 2006) and shorter retention times in the range of 30-90 min (Esmaeili et al., 2015; Rezaee and Ramavandi, 2006). Though the cation removal efficiencies of the other adsorbents such as activated carbon from carbonized eucalyptus wood, rice husk ash and 2-mercaptobenzimidazole loaded natural clay were also high (>90- >99%), they are most efficient at high initial mercury concentrations (40-100 mg L^{-1}) (Manohar et al., 2002; Silva et al., 2010; Tiwari et al., 1995); thus they are not suitable for the intended purpose of this study, since Hg is present in very low concentrations in the environment.

4.8.7.1 Distribution coefficients of competing cations

The distribution coefficients for the Cu^{2+}, Co^{2+}, Zn^{2+}, Fe^{2+} and Hg^{2+} cations used were calculated using equation (4.2). As shown in Table 4.6, the distribution coefficient was highest for Hg^{2+} (386.5 L mol^{-1}) followed by Fe^{2+} (241.5 L mol^{-1}) and Cu^{2+} (19.3 L mol^{-1}) and it remained at zero

for both Co^{2+} and Zn^{2+}. These results show that *Cladophora* sp. has a higher sorption capacity for Hg^{2+} compared to Fe^{2+}, Cu^{2+}, Zn^{2+} and Co^{2+} under the same experimental conditions (Alloway, 1995).

Table 4.6: Distribution coefficients of mercury and competing cations

Distribution coefficient: K_d (L mol^{-1})

Cu^{2+}	Co^{2+}	Zn^{2+}	Fe^{2+}	Hg^{2+}
19.3	0	0	241.5	386.5

4.9.8 Kinetic modeling

Results of the pseudo 1st and 2nd order kinetic models are given in this section. The model which best represents the experimental data is also selected.

4.8.8.1 Pseudo first and second order kinetic models

The pseudo second order model (Fig. 4.10 (b)) showed the best linearization with $R^2 = 1$ compared to the pseudo first order model (R^2=0.92) (Fig. 4.10 (a)). Thus, chemisorption is the rate limiting step in the interaction between Hg^{2+} ions and *Cladophora* sp. In addition, the calculated adsorption capacity (q_e) for the pseudo second order model is 833 mg kg^{-1} and this is very close to the experimental value of 805 mg kg^{-1}.

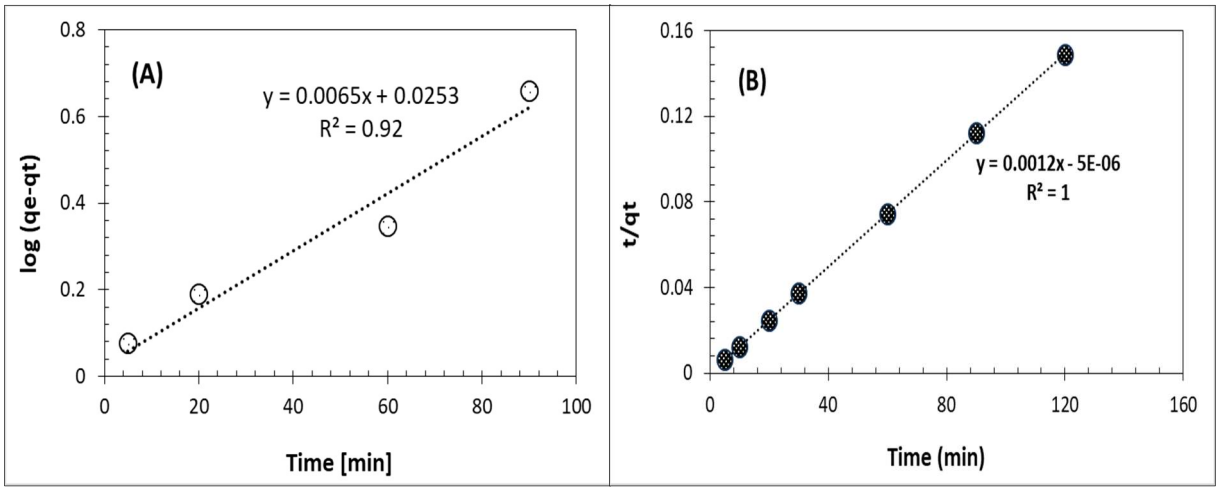

Fig. 4.10: (a) Pseudo first and (b) Pseudo second order kinetic models

4.8.8.2 Intra-particle diffusion model

The Intra-particle diffusion model exhibited two distinct regions (Li et al., 2012): (i) initial pore diffusion due to external mass transfer effects (R^2=1) followed by (ii) intra-particle diffusion (R^2=0.2349) (Fig. 4.11). However, the y-intercept does not pass through the origin, therefore, pore diffusion is not the only rate limiting step.

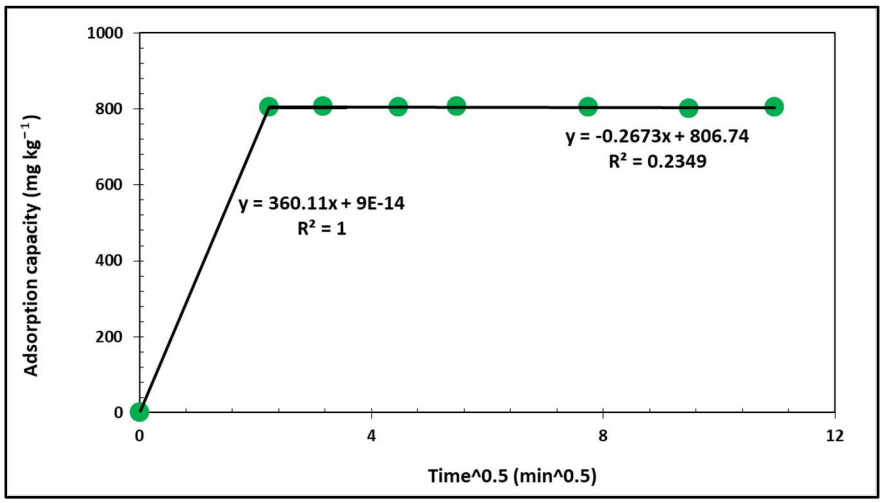

Fig. 4.11: Intra-particle diffusion model

4.8.9 Equilibrium adsorption isotherm models

The equilibrium adsorption isotherm models for the single and multi-component systems are given. The best model for each category is also selected.

4.8.9.1 Single component system

The data obtained from the study of the effect of initial Hg^{2+} concentration was used to fit both the Langmuir and Freundlich equilibrium isotherm models as shown in Table 4.7. The Langmuir equilibrium isotherm model best represented the results with an $R^2 = 1.00$ compared to $R^2 = 0.02$ in the Freundlich isotherm. The maximum adsorption capacity (q_e) of *Cladophora* sp. assuming a monolayer surface was found to be 1010 mg kg^{-1}.

Table 4.7: Coefficients of Langmuir and Freundlich isotherms

Langmuir isotherm			Freundlich isotherm		
R^2	q_m (mg g^{-1})	b (L mg^{-1})	R^2	K_f (L g^{-1})	n (-)
1.00	1.01	11.14	0.02	0.55	27.93

4.8.9.2 Multi-component system

Competitive adsorption studies showed that Fe^{2+} is the major competitor in the adsorption of Hg^{2+} on *Cladophora* sp. algae compared to (Cu^{2+}, $Zn^{2+}$and Co^{2+}). Therefore, assuming that the effect of other cations is negligible, equilibrium isotherm models were studied for a binary system (Hg^{2+} and Fe^{2+}) only. The Sips equilibrium isotherm model best described the results with an R^2 value of 0.93 compared to the Extended Langmuir (R^2=0.84) and Extended Freundlich (R^2=0.72) equilibrium isotherm models (Table 4.8).

Table 4.8: Coefficients of Extended Langmuir, Extended Freundlich and Sips Equilibrium Isotherms

Extended Langmuir equilibrium isotherm		Extended Freundlich equilibrium isotherm		Sips equilibrium isotherm	
q_m (mg g^{-1})	0.79	kf_1 (L g^{-1})	0.51	y_2 (-)	0.04
b_1 (L mg^{-1})	4.42	n_1 (-)	0.04	as_2 (L mg^{-1})	0.15
b_2 (L mg^{-1})	0.02	n_2 (-)	1.00	y_1 (-)	1.00
				as_1 (L mg^{-1})	5.07
				K_s (L g^{-1})	3.48
R^2 (-)	0.84	R^2 (-)	0.72	R^2 (-)	0.93

4.9 Conclusions

The dilapidated economy of developing countries such as Brazil, Tanzania and Zimbabwe amongst others; makes conventional and passive heavy metal removal technologies from contaminated waters impossible due to their high capital and maintenance costs respectively. The persistence of

Hg in the environment, its biogeochemical transformations in aquatic environments, especially the production of methylmercury a known neurotoxin which has a great tendency to biomagnify within the different trophic levels of the aquatic food chain; makes mercury removal from polluted potable water sources a priority. For poverty stricken communities located downstream of the ASGM activities; were river and stream water is the only source of potable water for domestic use, people and animals are at risk of Hg exposure through methylmercury contaminated fish and water consumption as well as through dermal contact. The abundance, adaptability, low cost, easy cultivation and harvest of *Cladophora* sp. algae makes them suitable candidates for heavy metal removal from contaminated waters in developing nations hence, they were tested in this study. Batch adsorption test results revealed that *Cladophora* sp. algae can be used as a low cost but highly effective sorbent material for the removal of Hg from contaminated waters in both single and multi-component solutions. More than 99% extraction efficiency was observed at an Hg concentration of 1.0 mg L^{-1} within 10 min at pH 3 in a single component solution. The rapid uptake of Hg and the high extraction efficiency displayed will result in huge cost savings during industrial and domestic applications and further treatment of the water for Hg removal is not required. However, for a multi-component system, a maximum Hg extraction efficiency of 67.2% was observed after a contact time of 60 min, for an initial cation (Hg^{2+}, Fe^{2+}, Cu^{2+}, Zn^{2+} and Co^{2+}) concentration of 1.0 mg L^{-1} and pH 3. The observed extraction efficiency is still high compared to other studies in literature, for example, Le Faucheur and colleagues (Faucheur et al., 2011). The adsorption selectivity of cations by *Cladophora* sp. was in the order: Hg^{2+} >Fe^{2+}>Cu^{2+}> Zn^{2+} > Co^{2+}. After the adsorption tests, the harvested algae biomass can be used to generate biodiesel or burned to generate heat and electricity after the recovery of the concentrated Hg (Tshumah-Mutingwende, 2014).

Chapter Five

Simulated Hg release and biosorption reactor design

This chapter focuses on simulating Hg release into the water column due to Hg^0 dissolution in freshwaters and also on designing a 1000 L batch reactor for the adsorption of the released Hg.

5.0 Introduction

The Minamata Convention on Hg use founded in October 2013 (UNEP, 2013), was finally enforced in August 2017 (UNEP, 2017). It is centered on protecting human health and the environment from anthropogenic release of Hg and Hg compounds (UNEP, 2017, 2013) With regards to this, this chapter focuses on simulating Hg release into the water column once an Hg^0 droplet of known surface area is discharged into a freshwater body. In order to protect humans from the effects of Hg-contaminated water use, a 1000 L batch reactor for the removal of dissolved Hg from water sources was designed.

5.1 Methodology

This section details the methodology followed together with the assumptions made.

5.1.1 Overall Hg multivariate dissolution model

Based on the dissolution tests findings (**Chapters 2 & 3**), a multivariate Hg^0 dissolution model (Eq. (5.1)) was proposed:

$$\hat{k} = \beta_0 + \beta_1 \log[H_3O^+] + \beta_2[SSA] + \beta_3[SRFA] \; + \; \beta_4 \, log[Re] \qquad (5.1)$$

Where;

$\hat{k}$ – is the predicted Hg^0 dissolution rate coefficient [min^{-1}]

β_0 – is the intercept [-]

$\beta_1, \beta_2, \beta_3 \; and \; \beta_4$ – are the model coefficients [-]

H^+ – solution pH (expressed as the concentration of hydronium ions in solution

SSA - Hg^0 droplet specific surface area [cm^2 cm^{-3}]

SRFA – Suwannee river fulvic acid concentration [mg-C L^{-1}]

Re – Reynolds number [-]

The following hypothesis were tested at the 5% significance level:

$$H_0: \beta_0, \beta_1, \beta_2, \beta_3, \beta_4 = 0 \qquad (5.2)$$

$$H_1: \beta_0, \beta_1, \beta_2, \beta_{3,}, \beta_4 \neq 0 \qquad (5.3)$$

Where;

β_0 – is the intercept

$\beta_1, \beta_2, \beta_3 \; and \; \beta_4$ – are the model coefficients (-)

5.1.2 Parametric sensitivity analysis

The sensitivity of the Hg^0 dissolution rate coefficient model parameters to changes in operational conditions was tested using arbitrary values of pH, Re and Hg^0 droplet surface area. The pH and Re were varied from 3.0 to 8.5 [-] and 13 000 to 95 000 [-] respectively. An Hg^0 droplet specific surface area range of 0.00084 to 0.03 cm^2 cm^{-3} was used. The SRFA concentration was varied from 0 – 150 mg-C L^{-1}. Reference conditions of pH 3 [-] (pH 3 was chosen since that is the optimum pH for Hg biosorption by *Cladophora* sp. (Chapter 4); SRFA concentration: 2 mg-C L^{-1}; Reynolds number: 37453.2 [-] and Hg^0 droplet specific surface area: 0.0015 cm^2 cm^{-3} (Hg^0 dissolution rate coefficient: 0.00075 min^{-1}) were used.

5.1.3 Hg released

The Hg^0 demand by each milling/amalgamation center is estimated to be about 2 kg-Hg^0 per week (Lassen et al., 2016). Since the whole ore amalgamation (WOA) technique on copper plates is mainly used by these ASGMs (Gunson et al., 2006), we assume that 70% (Chouinard and Veiga, 2008) of the Hg^0 used in the amalgamation process is lost into nearby creeks, rivers and streams via tailings Most ASGMs work an average of 7.3 h per day (PACT, 2015). The concentration of Hg released into the water column was calculated by assuming that 20 milling centers discharge Hg^0- rich amalgamation tailings into a creek with a capacity of 1 000 L.

5.1.4 Batch reactor design

By considering the optimum adsorption conditions (**Chapter 4**), a 1000 L batch reactor was designed based on the following assumptions: (i) equilibrium is reached in the batch adsorber (ii) the equilibrium saturation capacities are correlated by the Langmuir equation (iii) equilibrium Hg^{2+} concentration is 6.0 µg L^{-1} (World Health Organization (WHO), 2005) (iv) 1000 L is to be treated per batch and (v) maximum retention time is 10 min (optimum adsorption time). The mass of algae required in a single component system was determined by substituting Eq. (4.6) into Eq. (4.7):

$$m(kg) = [V(C_o - C_e)(1 + bC_e)/1000q_m bC_e\,] \quad (5.4)$$

Where;

$q_e\ (mg - Hg\ g^{-1}\ algae)$ - is the amount of metal adsorbed per gram of adsorbent (algae),

$q_m(mg - Hg\ g^{-1}\ algae)$ - is the amount of adsorption corresponding to complete monolayer coverage (i.e. maximum adsorption capacity)

$b\ (L\ mg^{-1})$ - is the adsorption constant related to binding energy

$C_e(mg\ L^{-1})$ - is the equilibrium metal ion concentration in media

$V(L)$ - is the volume of media

$C_o(mg\ L^{-1})$ - is the initial metal ion concentration in media

5.2 Results and discussions

The results of the overall Hg dissolution rate coefficient and batch reactor design amongst others are reported and discussed in this section.

5.2.1 Overall Hg multivariate dissolution model

Based on the pH (Chapters 2 (Fig. 2.3 C) & 3 (Fig. 3.2 B)), Re (Fig. 2.7), Hg^0 droplet specific surface area (Fig. 2.4C) and SRFA concentration (Fig. 3.5 B) dissolution results; an overall Hg^0 multivariate dissolution model was proposed:

$$\hat{k} = -2.6\times10^{-3} + 7.3\times10^{-4}\log[Re] + 8.3\times10^{-5}\log H_3O^+ + 0.12[SSA] + 3.7\times10^{-5}[SRFA] \quad (5.5)$$

But;

$$pH = -\log[H_3O^+] \quad (2.8)$$

Thus;

$$\hat{k} = -2.6\times10^{-3} + 7.3\times10^{-4}\log[Re] - 8.3\times10^{-5}pH + 0.12[SSA] + 3.7\times10^{-5}[SRFA] \quad (5.6)$$

The model adjusted R^2 of 0.98 implies that the regression is a good fit. Also, as shown in Table 5.1, the p-values of the model coefficients were less than 0.05, thus, H_0 was rejected.

Table 5.1: ANOVA statistical analysis results

	df	*SS*	*MS*	*F*
Regression	4	4.3×10^{-6}	1.1×10^{-6}	386.1
Residual	24	6.7×10^{-8}	2.8×10^{-9}	
Total	28	4.4×10^{-6}		

	Coefficients	*Standard Error*	*t Stat*	*P-value*
Intercept	-2.6×10^{-3}	1.6×10^{-4}	-16.4	1.4×10^{-14}
log [pH] [-]	8.3×10^{-5}	4.4×10^{-6}	18.8	7.3×10^{-16}
SRFA concentration [mg-C L^{-1}]	3.7×10^{-5}	1.6×10^{-6}	23.3	5.3×10^{-18}
log [Re] [-]	7.3×10^{-4}	3.7×10^{-5}	19.8	2.2×10^{-16}
Hg^0 droplet specific surface area [cm^2 cm^{-3}]	0.12	6.6×10^{-3}	18.8	7.6×10^{-16}

5.2.1.1 Model evaluation

The predicted Hg^0 dissolution rate coefficient was close to the experimental values (R^2: 0.98) (Fig. 5.1). Thus, for a known Hg^0 droplet specific surface area, Re, pH and SRFA (humic substances) concentration, this model can be used to determine the Hg^0 dissolution rate coefficient.

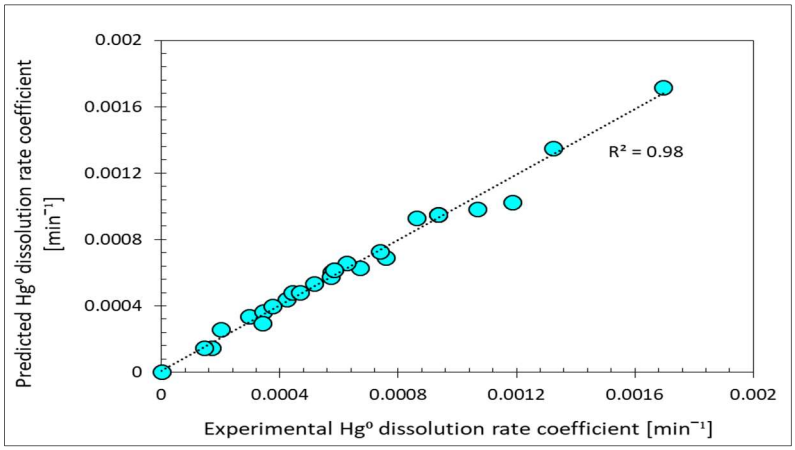

Fig.5.1: Comparison of observed and predicted data

5.2.1.2 Heteroscedasticity test of error terms

From an eye observation of the plot of residuals (Fig. 5.2), the possibility of heteroscedasticity was suspected.

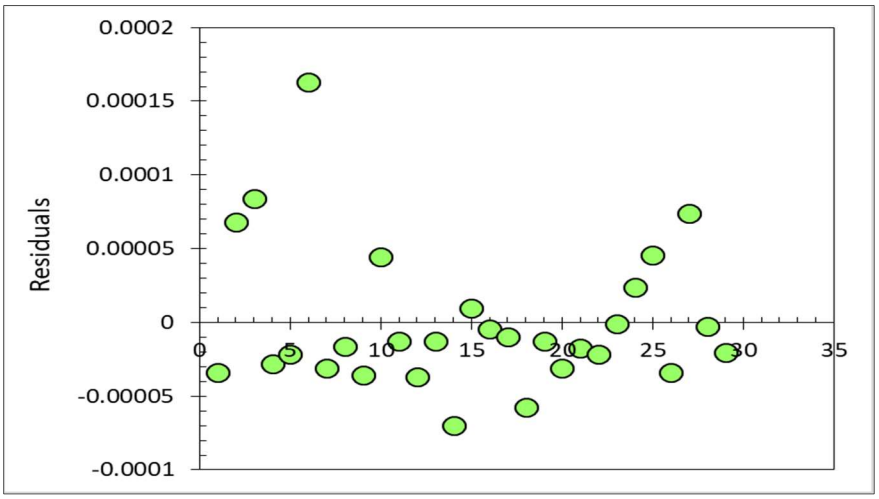

Fig. 5.2: Plot of the residuals

Thus, it was tested on the 5% significance level based on the following hypotheses:

$$H_0: the\ residuals\ are\ homoscedastic$$

$$H_1: the\ residuals\ are\ heteroscedastic$$

For both the Breusch-Pagan and White heteroscedasticity test models, the computed p-values (0.72 and 0.07 for the Breusch-Pagan and White test respectively) are greater than the significance level ($\alpha = 0.05$) (Table 5.2), thus, the residuals are homoscedastic and the null hypothesis (H_0) cannot be rejected.

Table 5.2: Heteroscedasticity test results

Parameter	Breusch-Pagan test	White test
LM (Observed value)	2.1	22.7
LM (Critical value)	9.5	23.7
DF	4	14
p-value (Two-tailed)	0.72	0.07
alpha	0.05	0.05

5.2.2 Parametric sensitivity analysis

The parametric sensitivity analysis revealed that the Hg^0 dissolution rate coefficient is sensitive to variations in SRFA concentration (0.00068 – 0.0062), pH (0.00029 – 0.00075), Re (0.00042 – 0.0010) and Hg^0 droplet specific surface area (0.00057 – 0.0043). They all resulted in an order of magnitude range difference in the simulated Hg^0 dissolution rate coefficient except for variations in pH which did not result in any order of magnitude range difference (Fig. 5.3).

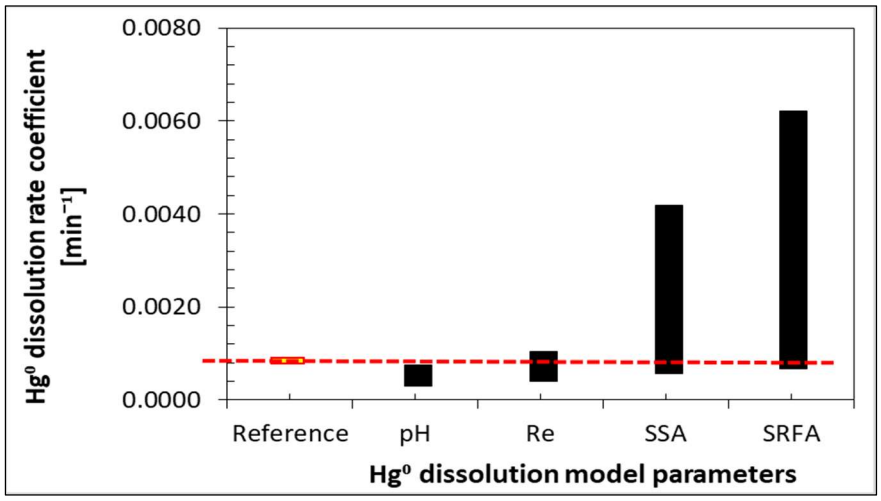

Fig.5.3: Sensitivity Analysis of Hg^0-dissolution model parameters

5.2.3 Hg released

The total Hg concentration released into the water column of a 1 000 L creek (pH 3) by an Hg^0 droplet with a specific surface area of 0.025 cm^2 cm^{-3}, dissolving at a rate of 0.0036 min^{-1} is 0.033 mg L^{-1}. Experimental observations in Chapter 3 revealed that acidic conditions do not favor the formation of Hg-SRFA soluble organic complex (Hg_{OC}); thus; we assume that 80% of the Hg in

solution is inorganic Hg^{2+} and 20% is in the form of Hg_{OC}. Thus, the total dissolved Hg concentration in the form of Hg^{2+} will be 0.026 mg-Hg L^{-1}.

5.2.4 Batch reactor design

Assuming that Hg biogeochemical processes (such as methylation and reduction) which depend on the presence of Hg^{2+} in environmental media are dormant; the mass of algae required at each initial concentration (C_0) in order to achieve the WHO standard of 0.006 mg-Hg L^{-1} was determined (Table 5.3). Generally, the mass of algae required increased with an increase in C_0. About 4 kg of *Cladophora* sp. algae is required for the removal of Hg in order to achieve the WHO standard of 0.006 mg-Hg L^{-1} when the C_0 is 0.26 mg-Hg L^{-1} compared to 0.32 kg when the C_0 is 0.026 mg-Hg L^{-1}. Favourable biosorption (large amount of adsorption at low Hg^{2+} concentrations (Gabelman, 2017)) of Hg^{2+} is expected to occur since the dimensionless separation coefficient (R_L) is between 0 and 1 $(0 < R_L < 1)$ (Hall et al., 1966).

Table 5.3 Mass of algae required for the different model scenarios

C_0 (Hg^{2+}) (mg-Hg L^{-1})	C_e (Hg^{2+}) (mg-Hg L^{-1})	Mass (kg)	R_L 1/(1+bCo) [-]
0.026	0.006	0.32	0.75
0.26	0.006	4.06	0.23
2.63	0.006	41.43	0.03

5.3 Conclusions

Hg release and potential adsorption of Hg^{2+} in a 1000 L batch reactor was simulated based on the results obtained in ***Chapters 2-4***. The overall model sensitivity analysis revealed that, the Hg^0 dissolution rate coefficient is sensitive to variations in SRFA concentration, Hg^0 droplet specific surface area and Re; for which a single order of magnitude range difference was observed in the simulated results. The required mass of algae in a 1000 L batch reactor depended on the concentration of Hg^{2+} available in solution and it increased with increase in concentration. About 4 kg of *Cladophora* sp. algae is required for the removal of Hg when the initial concentration is 0.26 mg-Hg L^{-1} in order to achieve the WHO standard of 0.006 mg-Hg L^{-1}.

Chapter Six

Conclusions and Recommendations

The general and overall conclusions of this study together with recommendations for future studies and or preventative measures for further Hg^0 pollution in ASGM sites are given in this chapter.

6.1 Overall Conclusions

Artisanal and small-scale gold mining is undeniable a lucrative source of income to impoverished communities of developing countries. However, owing to the unregulated use of Hg^0 and the lack of reputable Hg^0-rich amalgamation tailings disposal facilities, its negative effects on the environment and human health tend to tarnish its economic benefits. Owing to the slow dissolution of Hg^0 in freshwaters, it is estimated that Hg^0 dissolution will continue for at least 40 years in previously contaminated freshwaters; even after Hg^0 use is banned and or completely substituted by non-Hg^0 gold mining methods such as the borax box. However, in the presence of humic substances dissolution will continue for at least 31 years but more Hg will be released into the water column. Thus, Hg environmental risk must always be considered and contaminated freshwaters must be monitored continuously. *Cladophora* sp. algae can be successfully used as cheap but highly effective biosorbent for the removal of Hg from contaminated freshwaters.

6.1.1 General conclusions

Chapter 2: The effect of freshwater physio-chemical properties such as pH, Re and the Hg droplet specific surface area discharged into the aquatic system as a result of ASGM was investigated. It was concluded that acidic waters which are turbulent and a large droplet surface area results in a rapid dissolution. Based on the parametric sensitivity analysis, Hg^0 dissolution is expected to continue for at 40 - 62 years in already contaminated freshwaters. Therefore, there is need to pay continuous attention to Hg environmental risk.

Chapter 3: Owing to the abundance of humic substances in the freshwater column and their tendency to influence several factors of the Hg biogeochemical cycle such as solubility, speciation and toxicity; their effect on the Hg dissolution rate coefficient was investigated using commercially available Suwannee river fulvic acid (SRFA). It was concluded that irrespective of the presence or absence of SRFA, acidic conditions enhance the dissolution of Hg in freshwaters. However, the formation of water soluble organic Hg-SRFA complexes increased with increase in pH. Ionic strength did not result in any significant increase in the dissolution rate coefficient. Furthermore, the Hg_T, dissolution rate coefficient and the concentration of Hg-SRFA soluble organic complexes was proportional to the concentration of SRFA. Compared to dissolution tests in the absence of humic substances (Chapter 2); Hg^0 dissolution is expected to continue for at 31 - 48 years in

already contaminated freshwaters. Though the estimated dissolution time is shorter, more Hg will be released into the water column. Thus, there is need to pay continuous attention to Hg environmental risk.

Chapter 4: The potential use of an abundant algae in freshwaters (*Cladophora* sp.) as an Hg biosorbent was investigated. A rapid uptake of Hg from solution was observed at low pH (pH 3) and a high extraction efficiency of more than 99% was observed within the first 5 mins of contact; with equilibrium being attained after 10 mins. Thus, it was concluded that *Cladophora* sp. algae can be successfully used as a low cost but highly effective sorbent material for the removal of mercury from acidic waters.

Chapter 5: Hg release and potential adsorption of Hg^{2+} in a 1000 L batch reactor was simulated based on the results obtained in ***Chapters 2-4***. The required mass of algae on depended on the concentration of Hg^{2+} available in solution and it increased with increase in concentration. About 4 kg of *Cladophora* sp. algae is required for the removal of Hg in order to achieve the WHO standard of 0.006 mg-Hg L^{-1} when the initial Hg concentration is 0.26 mg-Hg L^{-1}.

6.2 Recommendations for further studies

1. The reducing effect of SRFA on dissolved Hg under acidic dark conditions must be investigated further. This is best done in a laboratory equipped with an Hg speciation analyzer machine such as a Milestone's direct analyzer, DMA 80 (Direct Mercury Analyzer) which can distinguish various Hg species by their release at different temperature ranges or by using an atomic absorption spectrometer (CG Analytica, model GBC 392 AA) coupled with a homemade thermal desorption oven (TDAAS). Differences in the Hg species can be determined by comparing the obtained thermal desorption profiles with the standard Hg profiles from literature (Milestone, 2019; Windmoller et al., 2017).
2. Cost reductions for large scale use can be achieved by the use of *Cladophora* sp. for the removal of mercury together with precious metals such as gold and silver which are present in trace quantities and can be recovered from algae; this possibility must be explored.
3. One of the limitations of this study is that the effect of pH on metabolic processes such as growth and reproduction (cell multiplication) were not quantified for the duration of the

dissolution tests. Thus, it is difficult to conclude if biosorption at pH 3 was metabolic - dependent or not. Therefore, we recommend that, the adaptive response of algae to Hg exposure with changing metabolism and photosynthesis be studied further at different environmental pHs.

6.2.1 Recommendations for preventing further Hg pollution in ASGM sites

1. Without advanced and ecologically friendly mine waste disposal facilities, ASGM will continue to discharge Hg^0-rich amalgamation tailings into nearby freshwaters. Thus, environmental agencies in the concerned countries must put such disposal facilities in ASGM sites.
2. Increased awareness on the consequences of reckless Hg^0 use on human health and the environment.
3. Local governments must increase availability and also subsidize the cost of chemical borax 'sodium borate', shaking tables, sluice boxes, spiral concentrators, and Hg retorts in order to facilitate a shift to non-Hg^0 and or reduced Hg^0 use ASGM technologies. Expertise training on how to use these alternative must also be readily available.
4. Stringent penalties and laws must be enforced on ASGM and medium scale miners who continuously use and pollute the environment with Hg^0. For example, according to the Environmental Management Act Cap (20:27); the current law in Zimbabwe which governs Hg^0 acquisition and use only states that; any person who imports, transports, stores or sells any hazardous substance (such as Hg) must have a license for each purpose. Such a regulation is not stringent enough to prohibit the illegal acquisition, trade and use of Hg^0.

References

Akkanen, J., 2002. Does dissolved organic matter matter? – Implications for bioavailability of organic chemicals. University of Joensuu.

Al-rub, F.A.A., Ashour, I., 2006. Biosorption of copper on Chlorella vulgaris from single , binary and ternary metal aqueous solutions 41, 457–464. https://doi.org/10.1016/j.procbio.2005.07.018

Alberts, J.J., Schindler, J.E., Miller, R.W., 1974. Elemental Mercury Evolution Mediated by Humic Acid. Science (80-.). 184, 895–897.

Alloway, B.., 1995. Heavy Metals in Soils, 2nd ed. Blackie Academic and Professional, London.

AMAP/UNEP, 2013. Technical Background Report for the Global Mercury Assessment 2013, Arctic Monitoring and Assessment Programme. Oslo, Norway/UNEP Chemicals Branch, Geneva, Switzerland.

Amyot, M., Morel, F.M.M., Ariya, P.A., 2005. Dark oxidation of dissolved and liquid elemental mercury in aquatic environments. Environ. Sci. Technol. 39, 110–114. https://doi.org/10.1021/es035444k

Andrade, A.D., Nobrega, J.A., 2005. Proton and metal binding capacity of the green freshwater alga Chaetophora elegans 40, 1931–1936. https://doi.org/10.1016/j.procbio.2004.07.007

Appleton, J.D., Williams, T.M., Breward, N., Apostol, A., Miguel, J., 1999. Mercury contamination associated with artisanal gold mining on the island of Mindanao , the Philippines 95–109.

Barsanti, L., Gualtieri, P., 2006. Algae: Anatomy, Biochemistry and Biotechnology, 2nd ed. Taylor and Francis, Boca Raton, FL.

Behar, S., 1996. Testing the Waters: Chemical and Physical Vital Signs of a River. River Watch Network, Montpelier, VT.

Bilal, M., Rasheed, T., Eduardo, J., 2018. Biosorption : An Interplay between Marine Algae and Potentially Toxic Elements — A Review. Mar. Drugs 16, 1–16. https://doi.org/10.3390/md16020065

Billaud, P., Laperche, V., Boudou, A., Maury-Brachet, R., Shoko, D., Kahwai, S., Freyssinet, P., 2004. Removal of barriers to the introduction of cleaner artisanal gold mining and extraction technologies in the Kadoma-Chakari area, Zimbabwe. Part A: Environmental assessment – Final Report.

Bloom, N.S., 1992. On the Chemical Form of Mercury in Edible Fish and Marine Invertebrate Tissue. Can. J. Fish. Aquat. Sci. 49, 1010–1017. https://doi.org/10.1139/f92-113

Boese-O´Reilly, S., Dahlmann, F., Lettmeier, B., Drasch, G., 2004. Removal of barriers to the introduction of cleaner artisanal gold mining and extraction technologie in Kadoma, Zimbabwe Part B: Health Assessment Final Report, UNIDO Project EG/GLO/01/G34 No.03/089 BRGM Project Nr 822657-3. Munich.

Boggs, S., Livermore, D., Seltz, M.G., 1985. Humic substances in natural waters and their complexation

with trace metals and radionuclides: A Review. Illinois.

Büchs, J., Maier, U., Milbradt, C., Zoels, B., 2000. Power consumption in shaking flasks on rotary shaking machines: I. Power consumption measurement in unbaffled flasks at low liquid viscosity. Biotechnol. Bioeng. 68, 589–593. https://doi.org/10.1002/(SICI)1097-0290(20000620)68:6<589::AID-BIT1>3.0.CO;2-J

Burkstaller, J.E., McCarty, P.L., Parks, G.A., 1975. Oxidation of Cinnabar by Fe(III) in Acid Mine Waters. Environ. Sci. Technol. 9, 676–678. https://doi.org/10.1021/es60105a004

Canela, M.C., Jardim, W.F., 1997. The Fate of Hg^0 in Natural Waters Intro duc ti on Expe ri men tal. J. Braz. Chem. Soc. 8, 421–426.

Castilhos, Z.C., Rodrigues-filho, S., Paula, A., Rodrigues, C., Villas-bôas, R.C., Siegel, S., Veiga, M.M., Beinhoff, C., 2006. Mercury contamination in fish from gold mining areas in Indonesia and human health risk assessment 368, 320–325. https://doi.org/10.1016/j.scitotenv.2006.01.039

Chakraborty, P., Vudamala, K., 2015. Reduction of mercury (II) by humic substances — influence of pH , salinity of aquatic system 10529–10538. https://doi.org/10.1007/s11356-015-4258-4

Chouinard, R., Veiga, M.M., 2008. Results of the Awareness Campaign and Technology Demonstration for Artisanal Gold Miners: Summary Report. Vienna.

Culture collection of alagae and protozoa (CCAP), 2013. List of media used to maintain strains at CCAP. Acidified Bold-Basal Medium with vitamins (ABM modified) [WWW Document]. URL www.ccap.ac.uk/media/pdfrecipes/ABM.htm (accessed 6.20.13).

De Haan, H., Jones, R.I., Salonen, K., 1987. Does ionic strength affect the configuration of aquatic humic substances , as indicated by gel filtration? Freshw. Biol. 17, 453–459. https://doi.org/10.1111/j.1365-2427.1987.tb01066.x

Deng, L., Su, Y., Su, H., Wang, X., Zhu, X., 2007. Sorption and desorption of lead (II) from wastewater by green algae Cladophora fascicularis 143, 220–225. https://doi.org/10.1016/j.jhazmat.2006.09.009

Drasch, G., Boese-O´Reilly, S., Beinhoff, C., Roider, G., Maydl, S., 2001. The Mt . Diwata study on the Philippines 1999 □ assessing mercury intoxication of the population by small scale gold mining.

Dutta, B.K., 2007. Principles of mass transfer and separation processes. Asoke K. Ghosh, PHI L earning Private Limited, New Delhi.

EPA, U.S.E.P.A., 2019. Health Effects of Exposures to Mercury [WWW Document]. URL https://www.epa.gov/mercury/health-effects-exposures-mercury#methyl (accessed 11.26.19).

Esdaile, L.J., Chalker, J.M., 2018. The Mercury Problem in Artisanal and Small-Scale Gold Mining 6905–6916. https://doi.org/10.1002/chem.201704840

Esmaeili, A., Saremnia, B., Kalantari, M., 2015. Removal of mercury (II) from aqueous solutions by biosorption on the biomass of Sargassum glaucescens and Gracilaria corticata. Arab. J. Chem. 8,

506–511. https://doi.org/10.1016/j.arabjc.2012.01.008

Faucheur, L., Tremblay, B.Y., A, C.C.F., 2011. Acidification increases mercury uptake by a freshwater alga , Chlamydomonas reinhardtii Acidification increases mercury uptake by a freshwater alga , Chlamydomonas reinhardtii. https://doi.org/10.1071/EN11006

Fitzgerald, W.., Clarkson, T.., 1991. Mercury and monomethyl mercury: present and future concerns. Environ. Health Perspect. 96, 159–166.

Freundlich, H.M.., 1907. Über die Adsorption in Lösungen. Zeitschrift für Phys. Chemie - Stöchiometrie und Verwandschaftslehre 57, 385–470.

Gabelman, A., 2017. Adsorption Basics: Part 1.

Gafur, N.A., Sakakibara, M., Sano, S., Sera, K., 2018. A Case Study of Heavy Metal Pollution in Water of Bone River by Artisanal Small-Scale Gold Mine 1–10. https://doi.org/10.3390/w10111507

Ghosh, K., Schinitzer, M., 1979. UV and Visible Absorption Spectroscopic Investigations in Relation to Macromolecular Characteristics of Humic Substances. Soil Sci. 30, 735–745. https://doi.org/https://doi.org/10.1111/j.1365-2389.1979.tb01023.x

Glew, D.N., Hames, D. a., 1971. Aqueous Nonelectrolyte Solutions. Part X. Mercury Solubility in Water. Can. J. Chem. 49, 3114–3118. https://doi.org/10.1139/v71-520

Goldman, C.R., Horne, A.J., 1983. Limnology. McGraw-Hill Book Co., New York.

Gunson, A., Thompson, M., Baker, R., Veiga, M.M., Spiegel, S., Cannon, M., 2006. Environmental and Health Assessment Report – Removal of Barriers to the Introduction of Cleaner Artisanal Gold Mining and Extraction Technologies. Vienna.

Hajahmadi, Z., Younesi, H., Bahramifar, N., Khakpour, H., 2015. Multicomponent isotherm for biosorption of Zn (II), CO (II) and Cd (II) from ternary mixture onto pretreated dried Aspergillus niger biomass. Water Resour. Ind. 11, 71–80. https://doi.org/10.1016/j.wri.2015.07.003

Hall, K.R., Eagleton, L.C., Acrivos, A., Vermeulen, T., 1966. Pore and solid diffusion Kinetics in fixed bed adsorption under constant pattern conditions. Ind. Eng. Chem. Fundam. 5, 212–223.

Henriques, B., Rocha, L.S., Lopes, C.B., Figueira, P., Monteiro, R.J.R., Duarte, A.C., Pardal, M.A., Pereira, E., 2015. Study on bioaccumulation and biosorption of mercury by living marine macroalgae : Prospecting for a new remediation biotechnology applied to saline waters. Chem. Eng. J. 281, 759–770. https://doi.org/10.1016/j.cej.2015.07.013

Hessen, D.O., Tranvik, L.J., 1998. Aquatic Humic Substances: Ecology and Biogeochemistry, 1st ed. Springer, Berlin, Heidelberg. https://doi.org/doi.org/10.1007/978-3-662-03736-2

Ho, Y.S., Mckay, G., 1999. Pseudo-second order model for sorption processes 34, 451–465.

IHSS, I.H.S.S., 2018. Elemental Compositions and Stable Isotopic Ratios of IHSS Samples [WWW Document]. URL https://humic-substances.org/elemental-compositions-and-stable-isotopic-ratios-

of-ihss-samples/ (accessed 2.16.18).

Janssen, P.H.M., Heuberger, P.S.C., 1995. Calibration of process-oriented models. Ecol. Modell. 83, 55–66. https://doi.org/10.1016/0304-3800(95)00084-9

Ji, L., Xie, S., Feng, J., Li, Y., Chen, L., 2012. Heavy metal uptake capacities by the common freshwater green alga Cladophora fracta 979–983. https://doi.org/10.1007/s10811-011-9721-0

Johnson, M., Shivkumar, S., Berlowitz-tarrant, L., 1996. Structure and properties of filamentous green algae 38, 103–108.

Jones, A.V., Clemmet, M., Highton, A., Golding, E., 1999. Access to Chemistry. The Royal Society of Chemistry, Cambridge.

Kelly, C.A., 2003. Effect of pH on Mercury Uptake by an Aquatic Bacterium : Implications for Hg Effect of pH on Mercury Uptake by an Aquatic Bacterium : Implications for Hg Cycling. https://doi.org/10.1021/es026366o

Kinniburgh, D.G., van Riemsdijk, W.H., Koopal, L.K., Benedetti, M.F., 1998. Ion Binding to Humic Substances: Measurements, Models, and Mechanisms, in: Adsorption of Metals by Geomedia. Elsevier, pp. 483–520. https://doi.org/10.1016/B978-012384245-9/50024-4

Klucakova, M., Lapcikova, B., Kucerik, J., 2000. Structure and properties of humic and fulvic acids . I . Properties and reactivity of humic acids and fulvic acids.

Lagergren., S., 1898. About the theory of so-called adsorption of soluble substances. K. Suensk Vetenskapsakademiens Handl. 241, 1–39.

Langmuir, I., 1918. The adsorption of gases on plane surfaces of glass, mica and platinum. J. Am. Chem. Soc. 40, 1361–1403.

Lassen, C., Warming, M., Maag, J., Jønsson, J.B., 2016. Mercury trade and use for artisanal and small-scale gold mining in Sub- Saharan Africa, Final Report. Kongens Lyngby.

Lewis, G.N., Randall, M., 1921. The activity coefficient of strong electrolytes. J. Am. Chem. Soc. 43, 1112–1154.

Li, Y., Du, Q., Liu, T., Sun, J., Jiao, Y., Xia, Y., Xia, L., Wang, Z., Zhang, W., Wang, K., Zhu, H., Wu, D., 2012. Equilibrium , kinetic and thermodynamic studies on the adsorption of phenol onto graphene. Mater. Res. Bull. 47, 1898–1904. https://doi.org/10.1016/j.materresbull.2012.04.021

Loux, N.T., 1998. An assessment of mercury-species-dependent binding with natural organic carbon. Chem. Speciat. Bioavailab. 10, 127–136. https://doi.org/10.3184/095422998782775754

MacCarthy, P., Suffet, I.H. (Mel), 1988. Aquatic Humic Substances and Their Influence on the Fate and Treatment of Pollutants, in: Aquatic Humic Substances: Advances in Chemistry. American Chemical Society, Washington, DC, pp. xiii–xxx. https://doi.org/10.1021/ba-1988-0219.pr001

Macingova, E., Luptakova, A., Schutz, T., 2012. Sulphates Removal from Acid Mine Drainage, in: The

12th International Multidisciplinary Scientific Geoconference (SGEM 2012). Albena, Bulgaria, pp. 825–831.

Malm, O., Branches, F.J.., Akagi, H., Castro, M.B., Pfeiffer, W.C., Harada, M., Bastos, W.R., Kato, H., 1995. Mercury and methylmercury in fish and human hair from the Tapajos river basin, Brazil. Sci. Total Environ. 75, 141–150.

Manohar, D.M., Krishnan, K.A., Anirudhan, T.S., 2002. Removal of mercury (II) from aqueous solutions and chlor-alkali industry wastewater using 36, 1609–1619.

Meech, J.A., Veiga, M.M., Tromans, D., 1998. Reactivity of Mercury from Gold Mining Activities in Darkwater Ecosystems. Springer behalf R. Swedish Acad. Sci. 27, 92–98.

Mehta, S.K., Gaur, J.., 2005. Use of Algae for Removing Heavy Metal Ions From Wastewater : Progress and Use of Algae for Removing Heavy Metal Ions From Wastewater : Progress and Prospects. Crit. Rev. Biotechnol. 25, 113–152. https://doi.org/10.1080/07388550500248571

Melamed, R., Bas, R.C.V., Gon, G.O., Paiva, E.C., 1997. Mechanisms of physico-chemical interaction of mercury with fiver sediments from a gold mining region in Brazil : Relative mobility of mercury species 58, 119–124.

Melamed, R., Trigueiro, F.E., Villas Bôas, R.C., 2000. The effect of humic acid on mercury solubility and complexation. Appl. Organomet. Chem. 14, 473–476. https://doi.org/10.1002/1099-0739(200009)14:9<473::AID-AOC25>3.0.CO;2-W

Milestone, 2019. DMA-80 evo [WWW Document]. URL https://www.milestonesrl.com/products/mercury-determination/dma-80-evo (accessed 12.6.19).

Mohamed, A.M.O., Anita, H.., 1998. Developments in Geotechnical Engineering. Geoenvironmental Engineering.

Monperrus, M., Tessier, E., Veschambre, S., Amouroux, D., Donard, O., 2005. Simultaneous speciation of mercury and butyltin compounds in natural waters and snow by propylation and species-specific isotope dilution mass spectrometry analysis. Anal. Bioanal. Chem. 381, 854–862.

Morel, F.M.M., Kraepiel, A.M.L., Amyot, M., 1998. the Chemical Cycle and Bioaccumulation of Mercury. Annu. Rev. Ecol. Syst. 29, 543–566. https://doi.org/10.1146/annurev.ecolsys.29.1.543

Mudyazhezha, S., Kanhukamwe, R., 2014. Environmental Monitoring of the Effects of Conventional and Artisanal Gold Mining on Water Quality in Ngwabalozi River, Southern Zimbabwe. Int. J. Eng. Appl. Sci. 4, 13–18.

Noyes, A.A., Whitney, W.R., 1897. The rate of solution of solid substances in their own solutions. J. Am. Chem. Soc. 19, 930–934. https://doi.org/10.1021/ja02086a003

Nsimba, E.B., 2012. Development of a biophysical system based on bentonite, zeolite and micro-organisms for remediating gold mine wastewaters and tailings ponds. University of the

Witwatersrand, Johannesburg.

Oriekhova, O., Stoll, S., 2016. Chemosphere Effects of pH and fulvic acids concentration on the stability of fulvic acids – cerium (IV) oxide nanoparticle complexes 144, 131–137. https://doi.org/10.1016/j.chemosphere.2015.08.057

PACT, 2015. A Golden Opportunity: Scoping Study of Artisanal and Small Scale Gold Mining in Zimbabwe. Washington, DC.

Pagano, T., Bida, M., Kenny, J.E., 2014. Trends in levels of allochthonous dissolved organic carbon in natural water: A review of potential mechanisms under a changing climate. Water (Switzerland) 6, 2862–2897. https://doi.org/10.3390/w6102862

Pansamrit, K. Ruangsomboon, S., 2010. Effect of pH on biosorption of basic dye Malachite green, in: The 8th International Symposium on Biocontrol and Biotechnolgy. Prattaya, Thailand, pp. 220–223.

Persaud, A., Telmer, K., 2015. Developing Baseline Estimates of Mercury Use in Artisanal and Small-scale Golg Mining Communities: A Practical Guide (Version 1.0), Artisanal Gold Council. Victoria, BC, Canada.

Plaza, J., Viera, M., Donati, E., Guibal, E., 2011. Biosorption of mercury by Macrocystis pyrifera and Undaria pinnatifida : Influence of zinc , cadmium and nickel. J. Environ. Sci. 23, 1778–1786. https://doi.org/10.1016/S1001-0742(10)60650-X

Ravichandran, M., 2004a. Interactions between mercury and dissolved organic matter — a review 55, 319–331. https://doi.org/10.1016/j.chemosphere.2003.11.011

Ravichandran, M., 2004b. Interactions between mercury and dissolved organic matter - A review. Chemosphere 55, 319–331. https://doi.org/10.1016/j.chemosphere.2003.11.011

Ravichandran, M., Aiken, G., Reddy, M., Ryan, J., 1998. Enhanced Dissolution of Cinnabar (Mercuric Sulfide) by Dissolved Organic Matter Isolated from the Florida Everglades. Environ. Sci. Technol. 32, 3305–3311. https://doi.org/10.1016/j.imlet.2006.02.006

Rezaee, A., Ramavandi, B., 2006. Biosorption of Mercury by Biomass of Filamentous Algae Spirogyra Species. https://doi.org/10.3923/jbs.2006.695.700

Salonen, J., Seppanen, K., Nyyssonen, K., Korpela, H., Kauhanen, J., Kantola, M., 1995. Intake of mercury from fish, lipid peroxidation, and the risk of myocardial infarction and coronary, cardiovascular and any death in Eastern Finnish men. Circulation 91, 645–655.

Sanemasa, I., 1977. Kinetics of the disproportionation reaction of mercury(I) in alkaline solutions 16, 2786–2788. https://doi.org/10.1021/ic50177a022

Satyanarayana, T., Johri, B.N., Prakash, A., 2012. Microorganisms in Environmental Management. Springer, Dordrecht. https://doi.org/doi.org/10.1007/978-94-007-2229-3

Schnitzer, M., Kerndorff, H., 1981. Reactions of fulvic acid with metal ions. Water. Air. Soil Pollut. 15,

97–108.

Shanab, S., Essa, A., Shalaby, E., 2012. by some microalgae species (Egyptian Isolates) Do not distribute . 1–8.

Silva, H.S., Ruiz, S.V., Granados, D.L., Santángelo, J.M., Nacional, U., Juan, D.S., 2010. Adsorption of Mercury (II) from Liquid Solutions Using Modified Activated Carbons 13, 129–134.

Skousen, J., Hilton, T., Faulkner, B., 1990. Overview of Acid Mine Drainage Treatment with Chemicals [WWW Document]. URL www.wvu.edu/~agexten/landrec/chemtrt.htm (accessed 2.24.15).

Stevenson, F.J., Cole, M.A., 1999. Cycles of soil: Carbon, Nitrogen, Phosphorus, Sulfur, Micronutrients, 2nd ed. John Wiley & Sons, INC, New York.

Stoffersen, B., Wu, P., Na-Oy, L.D., Sekamane, A.S., Ruiz, Z.I., Koster-Rasmussen, R., 2018. Introduction of Mercury-Free Gold Extraction to Small-Scale Miners in the Cabo Delgado Province in Mozambique. J. Heal. Pollut. 8, 1–5.

Strydom, H.A., King, N.., 2009. Environmental Management in South Africa, 2nd Revise. ed. Cape Town, South Africa.

Sullivan, J.B.J., Krieger, G.R., 2001. Clinical Environmental Health and Toxic Exposures, 2nd ed. Lippincott Williams and Wilkins, Philadephia.

Takahashi, F., 2017. Uncertainty analysis of simulated mercury exposure using a mercury environmental fate model for environmental risk estimate. J. Japan Soc. Civ. Eng. 73, 307–314.

Telmer, K., Veiga, M.M., 2009. World Emissions of Mercury from Artisanal and Small Scale Gold Mining, in: Pirrone, N., Mason, R. (Eds.), Mercury Fate and Transport in the Global Atmosphere Emissions,Measurements and Models. Springer Science+Business Media, Dordrecht, Heidelberg, London, New York, pp. 131–172. https://doi.org/10.1007/978-0-387-93958-2_6

Thurman, E.M., 1985. Developments in Biogeochemistry: Organic Geochemistry of Natural Waters. Martinus Nijhoff/Dr W. Junk Publishers, Dordrecht. https://doi.org/10.1007/978-94-009-5095-5

Tipping, E., 2002. Cation binding by humic substances. Cambridge University Press, Cambridge. https://doi.org/10.1017/CBO9780511535598

Tiwari, D.P., Singh, D.K., Saksena, D.., 1995. Hg(II) Adsorption from Aqueous Solutions Using Rice-Husk Ash. J. Environ. Eng. 121.

Tromans, D., Meech, J.A., Veiga, M.M., 1996. Natural Organics and the Environmental Stability of Mercury: Electrochemical Considerations. J. Electrochem. Soc. 143, L123-126. https://doi.org/10.1149/1.1836897

Tshumah-Mutingwende, R.R.M.., 2014. Assessment of Algae as Mercury Bioindicators in Acid Mine Drainage waters and their potential for Phytoremediation. University of the Witwatersrand, Johannesburg, South Africa.

Tshumah-Mutingwende, R.R.M.S., Takahashi, F., 2019. Physio-chemical effects of freshwaters on the dissolution of elementary mercury. Environ. Pollut. https://doi.org/10.1016/j.envpol.2019.05.130

U. S. Geological Survey, 1995. Mercury contamination of aquatic ecosystems: U. S. Geological Survey Fact Sheet FS-216-95.

U.S. Environmental Protection Agency (U.S. EPA), 1999. Understanding Variation in Partition Coefficient, Kd, values, The Kd Model, Methods of Measurement, and Application of Chemical Reaction Codes [WWW Document]. Vol. 1. URL https://www.orau.org/PTP/PTP Library/library/Subject/Environmental/kdsa.p%0Adf (accessed 11.30.13).

Udayabhanu, S.G., Prasad, B., 2010. Studies on Environmental Impact of Acid Mine Drainage Generation and its Treatment: An Appraisal. Indian J. Envionmental Prot. 30, 953–967.

UNEP, U.N.E.P., 2017. At a glance : Minamata Convention on Mercury. Geneva.

UNEP, U.N.E.P., 2013. Minamata Convention on Mercury Text and Annexes, Minamata Convention on Mercury. Geneva.

United States Environmental Protection Agency, U., 2002. Method 1631, Revision E: Mercury in Water by Oxidation, Purge and Trap, and Cold Vapor Atomic Fluorescence Spectrometry. Washington, DC.

Veglio, F., Beolchini, F., 1997. Removal of metals by biosorption : a review 44, 301–316.

Veiga, M.M., Angeloci, G., Hitch, M., Velasquez-lopez, P.C., 2014. Processing centres in artisanal gold mining. J. Clean. Prod. 64, 535–544. https://doi.org/10.1016/j.jclepro.2013.08.015

Veiga, M.M., Baker, R.F., 2004. Protocols for Environmental and Health Assessment of Mercury Released by Artisanal and Small-Scale Gold Miners. Vienna.

Veiga, M.M., Maxson, P.A., Hylander, L.D., 2006. Origin and consumption of mercury in small-scale gold mining. J. Clean. Prod. 14, 436–447. https://doi.org/10.1016/J.JCLEPRO.2004.08.010

Waples, J.S., Nagy, K.L., Aiken, G.R., Ryan, J.N., 2005. Dissolution of cinnabar (HgS) in the presence of natural organic matter. Geochim. Cosmochim. Acta 69, 1575–1588. https://doi.org/10.1016/j.gca.2004.09.029

Weber, W.J., Morris, J.., 1963. Kinetics of adsorption carbon from solutions. ournal Sanit. Eng. Div. 89, 31–60.

Windmoller, C.C., Silva, N.C., Andrade, P.H.M., Mendes, L.A., do Valle, C.M., 2017. Analytical Methods Use of a direct mercury analyzer ® for mercury speciation in di ff erent matrices without sample preparation. Anal. Methods 9, 2159–2167. https://doi.org/10.1039/c6ay03041f

World Health Organization, 1990. International Programme on Chemical Safety: Methylmercury in Environmental Health Criteria 101. Geneva.

World Health Organization (WHO), 2016. Artisanal and small-scale gold mining and health-Technical

Paper #1: Environmental and Occupational Health Hazards Associated with Artisanal and Small-scale Gold Mining. Geneva.

World Health Organization (WHO), 2005. Mercury in Drinking-water Background document for development of WHO Guidelines for Drinking-water Quality. Geneva.

WQA, W.Q.A., 2019. Mercury in Drinking Water [WWW Document]. URL https://www.wqa.org/learn-about-water/common-contaminants/mercury (accessed 11.26.19).

Yalcin, E., Cavusosoglu, K., Maras, M., Biyikoglu, M., 2008. Biosorption of Lead (II) and Cu (II) metal ions on Cladophora glomerata (L.) Kutz. (Chlorophyta) Algae: Effect of Algal surface modification. Acta Chim. Slov. 55, 228–232.

Yamamoto, M., 1996. Stimulation of elemental mercury oxidation in the presence of chloride ion in aquatic environments. Chemosphere 32, 1217–1224.

Appendix A

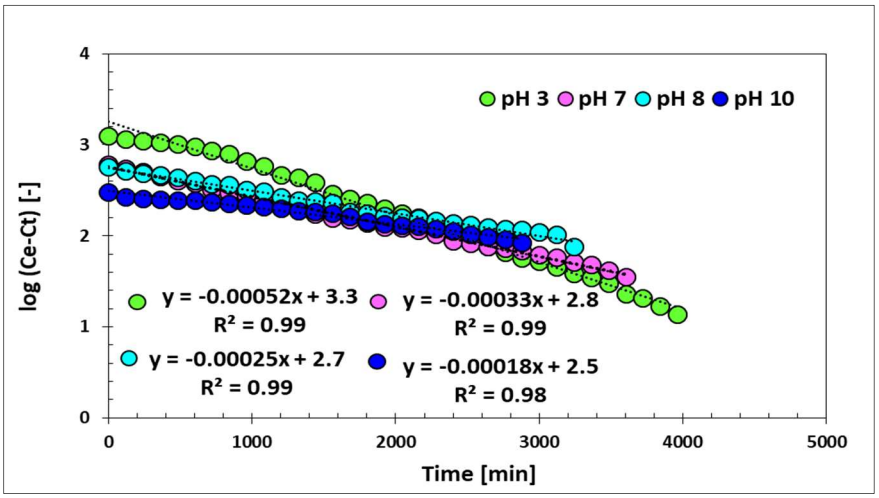

Fig. S3.2: Fitting effect of pH dissolution data on the Noyes-Whitney dissolution model.

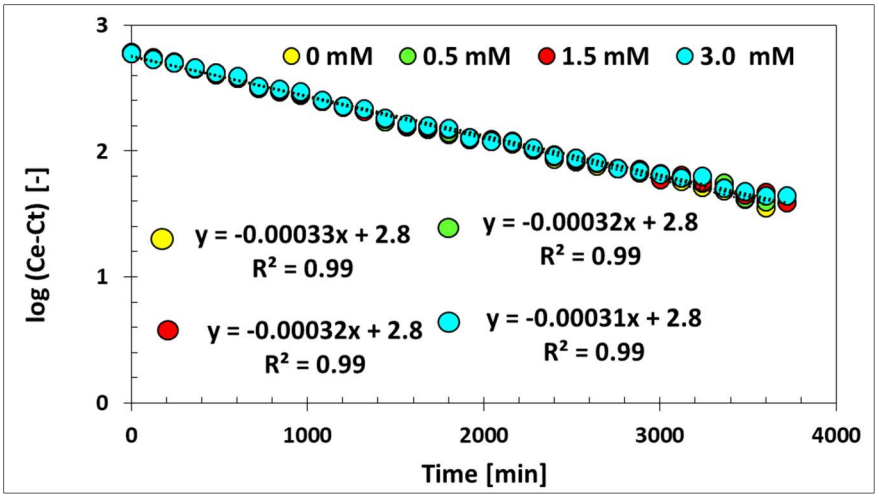

Fig. S3.5: Fitting effect of ionic strength dissolution data on the Noyes-Whitney dissolution model.

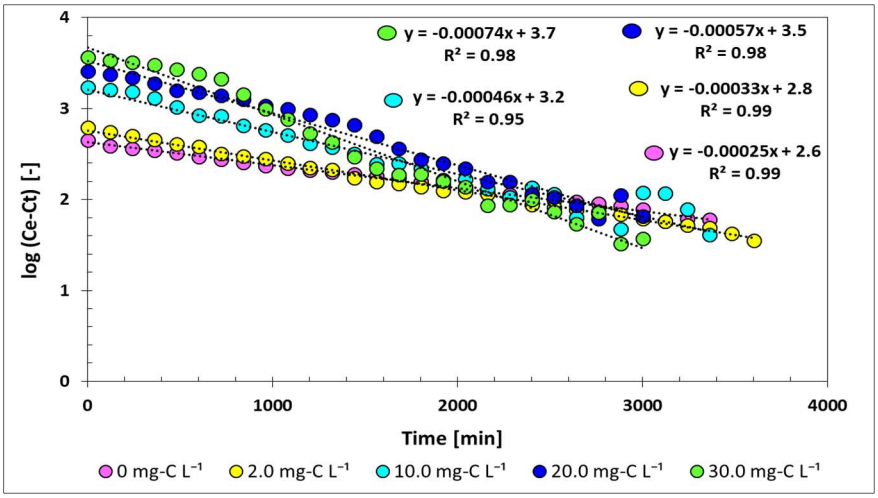

Fig. S3.6: Fitting effect of SRFA concentration dissolution data on the Noyes-Whitney dissolution model.

Combined Hg^0 multivariate dissolution model

$$\hat{k} = -2.6 \times 10^{-3} + 7.3 \times 10^{-4} \log[Re] - 8.3 \times 10^{-5} pH + 0.12[SSA] + 3.7 \times 10^{-5}[SRFA] \quad (5.6)$$

Table S1 Calculated Hg^0 dissolution rate coefficient (for Chapter 3; Section 3.5)

Parameter	Value
pH	7
Re	37453.18
SSA(cm^2 cm^{-3})	0.0015
SRFA (mg-C L^{-1})	2
k (min^{-1})	0.00042

Table S2: ANOVA statistical analysis results

	df	*SS*	*MS*	*F*
Regression	3	1.61×10^{-6}	5.37×10^{-7}	293.33
Residual	10	1.83×10^{-8}	1.83×10^{-9}	
Total	13	1.63×10^{-6}		

	Coefficients	*Standard Error*	*t Stat*	*P-value*
Intercept	1.43×10^{-3}	6.12×10^{-5}	23.32	4.76×10^{-10}
pH [-]	-1.11×10^{-4}	8.39×10^{-6}	-13.28	1.12×10^{-7}
Cl- [mM]	1.01×10^{-7}	1.14×10^{-5}	0.01	9.93×10^{-1}
SRFA concentration [mg-C/L]	3.53×10^{-5}	1.41×10^{-6}	25.01	2.39×10^{-10}